

Development of X-ray shielding material from combination of amorphous cellulose
of used paper, barium sulphate, and natural rubber



A Dissertation Submitted in Partial Fulfillment of the Requirements
for the Degree of Doctor of Philosophy in Environmental Science
Inter-Department of Environmental Science
GRADUATE SCHOOL
Chulalongkorn University
Academic Year 2020
Copyright of Chulalongkorn University

การพัฒนาวัสดุกำบังรังสีเอกซ์จากสารผสมของเซลลูโลสอสัณฐานจากกระดาษใช้แล้ว แบบเรียบซัลเฟต
และยางธรรมชาติ



วิทยานิพนธ์นี้เป็นส่วนหนึ่งของการศึกษาตามหลักสูตรปริญญาวิทยาศาสตรดุษฎีบัณฑิต
สาขาวิชาวิทยาศาสตร์สิ่งแวดล้อม สหสาขาวิชาวิทยาศาสตร์สิ่งแวดล้อม
บัณฑิตวิทยาลัย จุฬาลงกรณ์มหาวิทยาลัย
ปีการศึกษา 2563
ลิขสิทธิ์ของจุฬาลงกรณ์มหาวิทยาลัย

Thesis Title	Development of X-ray shielding material from combination of amorphous cellulose of used paper, barium sulphate, and natural rubber
By	Miss Harinate Mungpayaban
Field of Study	Environmental Science
Thesis Advisor	Associate Professor SOMCHAI PENGPRECHA, Ph.D.
Thesis Co Advisor	Professor SANONG EKGASIT, Ph.D.

Accepted by the GRADUATE SCHOOL, Chulalongkorn University in Partial Fulfillment of the Requirement for the Doctor of Philosophy

..... Dean of the GRADUATE SCHOOL
(Associate Professor THUMNOON NHUJAK, Ph.D.)

DISSERTATION COMMITTEE

..... Chairman
(Assistant Professor TASSANEE CHETWITTAYACHAN, Ph.D.)

..... Thesis Advisor
(Associate Professor SOMCHAI PENGPRECHA, Ph.D.)

..... Thesis Co-Advisor
(Professor SANONG EKGASIT, Ph.D.)

..... Examiner
(Associate Professor DOONYAPONG WONGSAWAENG, Ph.D.)

..... Examiner
(Associate Professor APICHAT IMYIM, Ph.D.)

..... External Examiner
(Associate Professor KIADTISAK SAENBOONRUANG, Ph.D.)

หริเนตร มุ่งพยาบาล : การพัฒนาวัสดุกำบังรังสีเอกซ์จากสารผสมของเซลลูโลสออสัญฐาน
จากกระดาษใช้แล้ว แบริยมซัลเฟต และยางธรรมชาติ. (Development of X-ray
shielding material from combination of amorphous cellulose of used
paper, barium sulphate, and natural rubber) อ.ที่ปรึกษาหลัก : รศ. ดร.สมใจ
เพ็งปรีชา, อ.ที่ปรึกษาร่วม : ศ. ดร.สนอง เอกสิทธิ์

งานวิจัยนี้มีวัตถุประสงค์เพื่อเตรียมสารตั้งต้นที่มีคุณสมบัติกำบังรังสีเอกซ์โดยใช้
เซลลูโลสออสัญฐานจากเยื่อกระดาษสำนักงานใช้แล้วและเยื่อคาลิปต์ผสมกับยางธรรมชาติเพื่อ
พัฒนาวัสดุต้นแบบ โดยคล้ายโครงสร้างเซลลูโลสส่วนผลึกให้เป็นส่วนออสัญฐานด้วยกรดซัลฟิวริก
อนุกรม 0 องศาเซลเซียส และรีเจนเนอเรท ด้วยสารละลายแบริยมคลอไรด์เกิดเป็นคอมโพสิต
แบริยมซัลเฟต/เซลลูโลสออสัญฐาน จากนั้นศึกษาคุณสมบัติการกำบังรังสีของสารผสมจากยาง
ธรรมชาติวัลคาไนซ์รังสีกับคอมโพสิตแบริยมซัลเฟต/เซลลูโลสออสัญฐาน จากกระดาษสำนักงานใช้
แล้ว (NR-W) รวมทั้งเปรียบเทียบประสิทธิภาพกับคอมโพสิตที่เตรียมจากเยื่อคาลิปต์ (NR-E) ซึ่ง
เป็นเซลลูโลสบริสุทธิ์กับผงแบริยมซัลเฟต (NR-P) ที่เป็นวัสดุกำบังรังสีเอกซ์ดั้งเดิม พบว่า NR-W
และ NR-E มีประสิทธิภาพในการกำบังรังสีเอกซ์สูงกว่า NR-P อย่างชัดเจน เนื่องจากเซลลูโลส
ออสัญฐานที่อยู่ล้อมรอบแบริยมซัลเฟตมีคุณสมบัติช่วยกระจายอนุภาคในเนื้อวัสดุได้อย่างทั่วถึงและ
ลดการเกาะรวมกันเป็นก้อน ส่งผลให้สามารถลดปริมาณช่องว่างของวัสดุได้ โดยรังสีเอกซ์ส่วนมาก
ที่ตกกระทบจะถูกดูดซับด้วยแบริยมซัลเฟตที่กระจายตัวอย่างสม่ำเสมอ มีรังสีเอกซ์เพียงส่วนน้อย
ที่สามารถทะลุทะลวงผ่านช่องว่างของวัสดุ จากนั้น ได้ศึกษาการเตรียมวัสดุต้นแบบให้มีคุณสมบัติ
กำบังรังสีเอกซ์เทียบเท่าตะกั่วหนา 0.25 mm ซึ่งเป็นไปตามข้อแนะนำในการป้องกันอันตราย
สำหรับผู้ป่วยและผู้ปฏิบัติงานกับเอกซเรย์ โดยผลิตวัสดุต้นแบบป้องกันรังสีปฐมภูมิ ได้แก่ หมวกกัน
รังสี ปกอกคอกันรังสี และเสื้อชั้นในกันรังสี รวมทั้งวัสดุต้นแบบเสื้อกาวน์กันรังสีสำหรับป้องกันรังสี
กระเจิง ที่สามารถย่อยสลายได้ในธรรมชาติ เป็นมิตรต่อสิ่งแวดล้อม ราคาถูก และปลอดภัย

สาขาวิชา วิทยาศาสตร์สิ่งแวดล้อม

ปีการศึกษา 2563

ลายมือชื่อนิสิต

ลายมือชื่อ อ.ที่ปรึกษาหลัก

ลายมือชื่อ อ.ที่ปรึกษาร่วม

5987846220 : MAJOR ENVIRONMENTAL SCIENCE

KEYWORD: amorphous cellulose, barium sulphate, X-ray shielding, natural rubber, prototype

Harinate Mungpayaban : Development of X-ray shielding material from combination of amorphous cellulose of used paper, barium sulphate, and natural rubber. Advisor: Assoc. Prof. SOMCHAI PENGPRECHA, Ph.D. Co-advisor: Prof. SANONG EKGASIT, Ph.D.

This research aimed to fabricate X-ray shielding substrates using amorphous cellulose from office waste paper and eucalyptus pulp mixed with natural rubber to produce the prototypes. The amorphous cellulose was prepared using only the sulfuric acid at 0 °C to rearrange the crystalline chain to the amorphous chain. After that, the barium sulfate/amorphous cellulose composite (Ba/AC) was regenerated using barium chloride solution. The shielding sheets were formulated by mixing vulcanization natural rubber individual with Ba/AC from office waste paper (NR-W), the purified eucalyptus pulp (NR-E), and barium sulfate powder (NR-P). The NR-W and NR-E were shown the predominant attenuation than the NR-P because of the amorphous cellulose surrounded barium sulfate distributed and reduced the particles aggregation; as a result, most incident X-rays have absorbed. The prototypes were developed at the equivalent of 0.25 mm Pb, complying with the recommendation for patients and occupational workers. The protective materials were formulated to prevent the primary radiation, comprising the shield of the head, thyroid, and breast, while the lab coat was produced to block the scatter radiation. The X-ray shielding prototypes present the benefits of biodegradable, eco-friendly, cost-effective, and non-toxic.

Field of Study: Environmental Science

Student's Signature

Academic Year: 2020

Advisor's Signature

Co-advisor's Signature

ACKNOWLEDGEMENTS

I wish to express my sincere appreciation for all the kind assistance and guidance from several people.

Firstly, I would like to extend my deepest gratitude to my thesis advisor, Associate Professor Dr. Somchai Pengprecha, for his strong support, encouragement, and kind recommendation. I also very much appreciated that he always puts a great effort into the benefit of my doctoral study at all times. This dissertation would not have been accomplished without his supervision.

I wish to express profound gratitude to my co-advisor, Professor Dr. Sanong Ekgasit, for the great opportunity to work on this project, including providing me with precious advice. I am very grateful for open my vision to do the research with valuable inspiration and dedicate the time to teaching me. This thesis has not successful without his advice and support.

Besides, I desire to thank Assistant Professor Dr. Tassanee Prueksasit, Associate Professor Dr. Doonyapong Wongsawaeng, Associate Professor Dr. Apichat Imyim, and Associated Professor Dr. Kiadtisak Saenboonruang as my dissertation committee for helpful recommendation to fulfill my research completely.

In addition, I gratefully acknowledge the Interdisciplinary Program in Environmental Science and the Sensor Research Unit (SRU), Chulalongkorn University for giving me valuable knowledge as well as kind assistance. My sincere special thanks to colleagues from the Office of Atoms for Peace for their strong encouragement and great support.

Finally, I take this opportunity to express my deepest gratitude to my beloved family, Mr. Sirichai Chaiyathammo and Ms. Phatcharin Lertsongkram, for their loving, inspiring, and patient throughout my entire study.

Harinate Mungpayaban

TABLE OF CONTENTS

	Page
ABSTRACT (THAI).....	iii
ABSTRACT (ENGLISH).....	iv
ACKNOWLEDGEMENTS.....	v
TABLE OF CONTENTS.....	vi
CHAPTER 1 INTRODUCTION.....	7
1.1 Research background.....	7
1.2 Objective.....	11
1.3 Scope of research.....	11
1.4 The benefit of this research.....	12
CHAPTER 2 THEORETICAL BACKGROUND.....	14
2.1 Radiation.....	14
2.1.1 Non-ionizing radiation.....	14
2.1.2 Ionizing radiation.....	14
2.2 X-rays.....	15
2.3 X-ray utilization in medicine.....	15
2.3.1 Radiation diagnosis.....	15
2.3.2 Radiation therapy.....	16
2.4 Radiation dose quantities [40], [43].....	16
2.4.1 Absorbed dose.....	16
2.4.2 Equivalent dose.....	16
2.4.3 Effective dose.....	18

2.5 Radiation effects.....	19
2.5.1 Deterministic effect	19
2.5.2 Stochastic effect.....	19
2.6 Radiation protection	19
2.6.1 Time.....	19
2.6.2 Distance	20
2.6.3 Shielding	20
2.7 Dose limit under law and regulations.....	21
2.8 X-ray interactions with matter.....	22
2.8.1 Photoelectric effect.....	22
2.8.2 Rayleigh scattering.....	23
2.8.3 Compton scattering.....	23
2.9 X-ray beam characterization in medicine	24
2.9.1 Primary radiation.....	24
2.9.2 Secondary Radiation.....	24
2.10 X-ray attenuation mechanism.....	25
2.11 X-ray attenuation materials	26
2.11.1 Lead.....	26
2.11.2 Barium sulphate.....	27
2.12 Cellulose.....	36
2.12.1 Amorphous cellulose.....	37
2.12.2 Cellulose from waste paper.....	37
2.13 Natural rubber	39
2.13.1 Property of natural rubber.....	39

2.13.2 Vulcanization of natural rubber.....	40
CHAPTER 3 EXPERIMENTAL SECTION	46
3.1 Chemicals and materials	46
3.2 Instruments.....	46
3.3 Regeneration of cellulose pulp from office waste papers.....	47
3.4 Preparation of amorphous cellulose	47
3.5 Fabrication of BaSO ₄ /amorphous cellulose.....	48
3.6 Preparation of BaSO ₄ /amorphous cellulose from eucalyptus pulp.....	48
3.7 Study of gamma dose for radiation vulcanized natural rubber.....	50
3.8 Formulation of BaSO ₄ /amorphous cellulose/natural rubber.....	52
3.9 Characterization techniques	53
3.9.1 Scanning electron microscope.....	53
3.9.2 X-ray diffractometer	54
3.9.3 Attenuated total reflectance Fourier transform infrared spectroscopy ...	54
3.10 Investigation of X-ray attenuation property	54
3.11 Prototype for x-ray protection products.....	56
3.12 Physical property of X-ray protection products	57
CHAPTER 4 RESULTS AND DISCUSSION	58
4.1 Preparation of amorphous cellulose	58
4.2 Fabrication of BaSO ₄ /amorphous cellulose composite.....	62
4.3 Preparation of radiation vulcanized natural rubber latex	65
4.4 Fabrication of BaSO ₄ /amorphous cellulose/natural rubber.....	66
4.5 Investigation of X-ray attenuation property.....	73
4.5.1 The radiation attenuation ratio.....	73

4.5.2 The linear attenuation coefficient.....	75
4.5.3 The half-value layer	76
4.5.4 The mass attenuation coefficient.....	78
4.6 Preparing of X-ray shielding protective prototypes.....	82
4.7 Interaction of X-ray with barium sulphate/amorphous cellulose/natural rubber using XCOM program.....	85
4.8 Physical property of X-ray protection products	87
4.9 Comparison of investment for X-ray shielding prototypes and commercial products.....	89
CHAPTER 5 CONCLUSION.....	90
REFERENCES	93
APPENDIX.....	101
VITA.....	108

LIST OF TABLES

	Page
Table 2.1 Recommended radiation weighing factors.....	17
Table 2.2 Recommended tissue weighing factors.....	18
Table 2.3 The dose limits under the ministerial regulation of radiation safety.....	21
Table 2.4 The composition example of the mixtures for preparing the sample sheets.....	30
Table 2.5 The radiation attenuation ratio and air permeability of the commercial filaments.....	31
Table 2.6 The composite of sample for coating on the textiles.....	34
Table 2.7 The radiation attenuation ratio of Sample A when exposed with 60-100 kVp.....	34
Table 2.8 The radiation attenuation radiation ratio of BaSO ₄ /cellulose nanocomposite membrane varying with BaSO ₄ concentration.....	35
Table 2.9 Compositions of the total solids content in natural rubber.....	40
Table 2.10 The combustion analysis of gases composition.....	44
Table 2.11 The potential application field of RVNR.....	45
Table 3.1 The sample code of X-ray shielding filler incorporated with RVNR.....	53
Table 3.2 The characteristics of narrow-spectrum series (N-series) for X-ray irradiation.....	55
Table 4.1 The density and mass attenuation coefficient of the varied thickness for RVNR composites.....	79
Table 4.2 The thickness of the sample sheet that array in the layer stack.....	81
Table 4.3 The linear attenuation coefficient and the half-value layer of samples.....	81
Table 4.4 The radiation attenuation ratio of X-ray shielding sheets of prototype development when exposed with 60, 80, and 100 kV.....	82

Table 4.5 The linear attenuation coefficient of X-ray shielding sheets to study the prototypes producing.....	83
Table 4.6 The required thickness of the prototypes that equivalency to 0.25 mm of Pb.....	83
Table 4.7 The physical property of representative for X-ray shielding sheets	87
Table 4.8 The comparison of price for X-ray shielding prototypes and commercial products.....	89



LIST OF FIGURES

	Page
Figure 1.1 Diagram of research.....	13
Figure 2.1 An overview of the electromagnetic spectrum.....	14
Figure 2.2 The mechanism of characteristic X-ray generation.....	15
Figure 2.3 The relationship between radiation weighting factor (W_R) for neutrons and neutron energy (E_n).....	17
Figure 2.4 The suitable shielding materials for the intervention of specific radiation.....	21
Figure 2.5 Interaction of X-rays incident with the matter; (A) no interaction, (B) Photoelectric effect, (C) Rayleigh scattering and (D) Compton scattering.....	22
Figure 2.6 The radiation exposures for X-ray utilization in medicine	17
Figure 2.7 Common exposures from X-ray scattering	28
Figure 2.8 X-ray shielding protective materials	29
Figure 2.9 The inside of the X-ray shielding garment; (2A) A layer construction of X-ray blocking garments following some embodiments, (2B) A detailed illustration of a filled polymer sheet, showing probable surface structure.....	29
Figure 2.10 Cross-section views of filaments structural; (A) Two layers array, and (B) One layer array.....	31
Figure 2.11 The BaSO ₄ mixed with silicone rubber and coated on the cotton fabric to use as X-ray shielding aspects	32
Figure 2.12 The radiation attenuation ratio of BaSO ₄ coated on cotton.....	32
Figure 2.13 The manufactured fiber for radiation dose reduction.....	33
Figure 2.14 The X-ray images of specimens under 50 kV when combining BaSO ₄ at concentration of 0% (CM), 5% (BSCM05), 10% (BSCM10), 15% (BSCM15), and 20% (BSCM20)	34

Figure 2.15 The natural rubber combined with metal oxide for radiation shielding....	35
Figure 2.16 Prototype of radiation shield clothing: (A) scarf made from PET containing BaSO ₄ and (B) inset produced from PET incorporation with BaSO ₄	36
Figure 2.17 The fibril of cellulose chain grouped by hydrogen bond	37
Figure 2.18 Chemical structure of natural rubber (cis-1,4 polyisoprene)	40
Figure 2.19 The sulfur vulcanization natural rubber (SVNR)	41
Figure 2.20 The mechanism of radiation vulcanization of natural rubber	42
Figure 2.21 Effect of leaching on aging properties of radiation vulcanization (RV).....	45
Figure 3.1 Defiber and deink of cellulose pulp from office waste paper.....	47
Figure 3.2 Fabrication of amorphous cellulose using iced-cold sulfuric acid.....	48
Figure 3.3 Regeneration of amorphous cellulose using barium chloride solution to produce Ba/AC.....	48
Figure 3.4 Fabrication of Ba/AC from eucalyptus pulp.....	49
Figure 3.5 Preparing the RVNR using Gamma ⁶⁰ Co irradiation.....	52
Figure 3.6 Schematic of X-ray attenuation study.....	55
Figure 3.7 The samples were exposed using the X-ray generator from SSDL.....	55
Figure 4.1 The SEM images of (A) cellulose pulp from office waste paper and (B) eucalyptus pulp.....	58
Figure 4.2 Schematic for preparation of amorphous cellulose.....	59
Figure 4.3 The SEM images of amorphous cellulose illustrate the submicron scale of particles: (A) AC-W and (B) AC-E.....	60
Figure 4.4 The XRD spectra; (A) cellulose pulp, (B) amorphous cellulose.....	60
Figure 4.5 The ATR-FTIR spectra of cellulose pulp from; (a) office waste paper, and (b) eucalyptus pulp.....	61
Figure 4.6 The ATR-FTIR spectra; (a) cellulose pulp from office waste paper, and (b) eucalyptus pulp.....	62

Figure 4.7 Schematic for preparation of Ba/AC by in situ regeneration of amorphous cellulose using BaCl ₂ solution.....	63
Figure 4.8 The SEM images of Ba/AC demonstrate the submicron scale of particles; (A) Ba-W and (B)-E.....	63
Figure 4.9 The XRD spectra of Ba/AC composites compared to the BaSO ₄ standard..	64
Figure 4.10 The ATR-FTIR of the Ba/AC-W compared with the Ba/AC-E.....	65
Figure 4.11 The relationship between gamma radiation dose (kGy) and RVNR properties; (A) swelling ratio, (B) crosslink density.....	66
Figure 4.12 Study of the suitable ratio between Ba/AC and RVNR to fabricate samples for shielding test.....	67
Figure 4.13 The RVNR sheets for shielding test; (A) RVNR without filler, and RVNR incorporated with filler (B-D).....	68
Figure 4.14 SEM/EDX results of RVNR without filler; (A) SEM images, and (B) EDX spectrum.....	69
Figure 4.15 SEM/EDX results of NR-W; (A) SEM image, and (B) EDX spectrum.....	70
Figure 4.16 SEM/EDX results of NR-E; (A) SEM image, and (B) EDX spectrum.....	71
Figure 4.17 SEM/EDX results of NR-P; (A) SEM image, and (B) EDX spectrum.....	72
Figure 4.18 The % RAR of RVNR samples mixed with BaSO ₄ fillers and irradiated at 30 kV X-ray tube voltage.....	73
Figure 4.19 The % RAR of RVNR samples mixed with BaSO ₄ fillers and irradiated at 40 kV X-ray tube voltage.....	74
Figure 4.20 The % RAR of RVNR samples mixed with BaSO ₄ fillers and irradiated at 60 kV X-ray tube voltage.....	74
Figure 4.21 BaSO ₄ particle distribution affects with X-ray transmittance; (A) BaSO ₄ powder, and (B) Ba/AC.....	75
Figure 4.22 The linear attenuation coefficient of RVNR samples mixed with BaSO ₄ fillers; (A) 40 %w/w, (B) 50 %w/w, and (C) 60 %w/w.....	76

Figure 4.23 The half-value layer of RVNR samples mixed with BaSO ₄ fillers ; (A) 40 %w/w, (B) 50 %w/w, and (C) 60 %w/w.....	77
Figure 4.24 The radiation attenuation ratio of NR-W and NR-E with different thickness compared to the lead sheet when exposing with 60 kV.....	80
Figure 4.25 The radiation attenuation ratio of NR-W and NR-E with different thickness compared to the lead sheet when exposing with 80 kV.....	80
Figure 4.26 Prototypes for X-ray protectives materials; (A1-A3) shielding sheets in various shapes and prototypes of (B1) head shield, (B2) thyroid shield, and (B3) breast shield.....	84
Figure 4.27 The X-ray shielding prototype; (A) shielding sheet prepared for attaching with the lab coat, and (B) lab coat for X-ray scattering attenuation.....	85
Figure 4.28 The X-ray interaction of BaSO ₄ amorphous cellulose/natural rubber.....	87
Figure 4.29 The Ba/AC particles dispersion in natural rubber; (A) Ba/AC NR-W60 PROTO and (B) Ba/AC NR-E60 PROTO.....	89

CHAPTER 1

INTRODUCTION

1.1 Research background

X-ray is generally employed in medical applications. The X-ray can be used for diagnostic (30-140 kV) and radiotherapy (40-300 kV). [1], [2] The diagnosis is used for medical imaging to diagnose the disorder symptoms in many organs. [3], [4] Besides, the X-ray in high energy can be utilized for killing skin cancer by selecting the optimized kilovoltage range for treatment. In general, radiation exposure from X-ray generators in medicine can produce in two main categories, which are primary radiation and secondary radiation. The primary radiation is the radiation that transmits from the X-ray tube, which affects significant hazards, even exposure in a short duration, while Secondary radiation is produced from primary radiation that incident to the matter and reflects other objects. Scatter radiation is one type of secondary radiation that is less hazardous compared to the primary beam, which normally affects the occupational worker in the hospital. [5], [6] The biological effects of X-ray radiation tending to damage the cell can classify into two types; deterministic effect and stochastic effect. The deterministic effect relates to the radiation exposure in high levels over the threshold in the short term, which depends on the radiation dose. The higher doses obtained, the greater the severity effect. The symptom of deterministic effect reveals skin burns, radiation sickness, cataracts, sterility, and tumor necrosis, while stochastic effect associates radiation exposure at a low level over a long time. The severity is independent of the dose received; however, the probability of appearing increased with the long-term exposure tends to risk with the apparent effect, for example, cancer, heritable effects, and genetic changes. [7], [8], [9]

Thailand complies with the Nuclear Energy for Peace Act, B.E. 2559 (2016) to regulate occupational exposure for radiation protection follows the ALARA principle by controlling the dose limit. The ministerial regulation of radiation safety, B.E. 2561 (2018)

defined as the radiation dose limit for public and occupational workers, according to the ICRP 103. [10] Moreover, to minimize the exposure of X-rays according to the ALARA principle, it is necessary to consider the benefits obtained by individuals exposed to radiation at a reasonable level. The radiation safety for external protection is time, distance, and shielding. Minimize spending time with radioactive sources can decrease the radiation exposure dose, increasing distance from the source of radiation will decrease the amount of radiation received, and selecting the appropriate shielding materials for reducing the external radiation risk are taken into consideration. [11]

Lead is generally used in medical facilities to prevent radiation exposure because it provides high atomic numbers ($Z=82$) and density (11.35g/cm^3). Lead can attenuate the primary X-ray and scattered X-ray with excellent performance. [12], [13], [14] However, lead is a dangerous material and detriment to health due to its toxicity. In addition, lead dust particles are formed on the object surfaces of the apron and protective materials, causing occupational exposure from dust removal from the surface when radiation incident to the object. The lead dust may contaminate the airborne, floors, and nearby places, tending to be inhaled or ingested by workers. [15], [16] Moreover, lead is a traditional material combined with a rubber, polymer, elastomer polymer with elastic properties. These materials are applied to garments, covers, and curtains for radiation attenuation purposes; however, the management of the disposal of Pb-based material when expired is still an environmental concern. The ICRP has also encouraged to study and development of shielding materials incorporating non-Pb materials either as single metal powders or as mixtures of metal powders. [17], [8]

Barium sulphate (BaSO_4) is environmentally friendly and economical to produce radiation shielding. BaSO_4 has an absorption edge of 37.4 keV to absorb the photoelectric effect, including can be absorbed the low energy through Compton scattering effectively. BaSO_4 is safe for humans and has normally been used in X-ray images for radiography by swallow since the early twentieth century. The predominant

function of BaSO₄ is the oral helpful diagnostic test for pharyngeal or esophageal symptoms, facilitating the selection of additional diagnostic procedures and guiding decisions about medical, endoscopic, or surgical treatment. Moreover, BaSO₄ is employed as the main component for producing radiation shielding fiber. It was because the absorption edge is lower than lead, which possesses a high atomic number with the energy of the photoelectric effect area. [18], [19], [20]

Cellulose is a biopolymer with high mechanical properties. Cellulose has the benefit of environment-friendly, biodegradable polymer, and renewable sources. Cellulose molecule composes of β -1, 4-D-linked glucose chains. The intra-chain and inter-molecule were linked with hydrogen bonds, which play a significant role in enhancing conformation and mechanical properties. [21], [22], [23] The cellulose chains are grouped into fibrils by hydrogen bonds, packed into larger microfibrils, and aligned in different directions. [24] Generally, the microfibrils consist of two main parts; the crystalline cellulose is in respect to the high ordered region, and the amorphous cellulose has a mainly disordered position. The crystalline chain has a hydroxy group orderly on the region showing the chemical resistance, while the amorphous cellulose has a hydroxy group aligned disordered in the domain chain. Most of the reactants are highly reactive with the amorphous region compared to the crystalline region, which results in employment for many purposes. [25], [26]

Amorphous cellulose has been applied in various applications. For example, the study of behavior in nanocrystalline domains [25], protein purification [27], and enzyme screening incorporated displaying materials. [28], [29], [30] The amorphous cellulose can prepare in many methods, for example, cellulose ball-milling, deacetylation of cellulose acetate under nonaqueous alkaline conditions, dissolving natural cellulose in an amine/inorganic salt solvent, associated with regenerate using organic solvents, such as methanol, ethanol, and acetone. [31], [32] However, these methods are complicated and require several chemical substances and solvents to achieve amorphous products.

Cellulose from recycled material is an interesting approach to reduce detrimental the ecology system. It is usually underutilized and finally achieves burning or slow biodegradation. [33] Recycling waste paper in one ton can preserve approximately 17 trees and 7000 gallons of water, which provides the advantage of environmental and economic. [34] Thailand has been employed office waste paper approximately 2 million tons per year and tends to expand continuously by 15% each year. [35] In terms of environmental aspects, office waste paper is wealth for recycling to reduce polluting the earth ecology. However, the maximum ratio for recycling from paper to paper is approximately 65 %, which may cause production in large quantities for its disposal. The higher cost of manufactured paper from recycled pulp and disposal of waste fibers are unfit for use. It is necessary to find alternative options to recycle waste paper. Several attempts have been considered in a new procedure to utilizing waste paper in terms of eco-friendly. The office waste paper provided a source of cellulose that can be utilized in many applications. [36], [37]

Natural rubber is normally utilized for many purposes due to its being eco-friendly and cost-effective. Radiation vulcanized natural rubber is non-toxic and eco-friendly compared to sulfur vulcanized natural rubber. Besides, the radiation vulcanized natural rubber would be economically acceptable to the latex industry when supplied on a large scale. [38], [39]

This research aims to fabricate a substrate of X-ray attenuation using amorphous cellulose. The amorphous cellulose was prepared from recycled pulp from office waste paper using only the ice-cold sulfuric acid to rearrange the crystalline order chain to the amorphous disorder chain. Due to the mild condition, almost the crystalline part in cellulose transformed into the amorphous part results in high production. The BaSO_4 /amorphous cellulose composite (Ba/AC) was prepared from regeneration with BaCl_2 solution as a substrate for the X-ray shielding prototype. After that, the X-ray shielding sheets were formulated by incorporation between the Ba/AC

and RVNR, including comparing with the Ba/AC from eucalyptus pulp and barium sulphate powder as conventional materials. The shielding sheets illustrate the X-ray attenuation efficiency. Subsequently, the protective prototypes for X-ray were studied and fabricated with equivalent to 0.25 mm Pb, regarding the Quality Standards of Medical Diagnostic X-ray Machines, Department of Medical Sciences. [4] The lab coat was produced to prevent the scatter radiation, while the X-ray protective materials (head shield, thyroid shield, and breast shield) were prepared for intervention in the primary radiation. The X-ray shielding prototypes present the benefits of biodegradable, eco-friendly, cost-effective, and non-toxic.

1.2 Objective

1.2.1 To fabricate composite of BaSO₄/amorphous cellulose from office waste paper as X-ray shielding substrate.

1.2.2 To formulate composite of BaSO₄/amorphous cellulose/natural rubber for X-ray shielding material.

1.2.3 To study X-ray attenuation property of BaSO₄/amorphous cellulose/natural rubber.

1.2.4 To prepare the prototype of X-ray shielding protective materials equivalency to 0.25 mm Pb.

1.3 Scope of research

1.3.1 Regenerate cellulose pulp from office waste paper.

1.3.2 Preparation of amorphous cellulose.

1.3.3 Fabrication of BaSO₄/amorphous cellulose.

1.3.4 Comparison of BaSO₄/amorphous cellulose from office waste paper (recycled pulp) with eucalyptus pulp (purified pulp).

1.3.5 Study of gamma dose for radiation vulcanized natural rubber.

1.3.6 Formulation of BaSO₄/amorphous cellulose/natural rubber.

1.3.7 Characterization of products.

1.3.8 Investigation of X-ray attenuation property.

1.3.9 Produce the prototypes of X-ray protective materials.

1.3.10 Study of the physical property of X-ray protection products.

1.4 The benefit of this research

1.4.1 The BaSO₄/amorphous cellulose can be used as a substrate for X-ray shielding materials, with the benefits of environmental-friendly, non-toxic, cost-effective, and appropriate scaling up for commercial purposes.

1.4.2 The BaSO₄/amorphous cellulose/natural rubber can attenuate X-ray efficiency with the flexible material that can apply in many applications.

1.4.3 The prototype of the lab coat for intervention the X-ray scatter produced at equivalency to 0.25 mm Pb can be used to prevent the occupational worker.

1.4.4 The X-ray protection prototypes (thyroid shield, breast shield, and head shield) from office waste paper as base materials can be employed for the direct X-ray beam equivalent to the thickness of lead 0.25 mm.

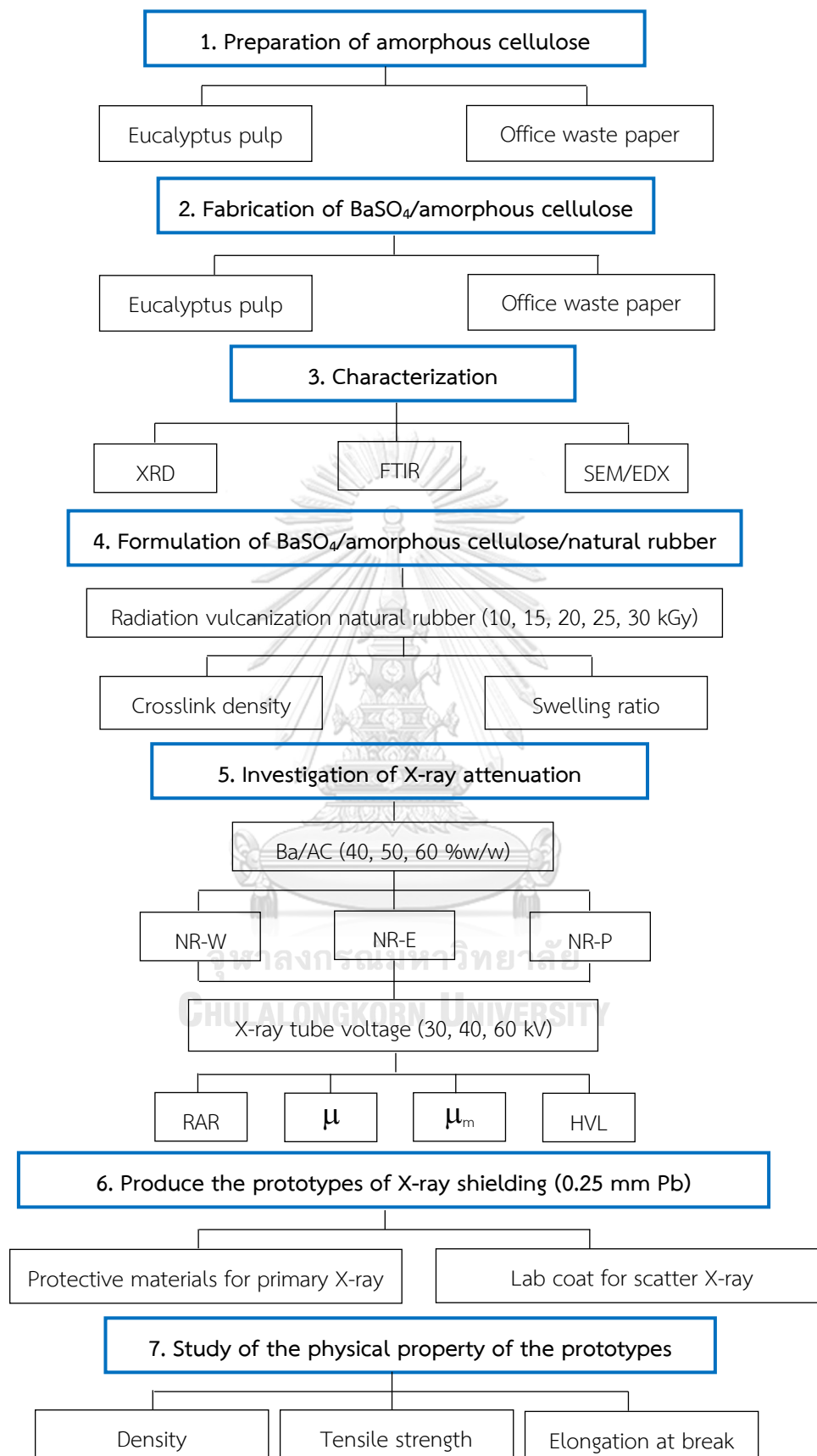


Figure 1.1 Diagram of research.

CHAPTER 2

THEORETICAL BACKGROUND

2.1 Radiation

Radiation is the energy of waves or particles that emit from sources and travels through space or other mediums. The radiation in waves form is light, heat, microwaves, X-rays, and gamma-rays, while the radiation in particles forms are alpha, beta, and neutron. The radiation can divide into two categories depending on the ionization properties; non-ionizing radiation and ionizing radiation. [40]

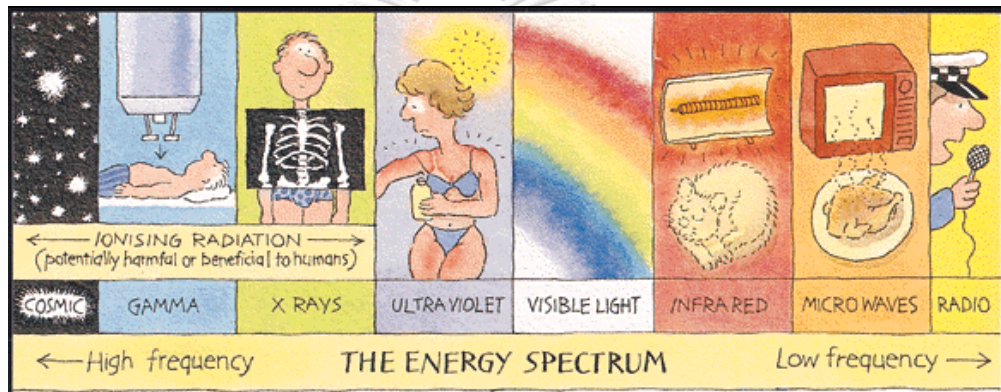


Figure 2.1 An overview of the electromagnetic spectrum. [41]

2.1.1 Non-ionizing radiation

Non-ionizing radiation provides low energy less than the ionizing radiation to produce ions; for example, ultraviolet, visible light, infrared, microwaves, and radio waves. The non-ionizing radiation has low-frequency waves and is not considered to health risk.

2.1.2 Ionizing radiation

Ionizing radiation is the electromagnetic wave or particles that possess high energy to ionize the atom or molecule in the medium to be the ions. The example of ionizing radiation is alpha particles, beta particles, gamma-rays, and X-rays. The ionizing

radiation is the radiation that can generate charged particles or ions in the matter composing of X-rays, gamma-rays, alpha particles, beta particles, and neutrons.

2.2 X-rays

X-ray is highly energetic electromagnetic radiation that originates from the electron shell of an atom. The X-ray is similar to visible light, which can penetrate the medium depending on the density and atomic weight of the matter. When X-rays incident to material, the inner atom will eject the electron and provide the hole in the electron shell. Subsequently, the electron from the outer shell that has higher energy will be released their energy to occupy the hole and create the characteristic X-ray as shown in Figure 2.2.

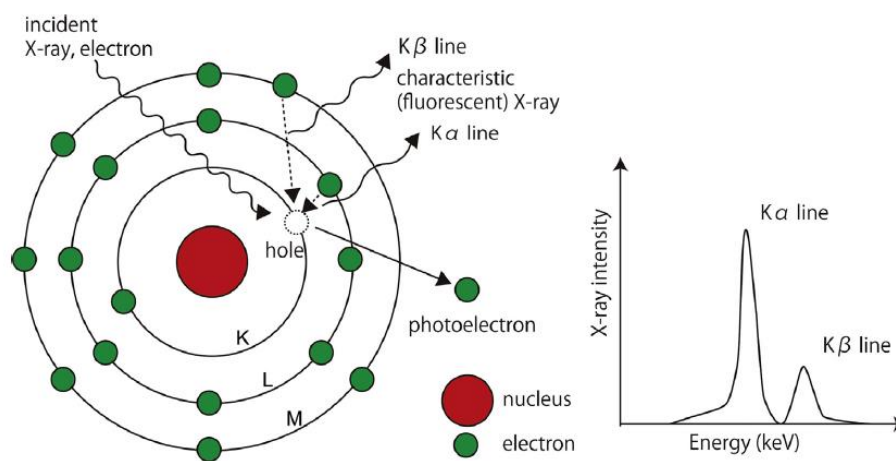


Figure 2.2 The mechanism of characteristic X-ray generation. [42]

2.3 X-ray utilization in medicine

X-ray is widely used in many applications, especially in medicine, which is classified into two categorized; diagnostic at the X-ray dose range of 30-140 kV, and radiotherapy at the dose range of 40-300 kV. [1], [2]

2.3.1 Radiation diagnosis

X-ray is utilized for medical imaging to diagnose the disorder's symptoms in many organs. The example of X-ray diagnostics is computerized tomography, digital

subtraction angiography, fluoroscopic X-ray, general radiographic X-ray, mobile X-ray, and dental X-rays unit. [3], [4]

2.3.2 Radiation therapy

The X-ray in high energy can be used for killing skin cancer by selecting the optimized kilovoltage range for treatment. X-ray therapy is conventionally divided into four ranges; Grenz ray (10-20 kV) using to cure skin disorders, contact therapy (40–50 kV) applying to treatment depths of 1–2mm, superficial therapy (50–150 kV) utilizing to injury treatment up to 5 mm deep, and orthovoltage therapy (150–300 kV) employing to skin tumor treatment to 2 cm depths. [2]

2.4 Radiation dose quantities [40], [43]

2.4.1 Absorbed dose

Absorbed dose (D) is the amount of energy deposited on the human body or object when exposed to ionizing radiation. The radiation exposure can measure in a unit called the gray (Gy). A dose of one gray is equal to a unit of energy in a joule accumulated in a kilogram of a substance (J/kg).

2.4.2 Equivalent dose

Equivalent dose relates the absorbed dose in human tissue to the effective biological damage of the radiation. The equivalent dose can calculate by multiplying the absorbed dose with the specified radiation weighting factor (w_R), which depends on the type of radiation as shown in Table 2.1. The equation for determining the equivalent dose is demonstrated in equation 2.1. The unit of equivalent dose is J/kg, and called in sievert (Sv).

$$H_T = \sum (D_{TR} \times w_R) \quad (2.1)$$

where;

H_T = the equivalent dose in tissue or organ T

D_{TR} = the average dose from radiation R in the tissue or organ T
(Table 2.1)

w_R = the radiation weighting factor for radiation

Table 2.1 Recommended radiation weighting factors.

Radiation type	Radiation weighting factor (w_R)
Photons	1
Electrons and muons	1
Protons and charged pions	2
Alpha particles, fission fragments, heavy ions	20
Neutrons	A continuous function of neutron energy can calculate according to the Figure 2.3 and equation 2.2

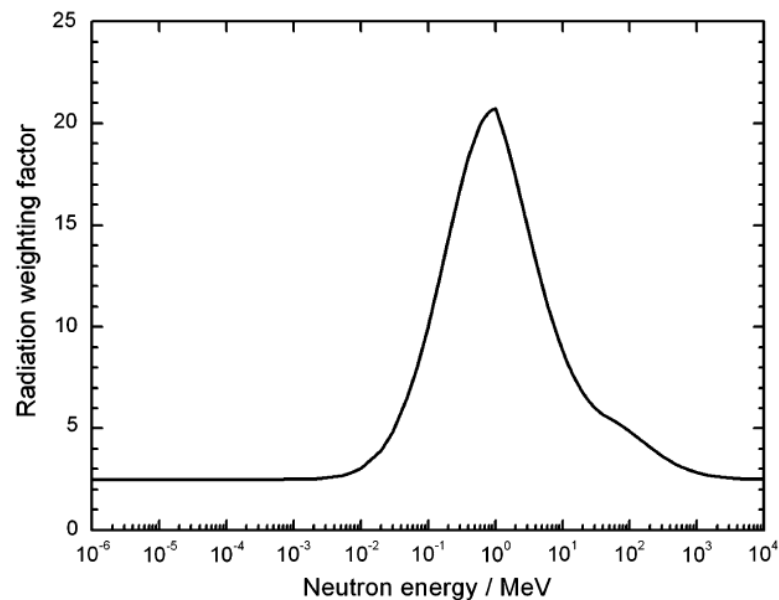


Figure 2.3 The relationship between radiation weighting factor (w_R) for neutrons and neutron energy (E_n). [43]

To determine the radiation weighting factor of the neutron, it is recommended to follow the continuous function of neutron energy (E_n) in Figure 2.3 and apply with the equation as follows;

$$\begin{aligned} E_n < 1 \text{ MeV}, & \quad w_R = 2.5 + 18.2e^{-[\ln(E_n)]^2/6} \\ 1 \text{ MeV} \leq E_n \leq 50 \text{ MeV}, & \quad w_R = 5.0 + 17.0e^{-[\ln(2E_n)]^2/6} \\ E_n > 50 \text{ MeV}, & \quad w_R = 2.5 + 3.25e^{-[\ln(0.04E_n)]^2/6} \end{aligned} \quad (2.2)$$

2.4.3 Effective dose

Effective dose indicates how radiation exposure can affect human health. The harmful risk depends on the exposed organ part, expressed by a tissue weighting factor (w_T) shown in Table 2.2. The equivalent dose can determine by multiplying the tissue weighting factor of the exposed organ with the equivalent dose and shown the unit in sievert.

$$E_T = \sum (H_T \times w_T) \quad (2.3)$$

where;

- E_T = the effective dose for organ or tissue T
 H_T = the equivalent dose in tissue or organ T
 w_T = the tissue weighting factor for tissue T

Table 2.2 Recommend tissue weighting factors.

Tissue	w_T
Bone-marrow (red), Colon, Lung, Stomach, Breast,	0.12
Remainder tissues*	
Gonads	0.08
Bladder, Oesophagus, Liver, Thyroid	0.04
Bone surface, Brain, Salivary glands, Skin	0.01

* Remainder Tissues (14 in total): Adrenals, Extrathoracic (ET) region, Gall bladder, Heart, Kidneys, Lymphatic nodes, Muscle, Oral mucosa, Pancreas, Prostate, Small intestine, Spleen, Thymus, Uterus/cervix.

2.5 Radiation effects

The radiation exposure potential to damage the body, which can classify into two types. The deterministic effect and stochastic effect described as follows. [7], [8], [9]

2.5.1 Deterministic effect

Deterministic effect associates the radiation exposure in high levels over the threshold in the short term, which depends on the radiation dose. The higher doses obtained, the greater the severity effect. The symptom of deterministic effect reveals skin burns, radiation sickness, cataracts, sterility, and tumor necrosis.

2.5.2 Stochastic effect

Stochastic effect relates to radiation exposure at a low level over a long time. The severity is independent of the dose obtained, but the probability of appearing increased. Long-term exposure tends to risk the obvious effect, for example, cancer, heritable effects, and genetic changes.

2.6 Radiation protection

The principle of radiation safety protection is to limit the exposure of ionizing radiation. The As Low As Reasonably Achievable (ALARA) principle is normally considered the benefits achieved by individuals exposed to radiation at a reasonable level. The radiation safety for external protection is time, distance, and shielding. [11]

2.6.1 Time

Minimize spending time with radioactive sources can decrease the radiation exposure dose. The less time spent with radioactive materials, the lower radiation absorbed. For radiation protection, the occupational worker is necessary to consider

the proper time to work. The appropriate time to be spent can calculate using equation 2.4.

$$\text{Dose} = \text{Dose Rate} \times \text{Time} \quad (2.4)$$

2.6.2 Distance

Increasing distance from the source of radiation will decrease the quantity of radiation acquired. The inverse-square law can use for calculating, which states that as the radiation travels out from the source, the dosage decreases inversely with the square of the distance.

$$I_1 d_1^2 = I_2 d_2^2 \quad (2.5)$$

where;

- I_1 = the intensity 1 at distance 1
- I_2 = the intensity 2 at distance 2
- d_1 = the distance 1 from radioactive source
- d_2 = the distance 2 from radioactive source

2.6.3 Shielding

In case decreasing time or increasing the distance may not be achievable. The shielding materials are necessary to select for reducing the external radiation risk efficiently. The appropriate shielding material was recommended by considering the activity, radiation type, energy, and dose limit for an occupational worker. The individual radiation type and energy will affect the transmittance of radiation which required specific shielding material.

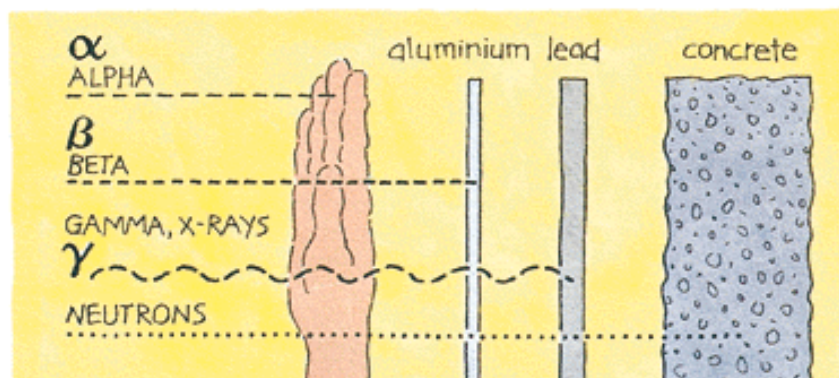


Figure 2.4 The suitable shielding material for the intervention of specific radiation. [44]

2.7 Dose limit under law and regulations

In terms of radiation protection, Thailand complies with the Nuclear Energy for Peace Act, B.E. 2559 (2016) for regulation the occupation exposure, following the ALARA principle by controlling the dose limit. The ministerial regulation of radiation safety, B.E. 2561 (2018) defined as the radiation dose limit for public and occupational workers, according to the ICRP 103, shown in Table 2.3. [10]

Table 2.3 The dose limits under the ministerial regulation of radiation safety.

Type of limit	Occupational	Public
Effective dose	20 mSv per year, averaged over defined periods of 5 years	1 mSv in a year
Annual equivalent dose in:		
Lens of the eye	150 mSv	15 mSv
Skin	500 mSv	50 mSv
Hands and feet	500 mSv	-

2.8 X-ray interactions with matter

In general, when X-ray incident with the matter, they will interact with atoms of the object and results in absorption or scattering. This behavior leads the beam to the trajectory direction, which may not interact and penetrate through the material. In terms of medical applications, the X-ray interactions related to medical are composed of photoelectric absorption, Rayleigh scattering, and Compton scattering are described as follows.

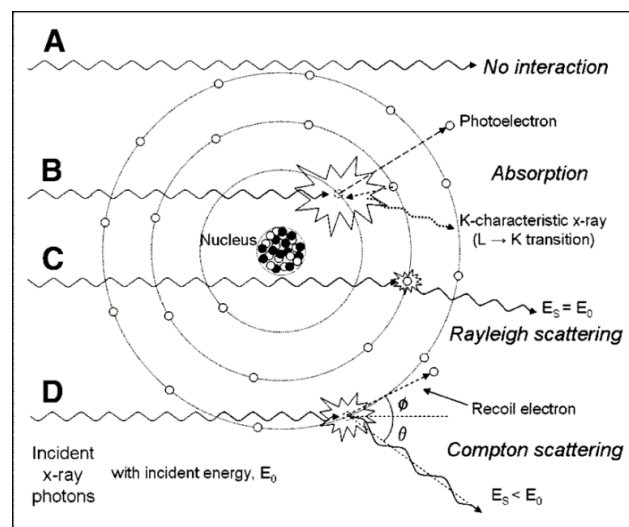


Figure 2.5 Interaction of X-rays incident with the matter; (A) no interaction, (B) Photoelectric effect, (C) Rayleigh scattering, and (D) Compton scattering. [45]

2.8.1 Photoelectric effect

The incident X-ray photon transfers its energy to the electron, which results in the ejection of the electron from its shell (usually the K shell) with a kinetic energy equal to the difference of the incident photon energy (E_0) and the electron shell binding energy (E_{BE}) as shown in Figure 2.5B. Subsequently, the vacancy electron shell was filled by an electron from an outer shell (L or M shell). After that, a characteristic X-ray has released that is equivalent to the different energy between binding energies of the source electron shell and the final electron shell. The photoelectric effect will not occur if the incident energy is less than the binding energy of the electron.

2.8.2 Rayleigh scattering

The Rayleigh scattering is a coherence scattering process that the incident X-ray is interacted with an electron and deflected or scattered without loss of energy. This process is elastic scattering that occurred by raising the electron energy without removing it from the atom. The electron returns to the previous energy level by emitting an X-ray equal to the incident energy, but slightly different direction. (Figure 2.5C) There is no absorption of energy, and most of the X-rays are scattered at a small angle. The Rayleigh scattering is possibly enhanced when increasing Z of the absorbed and decreasing X-ray energy.

2.8.3 Compton scattering

The Compton scattering is an incoherence scattering process that inelastic interaction between the energy of X-ray (E_0), which is greater than the binding energy of an atomic electron. Partial energy transfers to the electron, causing recoil and removal from the atom at an angle. The remainder of the energy (E_s) is transferred to a scattered X-ray with a trajectory of angle relative to the trajectory of the incident photon (Figure 2.5D).

2.9 X-ray beam characterization in medicine

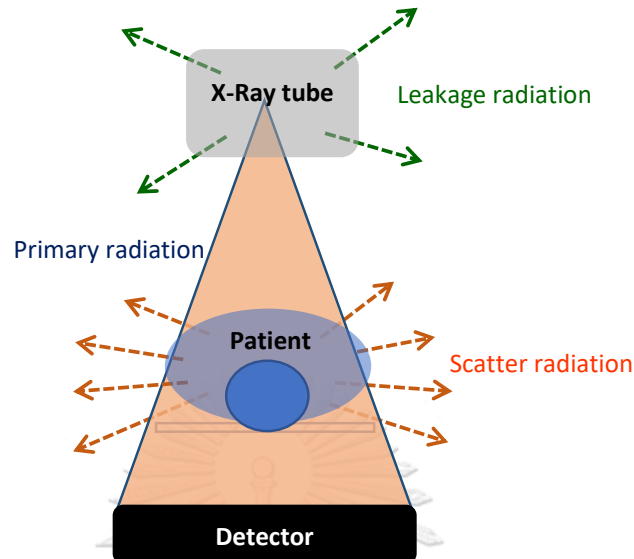


Figure 2.6 The radiation exposure for X-ray utilization in medicine.

Radiation exposure from X-ray generators in medicine can produce in two main categories, which are comprised of primary radiation and secondary radiation as follows. [5], [6]

2.9.1 Primary radiation

The radiation that transmits from the X-ray tube is called primary radiation. The primary beam is a significant hazard even exposure in a very short duration can lead to severe radiation burns.

2.9.2 Secondary Radiation

1) Scatter radiation

When the primary X-ray incident with the patient, they will produce the scatter radiation that generates less energy than the primary X-ray. The scatter radiation has less hazard than the primary beam, which affects the occupational worker in the hospital.

2) Leakage radiation

Leakage radiation comes from the x-ray tube, providing very low radiation that is not a hazard in case the tube housing is intact.

2.10 X-ray attenuation mechanism

The opportunity of X-rays to interact with matter varies according to the incident energy and the medium of the barrier, which can define the attenuation efficiency by linear attenuation coefficient, mass attenuation coefficient, and half-value layer. The X-ray attenuation can explain by Lambert's law by following equations. [11]

$$I = I_0 e^{-\mu x} \quad (2.6)$$

$$\mu = \frac{1}{x} \ln \left(\frac{I_0}{I} \right) \quad (2.7)$$

$$\mu_m = \frac{1}{\rho x} \ln \left(\frac{I_0}{I} \right) \quad (2.8)$$

where;

I = the intensity of the attenuated beam

I_0 = the initial intensity without shielding material

x = the thickness of the shielding material (cm)

μ = the linear attenuation coefficient (cm^{-1})

μ_m = the mass attenuation coefficient (cm^2g^{-1})

ρ = the density of material (gcm^{-3})

The linear attenuation coefficient is the possibility per unit length that X-ray will undergo an interaction in the material. For example, if the value of the linear attenuation coefficient is high, the possibility of the interaction is increased, which means the radiation can attenuate in a short distance. The mass attenuation coefficient

is dependent on the nature of the material, which does not relate to density but rather the atomic composition. The half-value layer (HVL) is the thickness of a shielding material required to attenuate the intensity of the radiation to half its initial value. [46]

$$\text{HVL} = \frac{\ln 2}{\mu} = \frac{0.693}{\mu} \quad (2.9)$$

The radiation attenuation ratio (%) also utilized to determine the X-ray shielding efficiency using the equation as follows. [47]

$$\text{RAR} (\%) = \frac{(I_0 - I)}{I_0} \times 100 \quad (2.10)$$

2.11 X-ray attenuation materials

2.11.1 Lead

Lead is generally used in medical facilities to prevent radiation exposure because it provides high atomic numbers ($Z=82$) and density (11.35 g/cm^3). Lead can attenuate the primary X-ray and scattered X-ray with excellent efficiency. [12], [13], [14] However, lead is a dangerous material and detriment to health due to its toxicity. Lead dust particles are formed on the object surfaces of the apron and protective materials, causing occupational exposure from dust removal from the surface when radiation incident to the object. The lead dust may contaminate airborne and floors tending to be inhaled or ingested by workers. [15], [16]

Burns et al. studied the lead-containing shields tend to provide lead dust on the external surface. The results indicated a significant proportion of shields (63%) used in hospitals were found the lead dust on the surface, which came from the occupational worker that worn to against the radiation exposure. [48]

In terms of environmental impact, lead is a traditional material combined with a rubber, polymer, elastomer polymer with elastic properties. These materials are

applied to garments, covers, and curtains for radiation attenuation purposes. However, the management of the disposal of Pb-based material when expired is still an environmental concern. Besides, the International Commission on Radiological Protection (ICRP) has also encouraged to study and develop shielding materials incorporating non-Pb materials either as single metal powders or as mixtures of metal powders. [17], [8]

2.11.2 Barium sulphate

Barium sulphate (BaSO_4) is environmentally friendly and economical to produce radiation shielding. BaSO_4 has an absorption edge of 37.4 keV to absorb the photoelectric effect, including can shield the low energy through Compton scattering effectively. BaSO_4 is safe for humans and can be used for X-ray images for radiography by swallow since the early twentieth century, which a dominant function of the oral helpful diagnostic test for pharyngeal or esophageal symptoms that facilitating the selection of additional diagnostic procedures and guiding decisions about medical, endoscopic, or surgical treatment. Moreover, BaSO_4 is used as the main component for producing radiation shielding fiber. It was because BaSO_4 possesses a high atomic number with the energy of the photoelectric effect area. [18], [19], [20] Many researchers studied the BaSO_4 for X-ray shielding aspects, which are summarized as follows.

Beck T.J. [5] developed the optional X-ray shielding material instead of lead for preventing the X-ray scatter at the energy of 110 keV. Multi-layer and flexible was produced in arrays to form a garment by combining the metal radiation absorption with the vinyl matrix or polyolefin. The bilayers were comprised 60-90% of barium oxide or barium sulphate for the outer layer, while the inner layer containing 60-90% of antimony that reduce the radiation to 90%. As the parts of the tri-layers, the outermost part produced from 60-90% of gadolinium in metal or oxide or salt form, the middle part was barium metals or barium oxide or barium sulphate, and the innermost part was 50-90% of antimony in the form of oxide or salts (chloride, iodide).

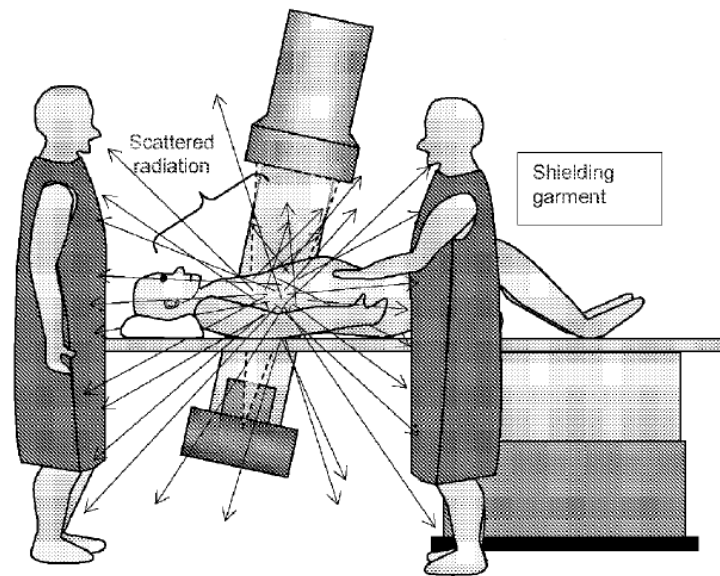


Figure 2.7 Common exposures from X-ray scattering.

Rebar et al. [49] invented the X-ray shielding material by incorporating the radiation shielding filler (Sb, W, Bi, BaSO₄) with several polymers (polyolefin elastomer, polyolefin copolymer, polyolefin terpolymer). The shielding products were vest-skirt combinations, frontal aprons, dental drapes, thyroid collars, gonad, providing the benefit of good mechanical properties and chemical resistance. The composites were comprised of two main layers; the outer layer is the nylon or polyester that does not absorb the radiation, while the middle layer contained the X-ray absorber that provides the material thickness of 10-12 μm . Since the metal fillers had various particle sizes between 1 to 70 μm , they caused some particles to stab out of the layer, as shown in Figure 2.9.

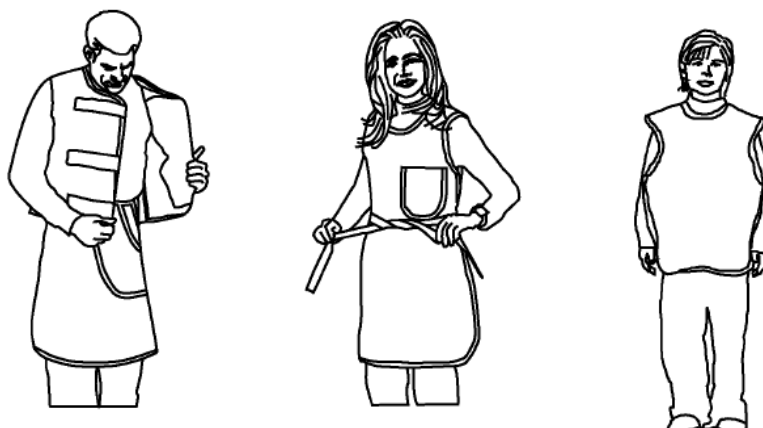


Figure 2.8 X-ray protective materials.

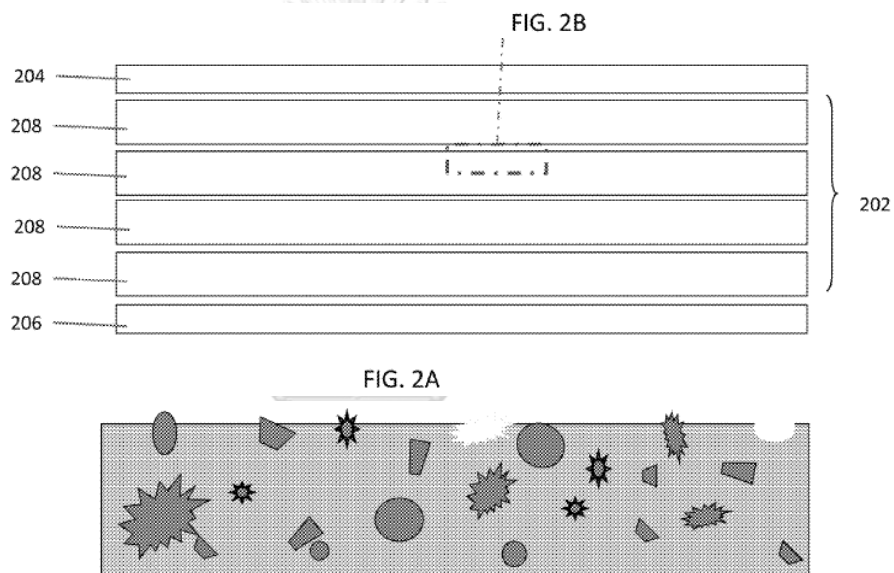


Figure 2.9 The inside of the X-ray shielding garment; (2A) A layer construction of X-ray blocking garments following some embodiments, (2B) A detailed illustration of a filled polymer sheet, showing probable surface structure.

The X-ray shielding sheets were prepared by mixing the chemical compositions shown in Table 2.4. The composites were agitated at 25-35 rpm, and then using a single screw extruder at 10 - 65 rpm with the temperature of 240 - 385 °F for 15 - 40 min to formulate the shielding sheets in thickness of 25-27 mm. All fillers were controlled the particle sizes lower than that of 44 μm .

Table 2.4 The composition example of the mixtures for preparing the sample sheets.

Composition	Ex1 (%w/w)	Ex2 (%w/w)	Ex3 (%w/w)
ENGAGE 8150	10.8	6.6	5.9
INFUSE 9000		6.6	5.9
Lead	28.7	-	-
Barium sulphate	4.3	71.2	43.9
Tungsten	1.3	-	-
Bismuth	-	10.8	13.2
Antimony	47.1	-	25.8
SUNPAR 2280 oil	7.4	4.6	5
BNX 1225	0.2	-	-
KEMAMIDE U	0.2	0.2	0.3

where;

ENGAGE 8150 = Polyolefin elastomer

INFUSE 9000 = Olefin block copolymer of ethylene and octene

SUNPAR 2280 oil = Paraffinic oil

BNX 1225 = Antioxidant and thermal stabilizer blend

KEMAMIDE U = Processing aid or slip agent comprising oleamide

จุฬาลงกรณ์มหาวิทยาลัย
CHULALONGKORN UNIVERSITY

Apell et al. [50] studied the X-ray shielding filaments that contained non-lead radiation absorbers (Sb, Ba, Sn, Ti, Bi, W) for medical purposes such as a drape, gonad, breast, face, and thyroid shield. Because lead is toxic, heavy, and impermeable, causing uncomfortable for the wearer. Therefore, the relationship between X-ray shielding efficiency and air-permeable were investigated using the commercial filaments were 1030-785/2 (Roney Industri AB, Vellinge, Sweden) contained with 61% BaSO₄ in polyvinyl chloride, and Barilen 60 (Saxa Syntape GmbH, Luebnitz, Germany) has 61% BaSO₄ in polypropylene. The radiation attenuation ratio was examined for interpreting the shielding performance, including the high value of air-permeable was selected for the practical filament's utilization.

Table 2.5 The radiation attenuation ratio and air permeability of the commercial filaments.

Number of layers	Penetrated dose (kGy)		% RAR		Air permeability (mm/s)	
	RONH	Barilen 60	RONH	Barilen 60	RONH	Barilen 60
	1030-785/2		1030-785/2		1030-785/2	
0	976	976	0	0	-	-
1	591	756	39	22	1528	454
2	379	594	61	39	1000	-
3	262	477	73	51	750	-
4	170	386	82	60	-	-
5	119	312	88	68	-	-
6	86	258	91	74	-	-

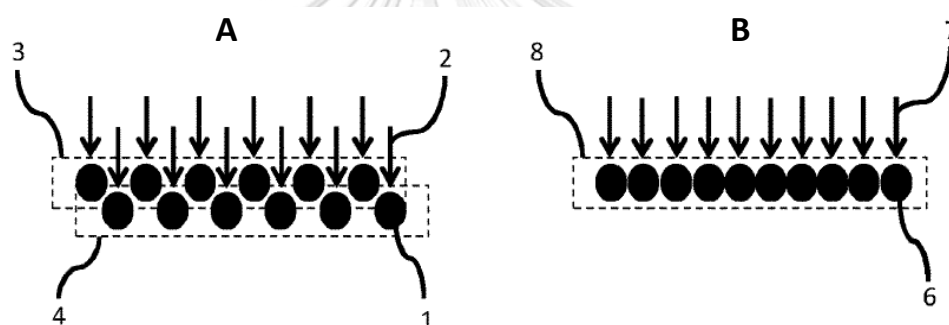


Figure 2.10 Cross-section views of filaments structural; (A) Two layers array, and (B) One layer array.

Aral et al. [47] developed a non-lead coating for applying to the textile surface. The metals to be used for non-lead materials are BaSO_4 , W, and Bi. The composites of silicone rubber (40 %w/w) were combined with fillers (60 %w/w) and then coated on the cotton fabrics. The radiation attenuation ratio (%RAR) studied the X-ray shielding performance, and the results demonstrated that the greater attenuation efficiency was $\text{Bi} > \text{W} > \text{BaSO}_4$. The experiments of BaSO_4 composites, when exposing at 80, 100, and 150 kV, illustrated %RAR was 21%, 19%, and 10%, respectively.



Figure 2.11 The BaSO_4 mixed with silicone rubber and coated on the cotton fabric to use as X-ray shielding aspects.

Kusuktham et al. [51] studied the X-ray shielding efficiency using BaSO_4 mixed with the thickener and coated on cotton from one to ten layers. The radiation attenuation was exposed at the energy of 50-100 kV, indicating the results of shielding performance at the range of 1.48-77 % with increased by enhancing the BaSO_4 ratio. The great shielding value was demonstrated of 77 % when incorporated 50 % BaSO_4 and coated on the fabrics into ten layers, as shown in Figure 2.12.

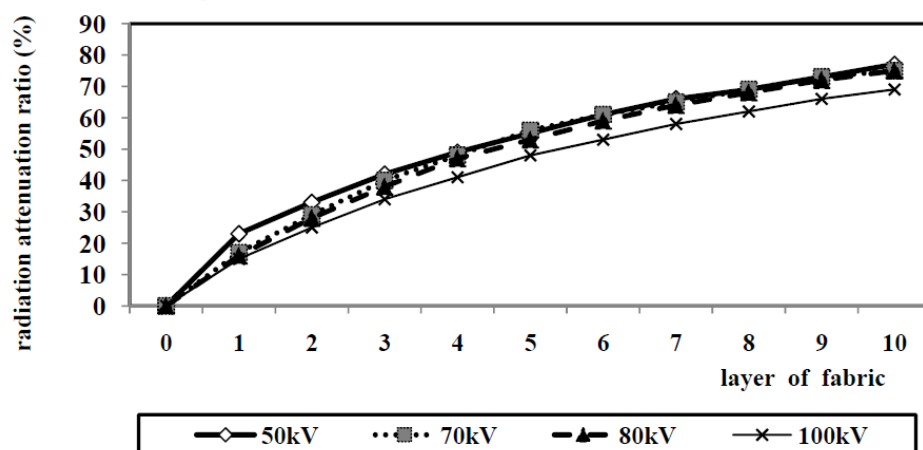


Figure 2.12 The radiation attenuation ratio of BaSO_4 coated on cotton and exposed at 50-100 kV.

Maghrabi et al. [52] studied the X-ray shielding performance using BaSO_4 coated on textiles, including compared it to Bi_2O_3 and $\text{BaSO}_4/\text{Bi}_2\text{O}_3$ composite at 80 kV. The results demonstrated that the attenuation efficiency increased when enhancing the BaSO_4 and Bi_2O_3 . The combination between BaSO_4 (20 %w/w) and Bi_2O_3 (13.3%) represented the highest absorbance of radiation (44.4%). While the BaSO_4 was coated on the fabrics at the ratios of 16.7 %w/w and 33.3 %w/w provided the results of 15.5% and 29.1%, respectively.

Kim et al. [53] developed a lightweight apron used for shielding the X-ray scatter in the medical room. Three kinds of textiles were produced by combining BaSO_4 and liquid silicone. The thickness of textile samples was 0.15 mm, 0.21 mm, and 0.29 mm conforming to lead equivalents of 0.039 mm Pb, 0.095 mm Pb, and 0.22 mm Pb, respectively. The shielding efficiency when exposed to radiation at 1.5 m was 97%. Consequently, the textiles were suitable for preventing the X-rays in low intensity, and also possible to reduce the weight of the apron to 1/5 compared to that of a commercial lead apron, which normally provides the weight of 3.25 kg for 0.25 mm Pb and 4.95 kg, for 0.50 mm Pb.



Figure 2.13 The manufactured fiber for radiation dose reduction.

Pulford et al. [54] produced the alternative X-ray shielding textile instead of lead by fabrication of three different samples; Sample A coated with BaSO_4 , Sample B with Bi_2O_3 , and Sample C with Na_2WO_4 . These samples have sandwiched a layer of chemically impregnated film between the textile substrate and an outer protective layer, demonstrated in Table 2.6.

Table 2.6 The composite of sample for coating on the textiles.

Layers	Sample A	Sample B	Sample C
1	Protective textile	Protective textile	Protective textile
2	BaSO ₄ film (70 %w/w)	Bi ₂ O ₃ film (70 %w/w)	Na ₂ WO ₄ film (70 %w/w)
3	85% polyolefin + 15 % viscose	85% polyolefin + 15 % viscose	85% polyolefin + 15 % viscose
Thickness (mm)	1.9	1.8	1.8

The results indicated that Sample A contains the BaSO₄ provided the radiation highest attenuation efficiency of 52.54 % when exposed at an X-ray tube voltage of 60–100 kVp as shown in Table 2.7.

Table 2.7 The radiation attenuation ratio of Sample A when exposed with 60-100 kVp.

X-ray tube voltage (kVp)	60	70	80	90	100
% RAR	52.54	49.41	42.57	21.44	4.75

Jiang et al. [55] produced a novel BaSO₄/cellulose nanocomposite membrane (BSCM) by incorporating the nano BaSO₄ (5-20%) and prepared in 0.3 mm thickness for X-ray shielding purposes. At the X-ray tube voltage of 50kV, the results demonstrated highest radiation attenuation ratio is 81.70 % when mixed with 20% BaSO₄. The nanocomposite membrane could be used as X-ray radiation shielding materials or filler membranes, providing the benefits of low toxicity and less expensive.

**Figure 2.14** The X-ray images of specimens under 50 kV when combining BaSO₄ at concentration of 0% (CM), 5% (BSCM05), 10% (BSCM10), 15% (BSCM15), and 20% (BSCM20).

Table 2.8 The radiation attenuation ratio of BaSO₄/cellulose nanocomposite membrane varying with BaSO₄ concentration.

Sample	BSCM05	BSCM10	BSCM15	BSCM20
% RAR	3.51	44.79	67.62	81.70

Kalkornsurapranee et al. [56] prepared and developed the natural rubber composite with BaCO₃, Bi₂O₃, and BaSO₄ to be used as X-ray shielding material. For the BaSO₄ composite, the natural rubber was vulcanized with sulfur to increase the mechanical properties and then combined with 57.80 %w/w BaSO₄ at the thickness of 13 mm. The composites were irradiated with X-ray at 120 kV to study the radiation attenuation. The X-ray shielding performance of the material is equivalent to 0.5 mm Pb, which represented the advantages of being flexible, light, safe, and eco-friendly.



Figure 2.15 The natural rubber combined with metal oxide for radiation shielding.

Kim et al. [57] developed the clothing for shielding aviation crew members from natural radiation of air travel. A tungsten double-layered composite yarn and a polyethylene terephthalate (PET) fiber fabric containing BaSO₄ was selected in this study. Then, the prototypes of a protective scarf (thyroid gland shielding) and apron (torso shielding) for flight attendants were invented. The shielding performances of the tungsten composite and PET fiber fabrics containing BaSO₄ were 0.018 Pb and 0.03 mm Pb, respectively. The results were illustrated the low-dose reduction that may be useful in preventing the aviation crew members from scattered rays. The radiation

shielding clothing tends to be used in aviation, medical, and other industries, especially in low-dose intervention.

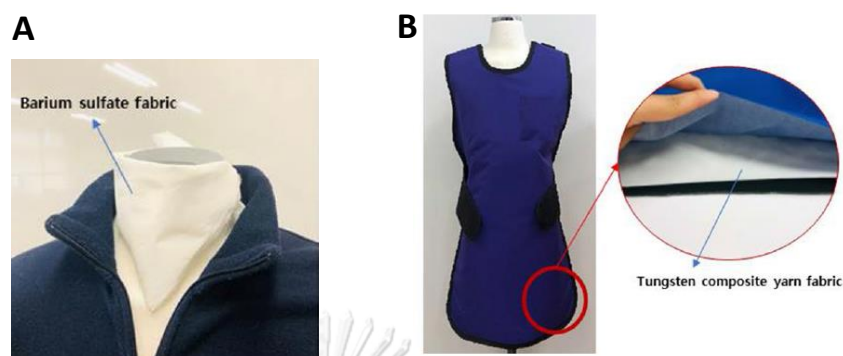


Figure 2.16 Prototype of radiation shield clothing: (A) scarf made from PET containing BaSO_4 and (B) inset produced from PET incorporation with BaSO_4 .

From the above applications, even though the BaSO_4 can be used for X-ray shielding purposes, it still provides a high particle aggregation because of low miscibility causing worst-distribute in the material. This problem affects the reproducibility for mass production when producing the shielding material in large amounts of shielding material with pure BaSO_4 . Moreover, the BaSO_4 packing in bulk particles tends to increase the space in the material that is inclined to reduce shielding performance because the radiation can penetrate to the holes compared to the well disperse material. [18], [19]

2.12 Cellulose

Cellulose is a biopolymer with high mechanical properties. Cellulose has the benefit of environment-friendly, biodegradable polymer, and renewable sources. Cellulose molecule composes of β -1, 4-D-linked glucose chains. The intra-chain and inter-molecule linked with hydrogen bonds play a significant role in enhancing conformation and mechanical properties. [21], [22], [23] The cellulose chains are grouped into fibrils by hydrogen bonds, packed into larger microfibrils, and aligned in different directions. [24] Generally, the microfibrils consist of two main parts; the

crystalline cellulose is in respect to the high ordered region, and the amorphous cellulose has a mainly disordered position. The crystalline chain has a hydroxy group orderly on the region showing the chemical resistance, while the amorphous cellulose has a hydroxy group aligned disordered in the domain chain. Most of the reactants are highly reactive with the amorphous domain, compared to the crystalline domain. This benefit leads the amorphous cellulose to employ for many purposes. [25], [26]

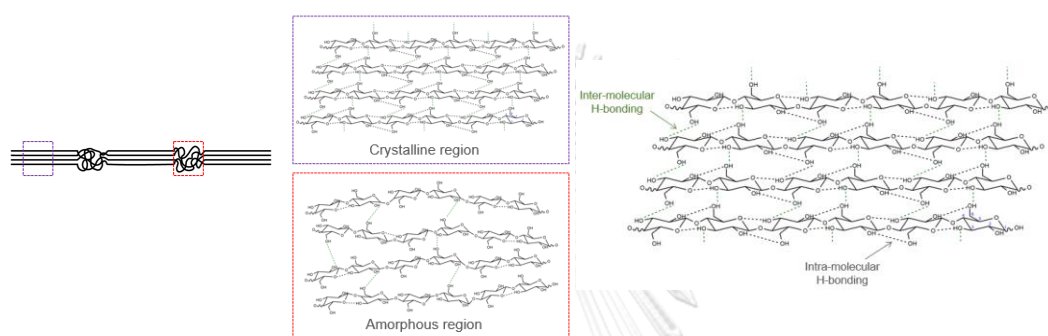


Figure 2.17 The fibril of cellulose chain grouped by hydrogen bond.

2.12.1 Amorphous cellulose

The amorphous cellulose has been applied in various applications. For example, the study of behavior in nanocrystalline domains [25], protein purification [27], and enzyme screening incorporated displaying materials. [28], [29], [30] The amorphous cellulose can prepare in many methods, for example, cellulose ball-milling, deacetylation of cellulose acetate under nonaqueous alkaline conditions, dissolving natural cellulose in an amine/inorganic salt solvent, associated with regenerate using organic solvents, such as methanol, ethanol, and acetone. [31], [32] However, these methods are complicated and require several chemical substances and solvents to achieve amorphous products.

2.12.2 Cellulose from waste paper

Cellulose from recycled material is an interesting approach to reduce detrimental the ecology system. It is usually underutilized and finally achieves burning

or slow biodegradation. [33] The recycling of waste paper in one ton can preserve approximately 17 trees and 7000 gallons of water, providing the advantage of environmental and economic. [34] The cellulose nanocrystal (CNC) is also isolated from waste paper using an alkali solution and following with acid hydrolysis. [58] The CNC was separated from residues of waste paper by employing sulfuric acid hydrolysis and assisted with the sonication process of the raw materials to achieve a fine powder with high properties for applying in other processes and techniques. This process can remove lignin and hemicellulose. [59] The waste paper was also converted into cellulose films according to rapid dissolution in pre-cooled H_2SO_4 aqueous solution by studying two types of waste paper; office paper and cardboard. The dissolution of waste cardboard was relatively slower than that of office waste paper and observed the several tiny undissolved pieces of cardboard due to the high lignin content. The CNC tends to prepare on a large scale by using sulfuric acid. [60] Besides, the office waste paper was utilized for CNC production by acid hydrolysis, providing the greatest crystallinity when using 59% sulfuric acid. Then, the CNC film was fabricated by convolution nanofibers to the transparent specimen with orientated nanofibers. After that, the CNC prepared from 65 % sulfuric acid was coated on PET sheets, which present the advantages of better water vapor barrier property and illustrate the transparency of PET that useful for applying when coating in packaging materials. [61] Some researchers presented that waste paper can produce CNC by extracting from waste paper, and used CNC as the organic filler to reinforce polyurethane elastomer in thermal properties by preparing from the in situ process in solvent N, N-dimethylformamide solution. The polyurethane nanocomposite with CNC of 2 %wt had provided better comprehensive properties with less water absorption, which made it appealing in load-bearing and outdoor applications. [62]

Thailand employed office waste paper approximately 2 million tons and increasing by 15% per year. [35] In terms of environmental aspects, office waste paper

is wealth for recycling to reduce polluted the earth ecology. However, the maximum ratio for recycling paper is approximately 65 %, causing produced disposal in large quantities when manufacturing in high production.

Besides, the higher cost of produced paper from recycled pulp and disposal of waste fibers is inappropriate for use. Therefore, it is necessary to find alternative options to recycle waste paper. Several attempts have been considered in a new approach to utilizing waste paper in terms of eco-friendly. The office waste paper provided a source of cellulose that can be applied in many applications. [36], [37]

2.13 Natural rubber

Natural rubber (NR) is normally utilized for many purposes due to its being eco-friendly, cost-effective, and plenty in Thailand. Generally, natural rubber is necessary to improve the mechanical properties before use. The vulcanization is employed to increase their quality, consisting of sulfur vulcanization and radiation vulcanization. The radiation vulcanization is free from undesired side reaction effects from high-temperature preparation compared to sulfur vulcanization. Besides, the radiation vulcanization is safe from chemical residue that is proper to use for direct skin application. [38]

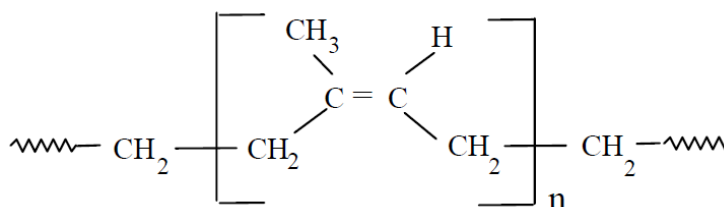
2.13.1 Property of natural rubber

The NR is a biopolymer extracted from a tropical plant in which cis-1,4-polyisoprene molecule. The natural rubber presents an amorphous composing solid contained shown in Table 2.9. The NR has a pH of 6.5-7.0 and a density of 0.98 g/cm³. The rubber particle sizes varied from 0.15 to 0.3 mm and molecular weight distribution 10⁵-10⁷ g/mol, depending on clone, weather, tapping frequency, and other factors.

Table 2.9 Compositions of the total solids content in natural rubber.

Composition	Percent by weight
cis-1,4-polyisoprene	>90
Acetone soluble	2.5-4.5
Nitrogen	0.3-0.5
Ash	0.2-0.4

The average rubber content of fresh NR is in the range of 30 to 45%. In general, the fresh NR can not be utilized directly due to it contains high water and susceptibility to bacterial attack. Therefore, it is necessary to concentrate the NR up to 60% and add the preservative to increase the stability before using it. The most common for increasing NR concentration is achieved by centrifugation, creaming, or by evaporation. In addition, ammonia is normally applied to preserve latex from bacterial attack, which generally used the High ammonia (HA) latex containing 0.7% ammonia in the latex. [63]

**Figure 2.18** Chemical structure of natural rubber (cis-1,4 polyisoprene).

The NR is renewable and does not contribute to global warming due to it initiating from carbon. If the end of its life, it decomposes to carbon dioxide, which no increase in gas. Moreover, NR is elasticity, which becomes an essential material for many applications. [64]

2.13.2 Vulcanization of natural rubber

Vulcanization is the process of converting natural rubber to crosslink polymer into more durable by curing process. The crosslinked rubber has improved mechanical

properties compared to unvulcanized rubber. In general, the process of rubber vulcanization is sulfur vulcanization natural (SVNR) and radiation vulcanization natural rubber (RVNR).

1) Sulfur vulcanization natural rubber (SVNR)

The SVNR is a process in which rubber is heated to induce a chemical reaction to form a three-dimensional network that imparts resilience and strength properties. The most common vulcanization agent is sulfur. It forms bridges between individual polymer molecules when heated with rubber. Ordinarily, a catalyst and initiator are added to accelerate the vulcanization process. Sulfur is generally used to crosslink NR because it consists of polyisoprene, which has many double bonds in its molecular chains and will be reacted with sulfur to form a network. [65]

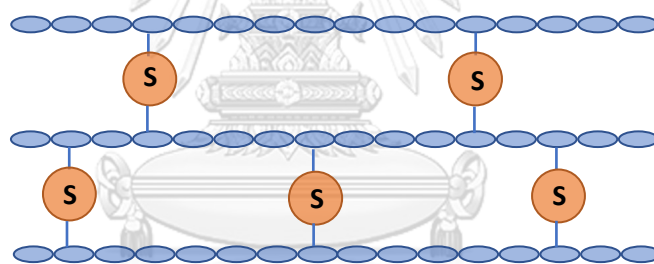


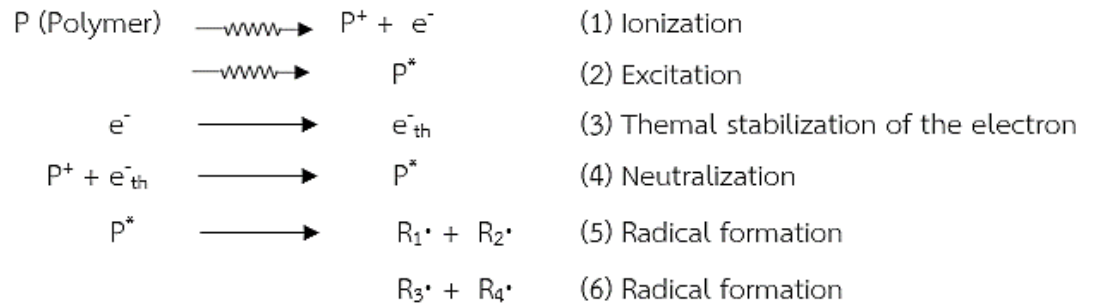
Figure 2.19 The sulfur vulcanization natural rubber (SVNR).

2) Radiation vulcanization natural rubber (RVNR) [38], [39]

In general, vulcanization to improve mechanical properties is utilizing sulfur or peroxide. However, these methods are necessary for the high temperature (150-180 °C), which cannot control the side effect of the reaction and provided the residue chemical. The RVNR advantages are presented in nitrosamines-free, SO₂ low emission, and degradable environment. The RVNR does not contain dithiocarbamates, sulfur, or zinc oxide. Therefore, the RVNR can overcome the drawbacks of chemical

vulcanization, for example, pollution, energy consumption, and time consuming. The mechanism of RVNR is demonstrated in Figure 2.20. [66]

Primary Process



Secondary Process

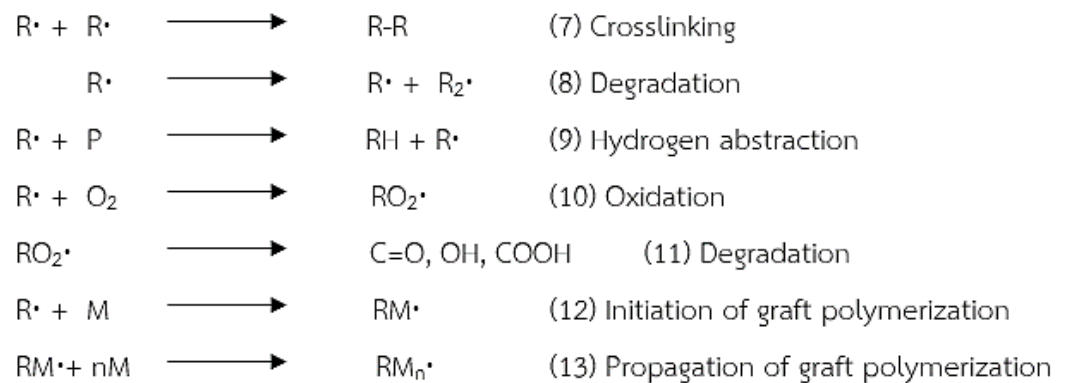


Figure 2.20 The mechanism of radiation vulcanization of natural rubber.

The RVNR can prepare in two types; mixing NR with sensitizer and then irradiating with gamma rays. The RVNR can be used for the manufacture of NR products by the conventional coagulant dipping process. The first progress was achieved by using the non-toxic sensitizer is n-butyl acrylate (n-BA) which plays a role in decrease the irradiation dose for vulcanization up to 15 kGy using 5 phr of n-BA. The properties of obtained RVNR can describe as follow.

1) Mechanical property

The mechanical property of RVNR depends on the origin of the latex. The processing factors such as leaching and drying also affect the qualities of the products. Tensile strength increased when drying in heat and leaching of the latex film because of better fusion of the rubber particles.

2) Nitrosamine free

Dithiocarbamates are used as accelerators for sulfur vulcanization, which may react with airborne nitrogen oxides to become nitrosamines. Nitrosamine is a carcinogen substance that not detect or found in low levels in the RVNR, which was notably below the allowable levels. The absence of dithiocarbamates in RVNR provided an advantage compared to SVNR due to the zinc dithiocarbamate residues can cause cell damage. Besides, commercial catheters, gloves, and RVNR latex films were tested for cell toxicity because the cytotoxicity related mainly to the content of dialkyl dithiocarbamate in the SVNR. The cytotoxicities of RVNR latex films were very low and decreased with increasing leaching time with an aqueous KOH solution at room temperature. It means that substances of low toxicity exist in RVNR latex films but can be removed by leaching. The very low cytotoxicity will be favorable for the biodegradation of RVNR products.

3) Low emission of SO₂

The results of the combustion test on RVNR and conventional sulfur vulcanized latex gloves are shown in Table 2.10. There was no detectable SO₂ from the RVNR while observing 19 mg/g of SO₂ in the conventional SVNR.

Table 2.10 The combustion analysis of gases composition.

Gases composition (mg/g)	RVNR	SVNR
SO _x	>1.0	19.0
HCl	>0.05	0.27
HCN	0.014	0.015
CO	>0.5	330
Ashes (%wt)	0.5	2.2

3) Degradability

According to the fabrication of RVNR, C-C bond crosslink structures are formed. While the SVNR, C-S-C, C-S-S-C, and C-S_n-C bonds are formed, depending on the utilization of the accelerator system. In addition, the C-C bonds have more powerful bond energies than C-S bonds, resulting in the temperature stability of an RVNR latex film is superior to that of sulfur vulcanization. However, under an oxidative atmosphere, the aging properties of the RVNR became very poor after leaching with ammonia solution compared to the SVNR as shown in Figure 2.21. The absence of dithiocarbamates plays a role in strong antioxidants in RVNR to affect improving the aging properties, for example, tris(nomiated phenyl) phosphite (TNPP) and 2,5- dessert amyhydroquinone (DAHQ).

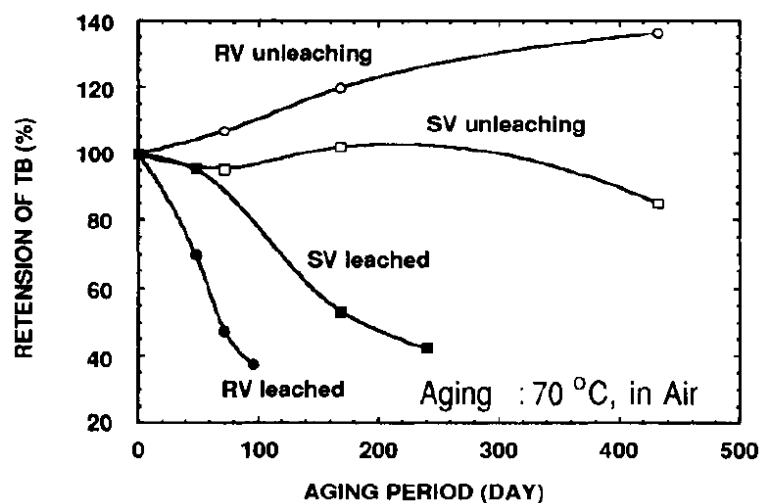


Figure 2.21 Effect of leaching on aging properties of radiation vulcanization (RV) and sulfur vulcanization (SV).

4) Application of RVNR

From all the above advantages of RVNR, it could be concluded that the RVNR is non-toxic and eco-friendly compared to SVNR. Besides, the RVNR would be economically acceptable to the latex industry when supplied on a large scale. The potential application for RVNR is demonstrated in Table 2.11.

Table 2.11 The potential application field of RVNR.

Advantages	Applications
Absence of nitrosamine	Teats, Balloons, Gloves
Very low cytotoxicity	Catheters, Medical tubing, Household gloves
Low emission of SO ₂	All medical/surgical products
Degradability	Toy balloons, Advertising balloons

CHAPTER 3

EXPERIMENTAL SECTION

3.1 Chemicals and materials

1. Office waste paper
2. Eucalyptus pulp, Siam Cement Group Public Co., Ltd.
3. Sulfuric acid (H_2SO_4 , 98% w/w), Merck, Ltd.
4. High-ammonia natural rubber latex (60% dry rubber contents), Chemical and Materials Co., Ltd.
5. Barium chloride (BaCl_2 , 99%), Gammaco Co., Ltd.
6. Barium sulphate (BaSO_4 , 99%), Gammaco Co., Ltd.
7. Potassium hydroxide (KOH, 99%), Gammaco Co., Ltd.
8. Ammonium solution (NH_3 , 27%), Gammaco Co., Ltd.
9. Normal butyl acrylate (n-BA), Miracle Chemical Industry Co., Ltd.
10. Sodium hydroxide (NaOH), Krungthepchemi Co., Ltd.
11. Hydrogen peroxide (H_2O_2 , 30%), Krungthepchemi Co., Ltd.
12. Sodium metasilicate (Na_2SiO_3), Krungthepchemi Co., Ltd.
13. Nonylphenol ethoxylate (NP-9) Krungthepchemi Co., Ltd.
14. Linear alkylbenzene sulfonate (LAS 24), Krungthepchemi Co., Ltd.

3.2 Instruments

1. Scanning Electron Microscope with Energy Dispersive X-ray Fluorescence (SEM/EDX) , TESCAN VEGA 3
2. X-Ray Diffractometer (XRD), Bruker D2 PHASER
3. Fourier transform infrared spectroscopy (FT-IR), Thermo Scientific Nicolet iS5
4. Gammacell 220 excel, Nordion

5. X-ray Generator, YXLON MGC41
6. Sputter coater, Ouorum Q150R ES
7. Homogenizer, IKA T25
8. Oven, BINDER FP 115
9. Electronic balance, METTLER TOLEDO MS204TS
10. Ultrasonic cleaner, CREST CP1000D
11. Centrifugal, OHAU FRONTIER 5706
12. Thickness gauge, Mitutoyo ID-C112EBS

3.3 Regeneration of cellulose pulp from office waste papers

Office waste paper (100 g) was cut into small pieces and soaked for 3 h with 1000 ml deink agents: NaOH (99 %, 450 g), H₂O₂ (30 %v/v, 300 ml), NaSiO₃ (99 %, 150 g), LAS (24%, 188.5 ml), and NP-9 (45 ml). Then, the mixer was agitated at 1,000 rpm for 2 h to defibrate, including deink the pulp from the waste paper. The defibrated waste paper was washed with water several times until the pH of the filtrate was neutral to obtain the cellulose pulp; subsequently, dried in an oven at 100 °C for 3 h. [61]



Figure 3.1 Defiber and deink of cellulose pulp from office waste papers.

3.4 Preparation of amorphous cellulose

The cellulose pulp from office waste paper (10 g) was dissolved in ice-cold H₂SO₄ (60% v/v, 150 ml) by controlling the temperature at 0 °C throughout the process to obtain a high yield of amorphous cellulose. The cellulose fiber was slowly

transformed into the gel of the amorphous region. The final product was illustrated the fibrous residue in the gel and required to remove using centrifugal at 3,000 rpm for 15 min. The clear gel of amorphous cellulose was separated, but it still observed ink residues in the product.

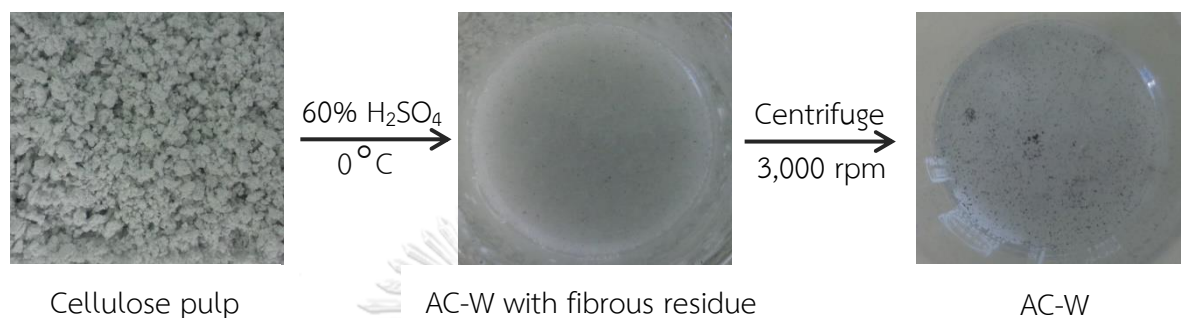


Figure 3.2 Fabrication of amorphous cellulose using iced-cold sulfuric acid.

3.5 Fabrication of BaSO₄/amorphous cellulose

The barium chloride solution (60 g, 800 ml) was vigorously stirred under 20,000 rpm using a homogenizer and slowly injected amorphous into the solution. The BaSO₄/amorphous cellulose (Ba/AC) occurred with a white suspension of Ba/AC particles. The product was washed with water several times until the pH is neutral.

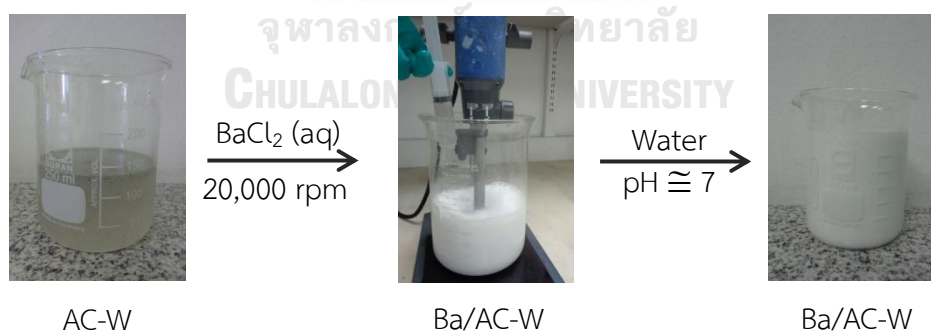


Figure 3.3 Regeneration of amorphous cellulose using barium sulphate chloride solution to produce Ba/AC.

3.6 Preparation of BaSO₄/amorphous cellulose from eucalyptus pulp

The Ba/AC was produced from eucalyptus pulp according to the procedure of office waste paper as described in the preparation of amorphous cellulose, including

Ba/AC. The eucalyptus pulp (10 g) was dissolved using ice-cold H_2SO_4 and maintained the temperature at $0\text{ }^\circ\text{C}$ until acquiring the clear gel solution. The Ba/AC was regenerated using barium chloride solution (60 g, 800 ml) by stirring the solution at 20,000 rpm, and then inject the amorphous gel into the solution during agitation. The Ba/AC occurred in a white suspension product, the process shown in Figure 3.4.



Figure 3.4 Fabrication of Ba/AC from eucalyptus pulp.

The BaSO_4 concentration was determined using the difference of decomposed temperature between cellulose at $400\text{ }^\circ\text{C}$ [67] and barium sulphate at $1580\text{ }^\circ\text{C}$. [68] The Ba/AC was weighed (0.1 g) using four digits electronic balance. The samples were dried using electronic oven ($120\text{ }^\circ\text{C}$, 3 h) and then ignited ($500\text{ }^\circ\text{C}$) using the furnace to decompose the cellulose and then recorded the weight after ignition. The BaSO_4 concentration was calculated using the equation as follows.

$$\% \text{BaSO}_4 = \frac{W_b - W_a}{W_b} \times 100 \quad (3.1)$$

where;

w_a = the weight of Ba/AC before ignition

w_b = the weight of Ba/AC after ignition

3.7 Study of gamma dose for radiation vulcanized natural rubber

NH_3 solution (1% v/v, 20 ml) was added into 100 g of high ammonia natural rubber latex (HA Latex) and stirred using a blender for 15 min. KOH (10%, 0.25 ml) was dropped into the solution, and further agitated for 15 min. Then, mixed with n-BA (5 ml) and stirred for another 1 h. The mixed HA Latex was exposed using ^{60}Co gamma radiation (Nordion Model: Gammacell 220 excel) at the dose 10, 15, 20, 25, and 30 kGy under a dose rate of 0.52 Gy/s. After that, the suitable irradiation dose was estimated from swelling ratio and crosslink density following the ASTM D471-06 testing method. The swelling ratio was tested by cutting in 2x2 cm and weighed for 1 g using four digits electronic balance (three repeats for each sample), including immersed in toluene for 24 h. The soaked specimens were recorded the weighed and calculated according to equation 3.1. [69], [70]

$$\text{Swelling ratio} = \frac{w_2 - w_1}{w_1} \times \frac{\rho_r}{\rho_s} \times 100 \quad (3.2)$$

where;

w_1 = the sample weight before immersion with the toluene

w_2 = the sample weight after immersion with the toluene

ρ_s = the density of RVNR

ρ_r = the density of toluene

The crosslink density was tested by immersion the samples in toluene for 72 h or three days to achieve the equilibrium swelling state. The crosslink density was calculated using the Flory-Rehner equation.

$$n = \frac{1 \ln(1 - V_r) + V_r + \chi V_1^2}{2 V_s (V_r^{\frac{1}{3}} - \frac{V_r}{2})} \quad (3.3)$$

The V_s is the molar volume of toluene (106.1 cm³/mol), χ is the parameter of interaction (0.393 for NR-toluene system), V_r is the volume fraction of RVNR, which was determined using equation 3.3.

$$\frac{1}{V_r} = 1 + \left(\frac{w_2 - w_1}{w_1} \times \frac{\rho_r}{\rho_s} \right) \quad (3.4)$$

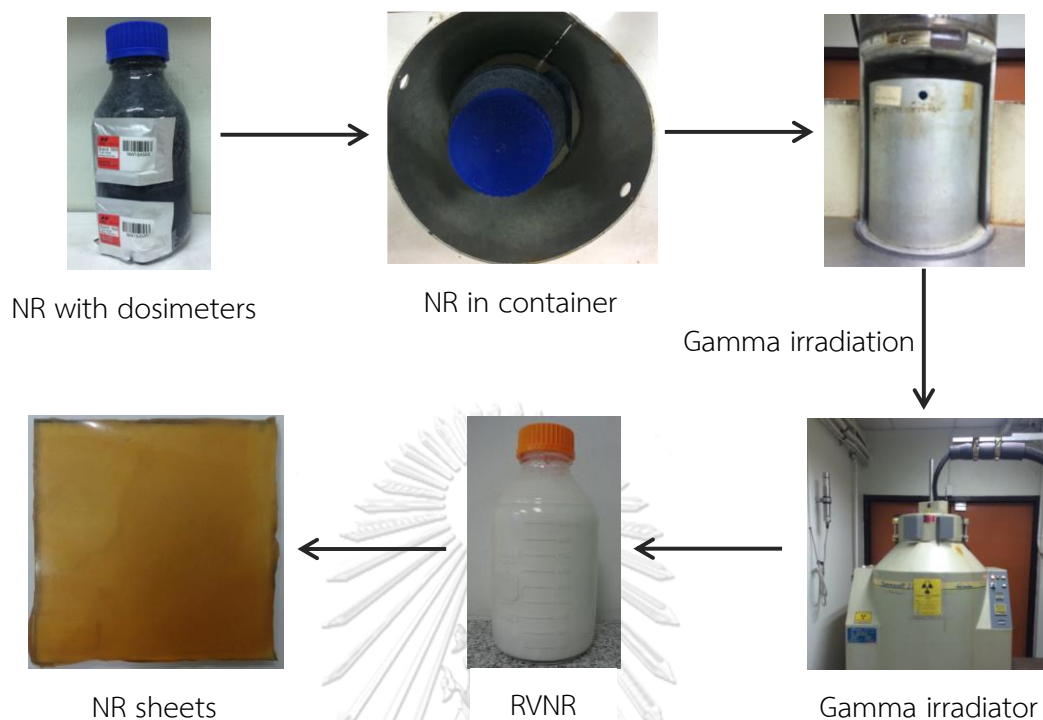


Figure 3.5 Preparing the RVNR using Gamma ^{60}Co Irradiation.

3.8 Formulation of BaSO_4 /amorphous cellulose/natural rubber

The ratio between Ba/AC and RVNR was studied for casting the testing sheet. The Ba/AC was added into RVNR by varying the concentration with 50, 55, 60, 65, and 70 %w/w and formulated by pouring on the glass square mold, including left to dry 2-3 days. The samples were immersed with water for 8 h to remove all remaining chemical agents, then dried with the electronic oven at the temperature of 80 °C for 3 h. The completed BaSO_4 /amorphous cellulose/natural rubber sheet was selected as a suitable ratio for preparing the BaSO_4 /amorphous cellulose/natural rubber for further X-ray shielding study.

The RVNR was combined individually with Ba/AC (NR-W) at the ratio of 40, 50, and 60 %w/w. The Ba/AC produced from the eucalyptus pulp (NR-E), and BaSO_4 powder (NR-P) was fabricated to compare with the conventional method. The NR-E represents the purified Ba/AC material and traditional material of X-ray shielding. The

homogeneity particle distribution can vividly observe by adding 5 %w/w of the pigment, which is green (NR-W), pink (NR-E), and yellow (NR-P). The dyes are specified for the natural rubber and do not affect the shielding sheet's properties. The composites for each sample indicate in Table 3.1.

Table 3.1 The sample code of X-ray shielding filler incorporated with RVNR.

Sample	Concentration of composites incorporated with RVNR
NR-W40	40% w/w Ba/AC (office waste paper)
NR-W50	50% w/w Ba/AC (office waste paper)
NR-W60	60% w/w Ba/AC (office waste paper)
NR-E40	40% w/w Ba/AC (eucalyptus pulp)
NR-E50	50% w/w Ba/AC (eucalyptus pulp)
NR-E60	60% w/w Ba/AC (eucalyptus pulp)
NR-P40	40% w/w BaSO ₄ powder
NR-P50	50% w/w BaSO ₄ powder
NR-P60	60% w/w BaSO ₄ powder

3.9 Characterization techniques

3.9.1 Scanning electron microscope

The morphology of Ba/AC was investigated using a scanning electron microscope. The ultrasonic bath was utilized to disperse the samples, dropped directly onto the aluminum stub, and dried at room temperature. Then, the microparticles of composites were coated with gold to obtain a surface thickness of 10 nm using a sputter coater for 30 s (20 kV of power voltage, 23 mA of current). The images and particle sizes were observed using an accelerating voltage of 10 kV with a secondary electron detector and TESCAN software. The NR specimens were prepared by cut into small pieces, attached to the aluminum stub, and then coated with the gold using sputter coater before study with SEM/EDX.

3.9.2 X-ray diffractometer

The X-ray diffractometer was utilized to collect the XRD spectra of samples. The cellulose pulp from office waste paper, eucalyptus pulp, including amorphous cellulose from the office waste paper (AC-W), and eucalyptus pulp (AC-E) were prepared for investigation. The Ba/AC substrates fabricated from the office waste paper (Ba-W) and eucalyptus pulp (Ba-E) were identified and compared to the BaSO₄ standard for confirming the fingerprint of produced substances. The X-ray diffraction patterns were collected with a scanning rate of 0.06 deg/ min, using Cu Ka irradiation (0.154 nm, 30 kV, 10 mA).

3.9.3 Attenuated total reflectance Fourier transform infrared spectroscopy

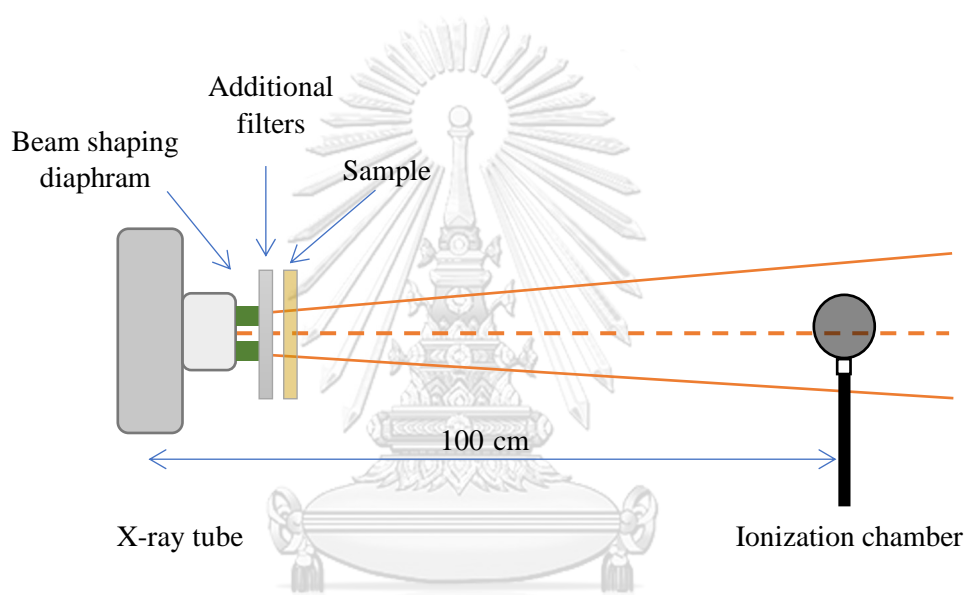
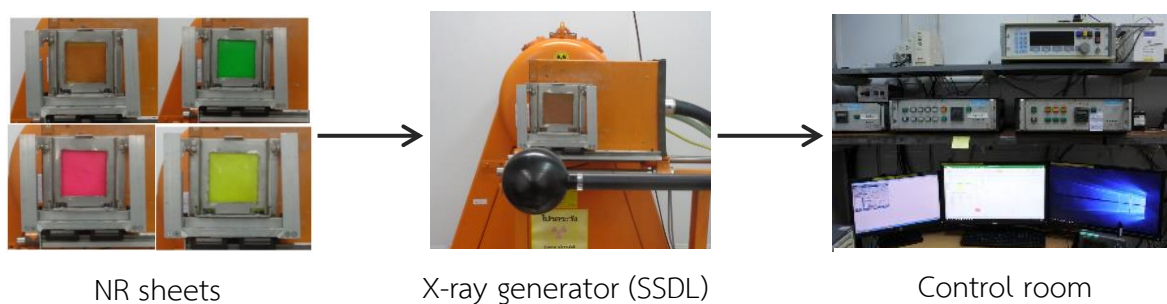
The eucalyptus pulp, office waste papers, and their products were analyzed the functional groups using infrared spectroscopy. The cumulative scans were obtained in the frequency of 4000 cm⁻¹ to 500 cm⁻¹ with a resolution of 4 cm⁻¹.

3.10 Investigation of X-ray attenuation property

The attenuation property was studied at the Secondary Standard Dosimetry Laboratory (SSDL). The NR-W and NR-E were cut into 10 cm x10 cm and placed between the X-ray tube and ionization chamber. The samples were irradiated using the X-ray generators (YXLON Model: MGC41) at the dose of 30, 40, and 60 kV by complying with the N-series of ISO 4037-1 [71], as shown in Table 3.2. The equipment has arranged concerning the settled condition to 2 mA in tube current and 60 sec of shooting time. The X-ray tube has maintained the distance to the ionizing detector is 100 cm, as demonstrated in Figures 3.6 and 3.7.

Table 3.2 The characteristics of narrow-spectrum series (N-series) for X-ray irradiation.

Code	Tube potential (kV)	Mean energy (keV)	Resolution (%)	Recommended inherent filtration	Additional filtration
N-30	30	24.6	32	1 mm Be	4.00 mm Al
N-40	40	33.3	30	4 mm Al	0.21 mm Cu
N-60	60	47.9	36	4 mm Al	0.60 mm Cu

**Figure 3.6** Schematic of X-ray attenuation study.**Figure 3.7** The samples were exposed using the X-ray generator from SSDL.

3.11 Prototype for x-ray protection products

The Ba/AC produced from the eucalyptus pulp and office waste paper were fabricated utilizing the BaCl₂ solution (120 g, 800 ml). The Ba/AC was incorporated with RVNR at the concentration of 40, 50, and 60 %w/w to obtain the sheets of BaSO₄/amorphous cellulose/natural rubber. The shielding samples were exposed with the X-ray generator at the tube voltage of 60, 80, and 100 kV. The comparative of the linear attenuation coefficients between the lead sheet (0.3 mm Pb) and the samples was calculated to achieve the thickness for the shielding prototype with equivalency to 0.25 mm Pb. Subsequently, the X-ray shielding sheets were formulated at the required thickness. The Ba/AC produced from eucalyptus pulp was selected for preparing the X-ray shielding lab coat, while the X-ray protective materials were prepared from the office waste paper. The required thickness for preparing the prototypes could be calculated according to the correlation from equation 2.6, which was expressed as follows;

$$I = I_0 e^{-\mu x}$$

The experiment was utilized the lead sheet at 0.3 mm thick of Pb to expose with 60 kV. Therefore, the linear attenuation coefficient of 0.3 mm Pb (4.034 mm⁻¹) and the desired thickness (0.25 mm) were replaced in the equation to calculate the I/I₀.

$$I/I_0 = e^{-(4.034 \text{ mm}^{-1})(0.25 \text{ mm})}$$

$$I/I_0 = 0.3648$$

Subsequently, the I/I₀ was substituted for equation 2.6, including the added linear attenuation coefficient of the sample that irradiated at 60 kV for calculating the required thickness.

$$0.3648 = e^{-(0.093 \text{ mm}^{-1})(x)}$$

$$x = 6.93 \text{ mm}$$

In summary, to prepare the sample equivalent to 0.25 mm of lead at 60 kV, it was necessary to fabricate the X-ray shielding at the thickness of 6.93 mm.

3.12 Physical property of X-ray protection products

The X-ray shielding sheets were prepared, which were eucalyptus pulp for a lab coat and office waste paper for X-ray protective materials. The physical properties of samples were studied, comprising density, tensile strength, and elongation at break. The density was determined according to the ASTM D792, while the tensile strength and elongation at break were tested following the ISO 37 (Type 1).



CHAPTER 4

RESULTS AND DISCUSSION

4.1 Preparation of amorphous cellulose

The office waste paper was defibered and deinked to obtain the cellulose pulp, which provided a production yield of 54.56 ± 4.07 %w/w. The morphology of recycled pulp was compared with the eucalyptus pulp as a purified substance, as shown in Figure 4.1.

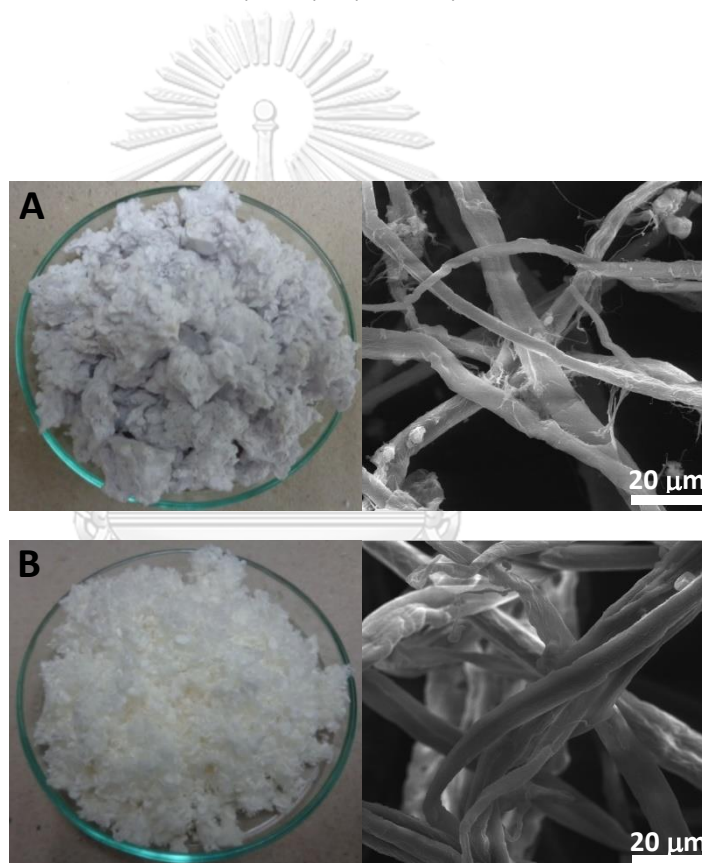


Figure 4.1 The SEM images of (A) cellulose pulp from office waste paper and (B) eucalyptus pulp.

The amorphous cellulose was prepared using ice-cold sulfuric acid to dissolve the fibrils and transform the order structure in the crystalline chain to the disorder arrangement. The transformation of order structure to disorder structure slowly

occurred in mild condition without destroying the crystalline chain, compared to utilize the high temperature. As a result, almost the crystalline part was converted to the amorphous form, as presented in Figure 4.2 and Figure 4.3.

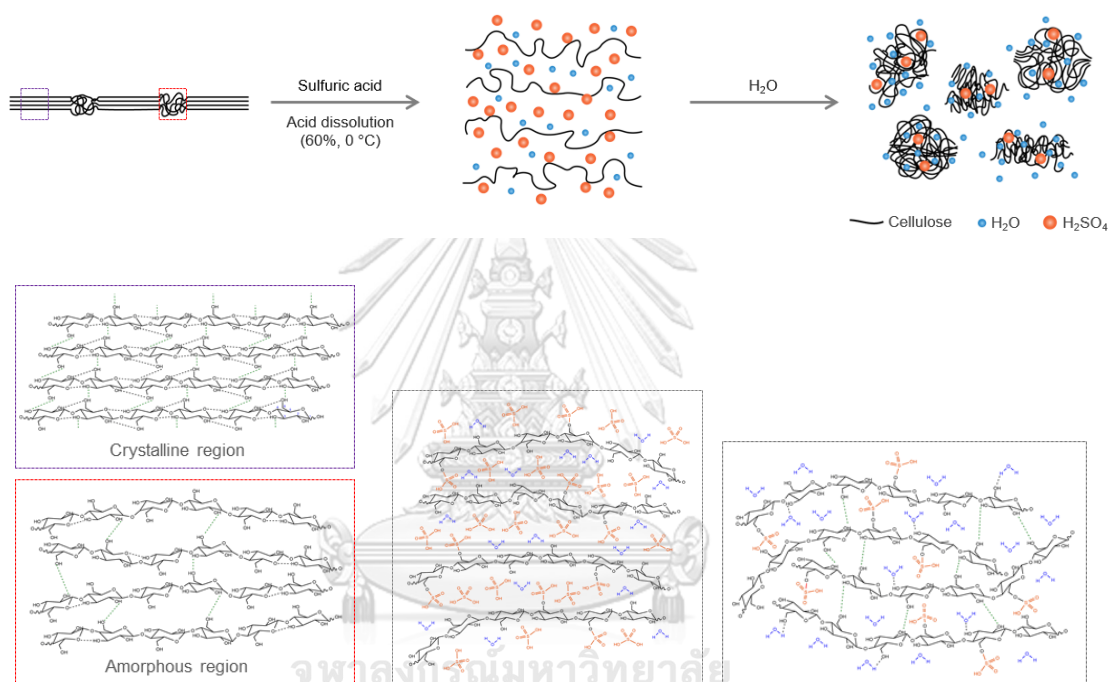
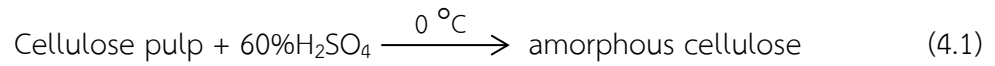


Figure 4.2 Schematic for preparation of amorphous cellulose using ice-cold sulfuric acid.

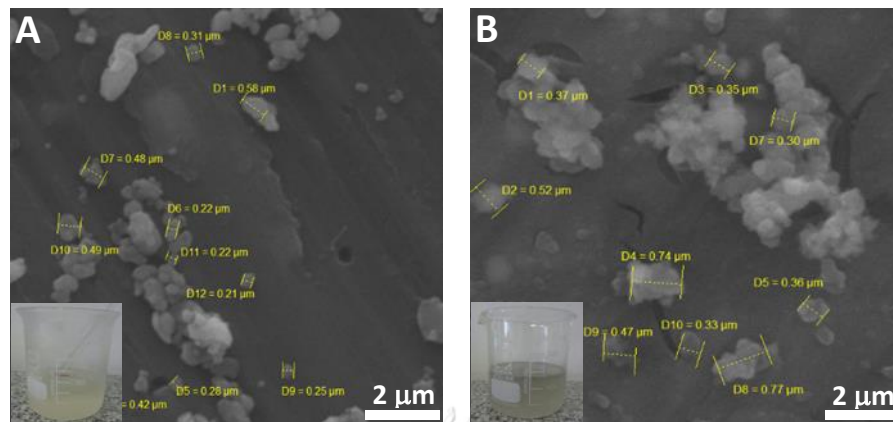


Figure 4.3 The SEM images of amorphous cellulose illustrate the submicron scale of particles; (A) AC-E and (B) AC-W.

The X-ray diffractograms demonstrated cellulose pulps completely converted to amorphous cellulose. The XRD patterns of cellulose pulps were indicated at the peak of 15° and 23° in Figure 4.4 (A). While the broad spectrum of the amorphous form in Figure 4.4 (B) occurred following the Ciolacu et al. studied. [25]

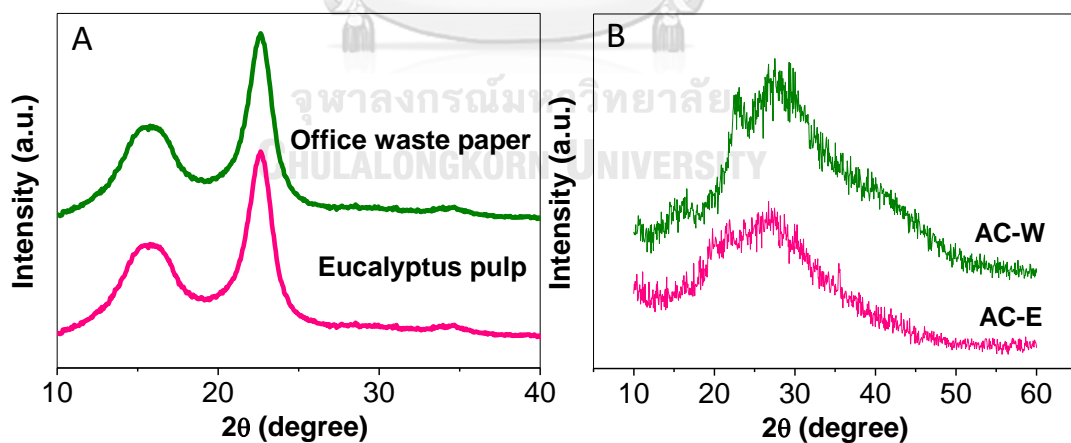


Figure 4.4 The XRD spectra; (A) cellulose pulp, (B) amorphous cellulose.

Figure 4.5 and Figure 4.6 show the ATR-FTIR spectra of the cellulose pulps and amorphous cellulose. The amorphous structure can confirm by the band shift from 2900 cm^{-1} , which represented the C-H stretching vibration at the wavenumber in the high region. The absorption bands on the $1500\text{-}899\text{ cm}^{-1}$ are strongly reduced the C-O-C stretching at β -(1-4) glycosidic linkage and increased in the intensity of the CH_2 absorption band at 898 cm^{-1} which represents the amorphous absorption band.

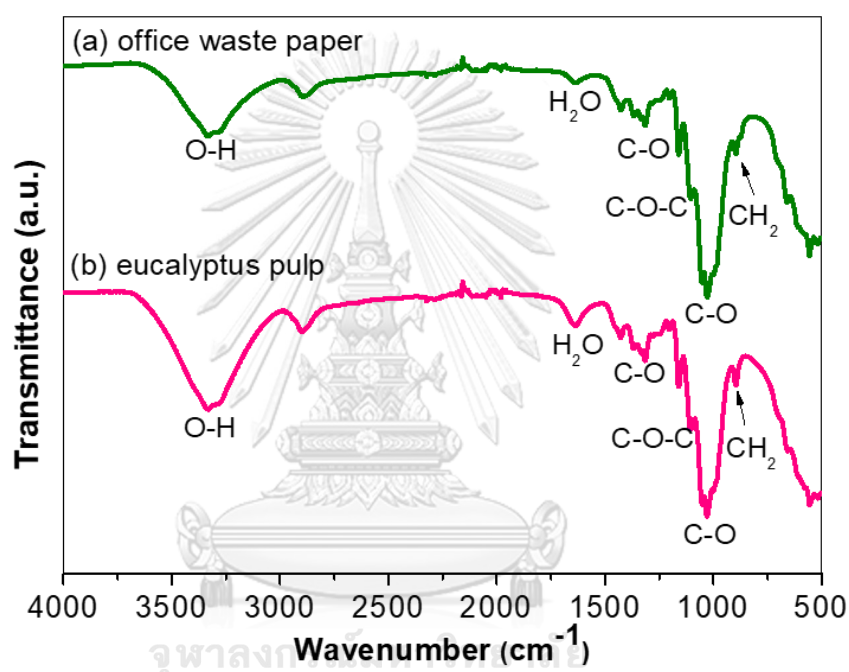


Figure 4.5 The ATR-FTIR spectra of cellulose pulp from: (a) office waste paper, and (b) eucalyptus pulp.

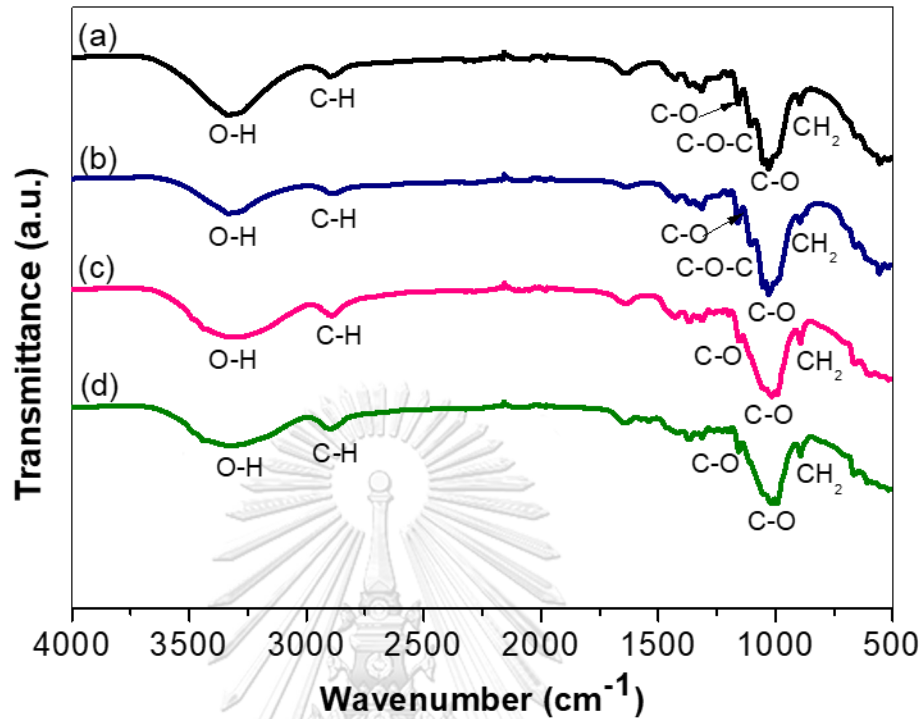


Figure 4.6 The ATR-FTIR spectra; (a) cellulose pulp from office waste paper, (b) eucalyptus pulp, (c) AC-W, and (d) AC-E.

4.2 Fabrication of BaSO₄/amorphous cellulose composite

The Ba/AC composite was produced from the in-situ regeneration by injecting the amorphous cellulose during the vigorous agitation of the BaCl₂ solution, resulting in the SO₄²⁻ in H₂SO₄ will be exchanged the ionic groups between the SO₄²⁻ and Cl₂⁻. Then, the white suspension product was occurred in the sub-micro scale, as shown in Figure 4.7 and Figure 4.8.



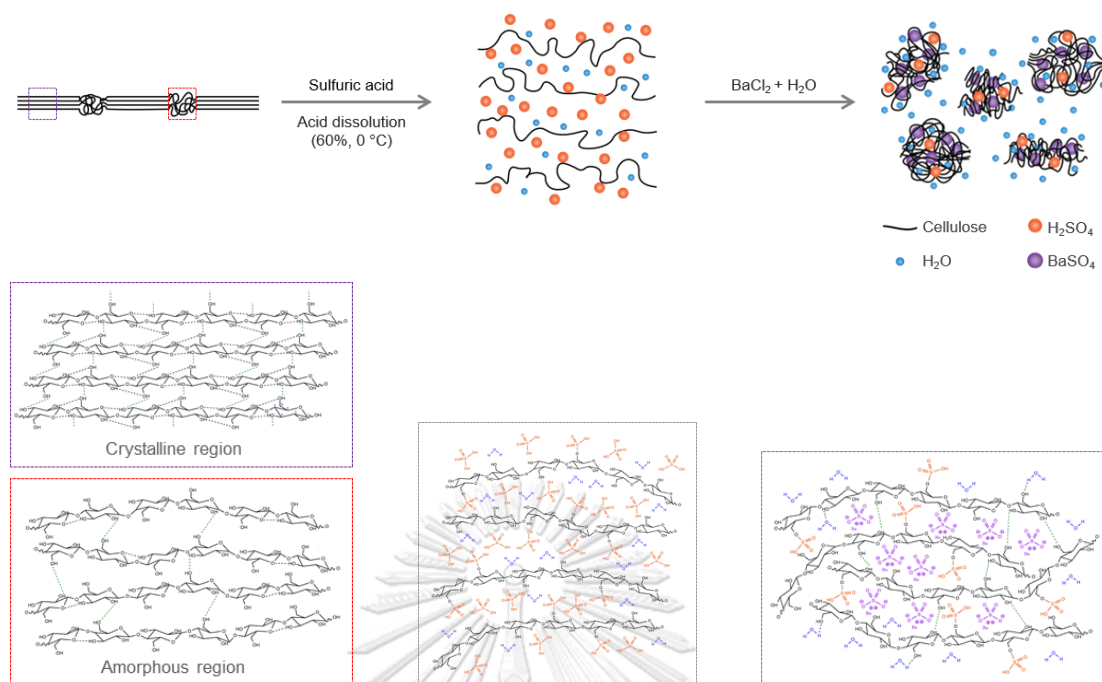


Figure 4.7 Schematic for preparation of Ba/AC by in situ regeneration of amorphous cellulose using BaCl₂ solution.

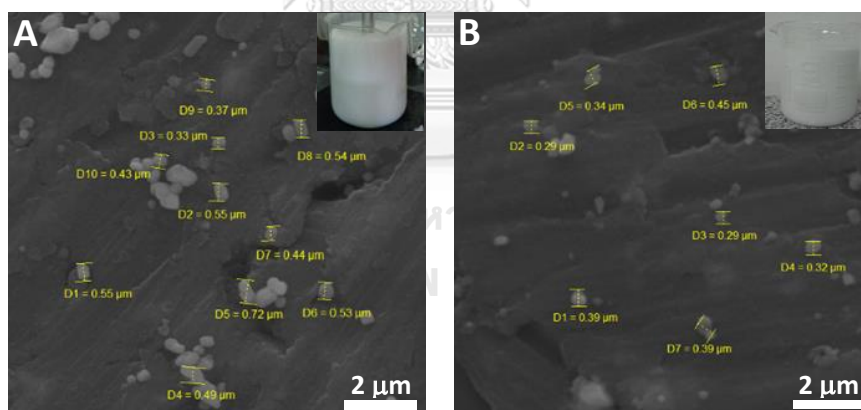


Figure 4.8 The SEM images of Ba/AC demonstrate the submicron scale of particles; (A) Ba-E and (B) Ba-W.

Figure 4.9 shows the XRD data of Ba/AC composite produced from AC-W and AC-E compared to the BaSO₄ standard. The results demonstrated the structure of Ba/AC-W and Ba/AC-E parallel with the BaSO₄ standard.

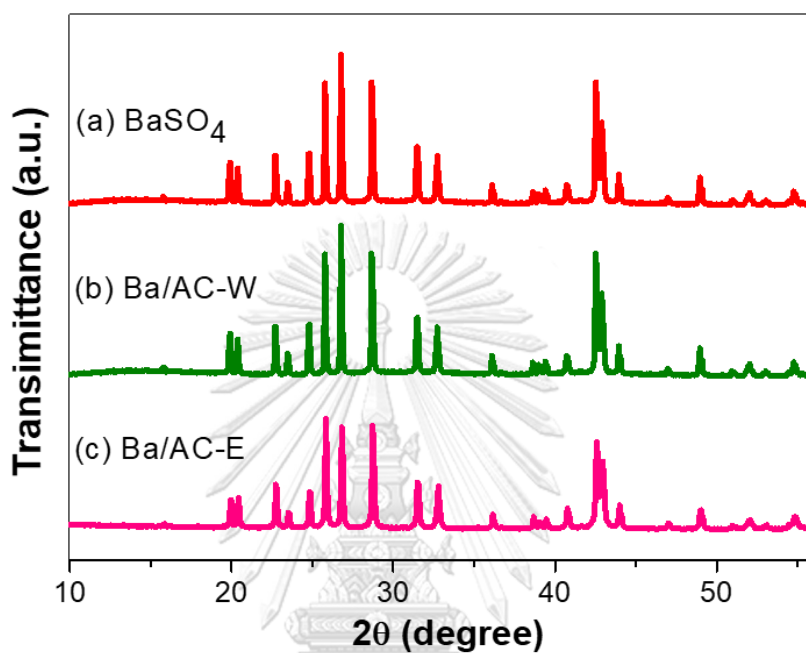


Figure 4.9 The XRD spectra Ba/AC composites compared to the BaSO₄ standard.

The ATR-FTIR spectra were carried out to investigate the functional groups present in samples. The spectra of Ba/AC composites were illustrated the disappear peak of OH stretching (333.6 cm^{-1}) and CH stretching (2897.6 cm^{-1}), while the peaks were shown SO_4^{2-} symmetrical vibration (983.5 cm^{-1}) and SO_4^{2-} out-of-plane bending vibration (638.3 and 605.1 cm^{-1}).

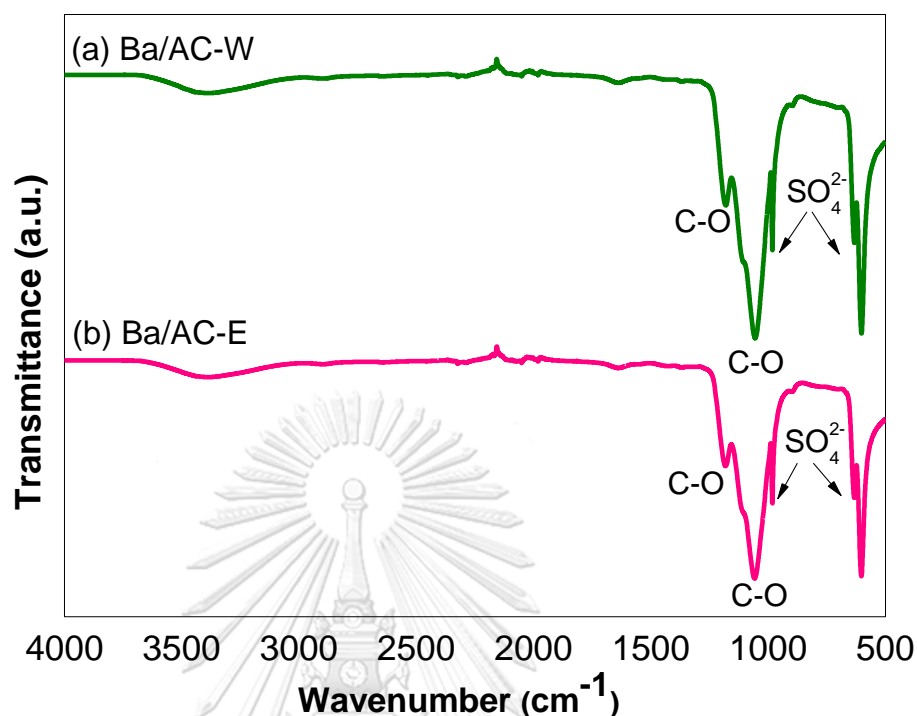


Figure 4.10 The ATR-FTIR of the Ba/AC-W compared with the Ba/AC-E

As observed in the characterization of purified pulp (eucalyptus pulp) and recycled pulp (office waste paper), it should be noted that there are no significant differences in terms of morphology, particle sizes, crystal structure, and functional groups. Besides, the BaSO_4 concentration in Ba/AC showed a similar concentration of 10.98 %w/w (Ba/AC-W) and 9.66 %w/w (Ba/AC-E). Consequently, the Ba/AC-W may be provided equality properties with the Ba/AC-E for utilizing in many applications.

4.3 Preparation of radiation vulcanized natural rubber latex

The swelling ratio and crosslink density were utilized to study the suitable irradiation dose for RVNR preparation. The cured natural rubber was exposed to gamma radiation at the dose of 10, 15, 20, 25, and 30 kGy. The results indicated that the swelling ratio decreased when increasing the irradiation dose, while crosslink density showed the opposite behavior.

The swelling ratio and crosslink density on gamma radiation could be described by the gamma-ray energy transferred to the natural rubber molecules, causing the natural rubber free radicals. Afterward, the free radicals will recombine to form the crosslink networks. [67] The swelling ratio was expressed as the dose level that the natural rubber was expanded until equilibrium, while the crosslink density shown the amounts of the crosslinked network in the natural rubber. It could be indicated that the dose of 20 kGy, which obtained the lowest swelling ratio and high crosslink is proper for preparing the RVNR.

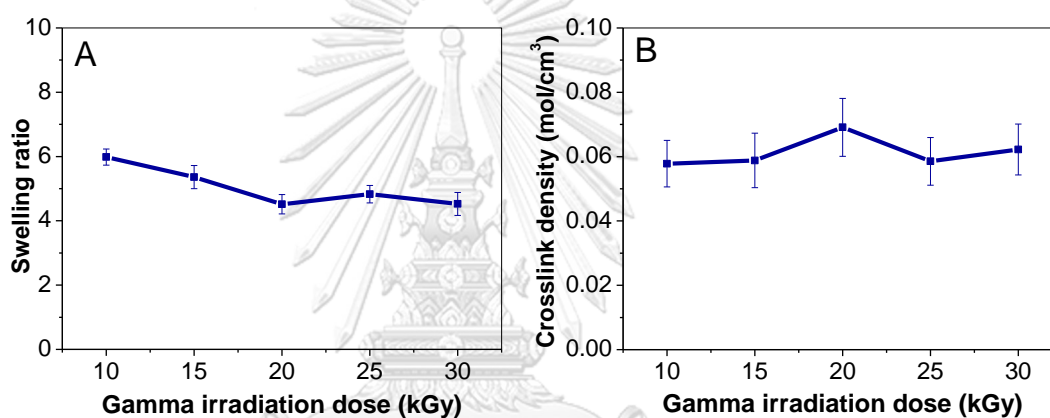


Figure 4.11 The relationship between gamma radiation dose (kGy) and RVNR properties; (A) swelling ratio, (B) crosslink density.

4.4 Fabrication of BaSO₄/amorphous cellulose/natural rubber

The highest filler loading that does not deteriorate the material was studied by incorporated the Ba/AC with concentrations at 50, 55, 60, 65, and 70 %w/w. It could be observed that the samples contained with filler loading of 65 and 70 %w/w provided the

deterioration of the rubber sheet, as shown in Figure 4.12. Consequently, the ratio of filler lower than 65 %w/w was selected for further study.

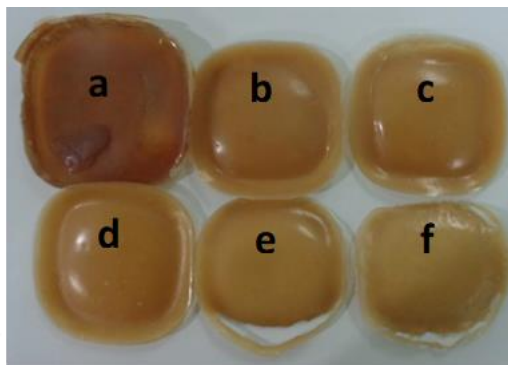


Figure 4.12 The Ba/AC concentration for fabrication of shielding sheet (a) 50 %w/w, (b) 55 %w/w, (c) 60 %w/w, (d) 65 %w/w, and (e) 70 %w/w.

The Ba/AC composites were combined with RVNR at the ratio of 40%, 50%, and 60 %w/w, comparing with BaSO_4 powder as the traditional material. It could be observed that the materials sheets of NR-W, NR-E, and NR-P provided well-distribute of particles without deterioration expressed in the material is shown in Figure 4.13.

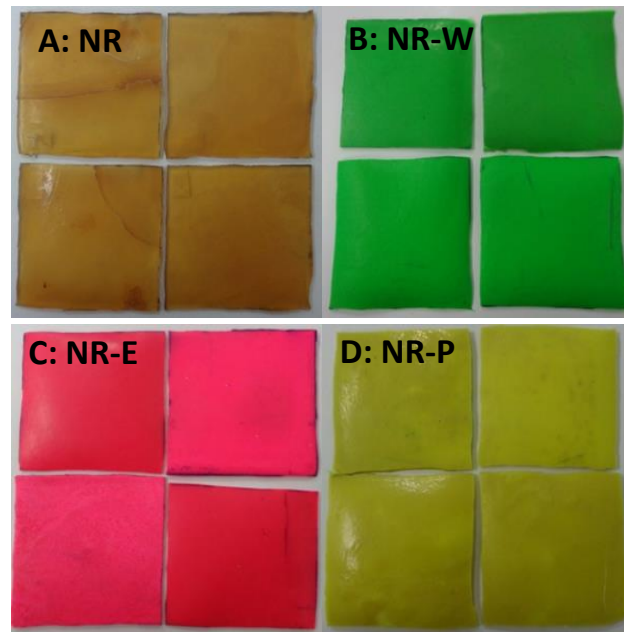


Figure 4.13 The RVNR sheets for shielding test; (A) RVNR without filler, and RVNR incorporated with fillers (B-D).

Figure 4.14 to Figure 4.17 show the BaSO_4 particle distribution of NR-W60, NR-E60, and NR-P60. The SEM images illustrated the white suspended particle of Ba/AC providing thorough distribution into the natural rubber. The Ba/AC plays a role in decreasing the agglomeration in the materials. The BaSO_4 powder demonstrated the aggregation of the particles, leading the several holes inside the natural rubber. Due to the BaSO_4 is low miscibility when combining in high amounts that tend to collect in large molecules, causing dispersion problems. [18], [71], [19] The amorphous cellulose surrounded with the BaSO_4 plays a significant role in dispersing the particle, including prevented the BaSO_4 gather in a large molecule.

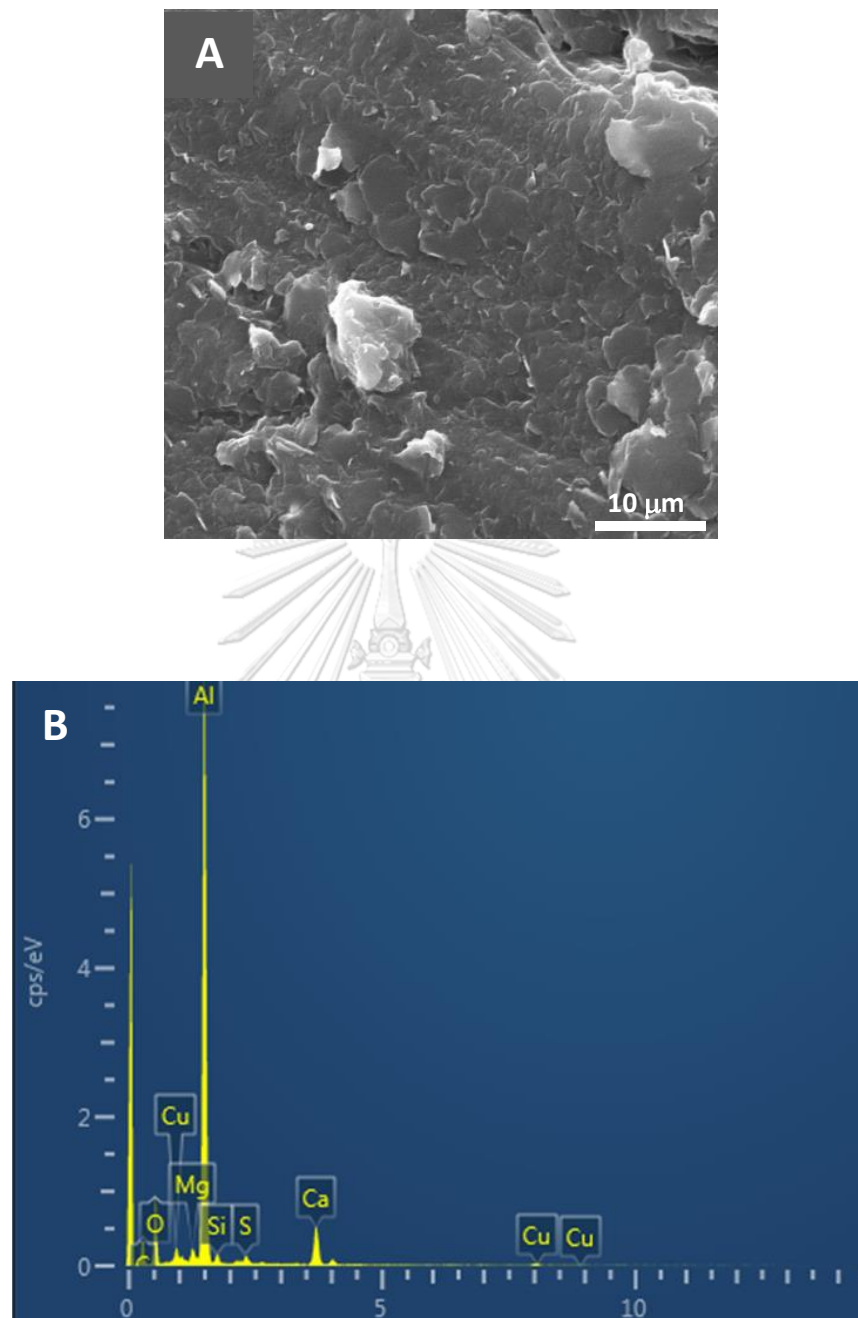


Figure 4.14 SEM/EDX results of RVNR without filler; (A) SEM image, and (B) EDX spectrum.

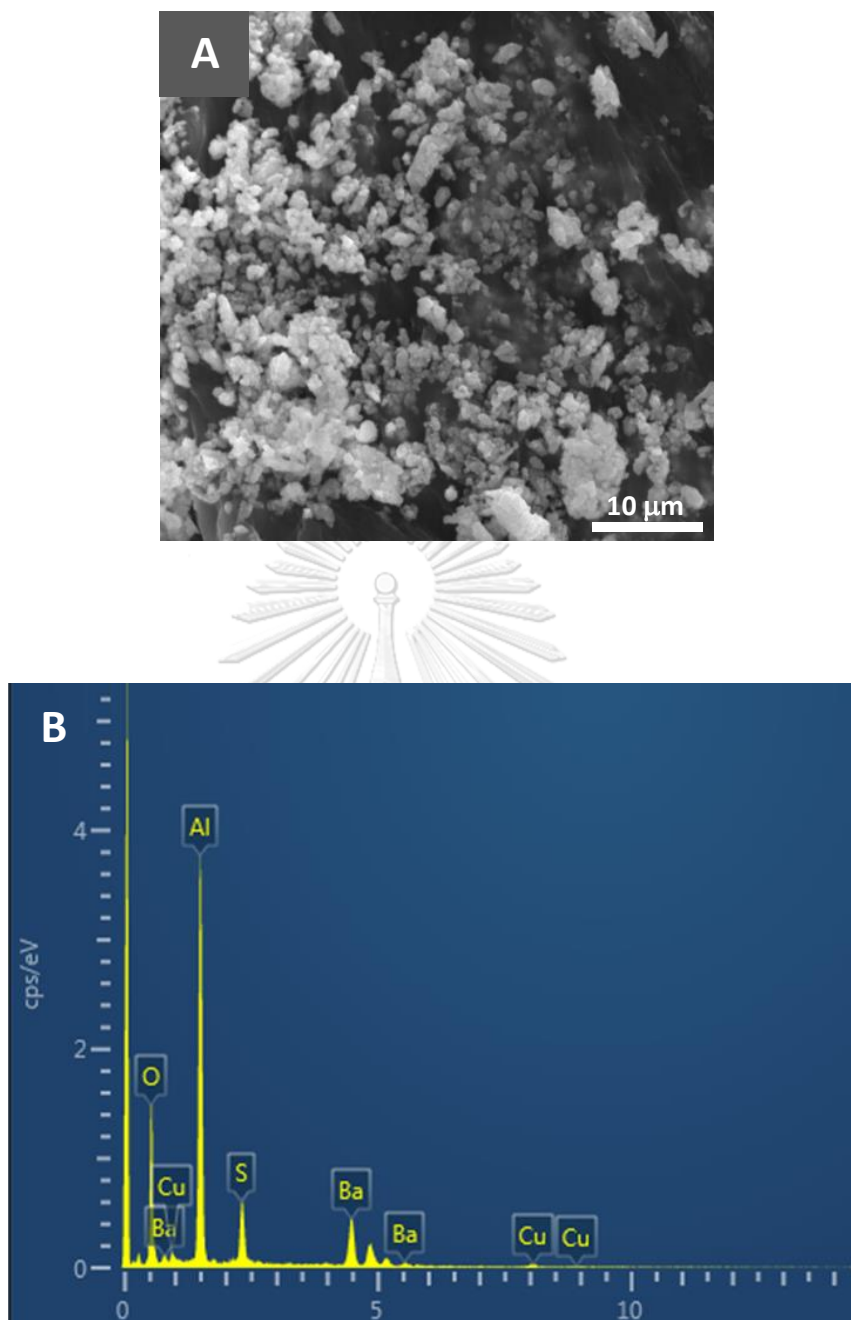


Figure 4.15 SEM/EDX results of NR-W; (A) SEM image, and (B) EDX spectrum.

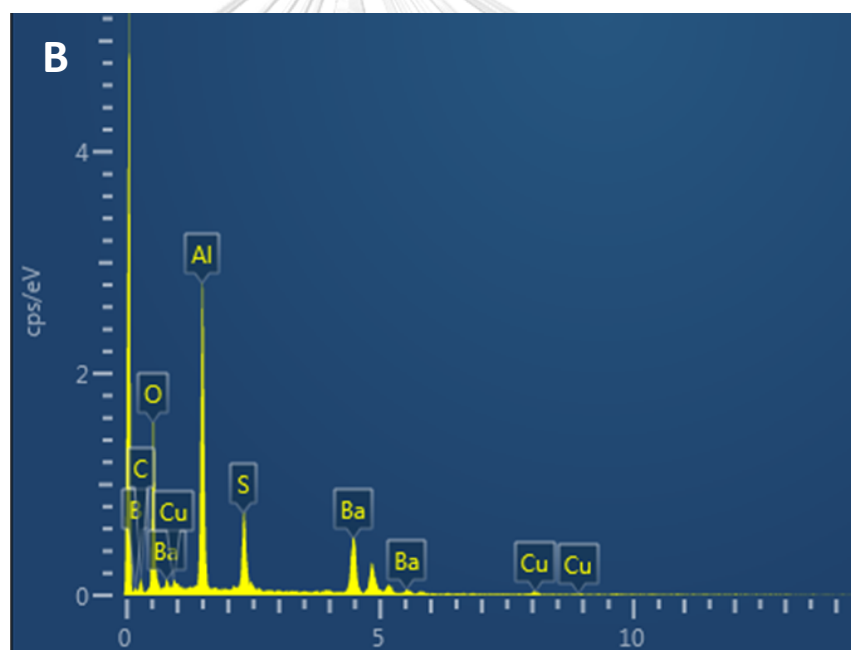
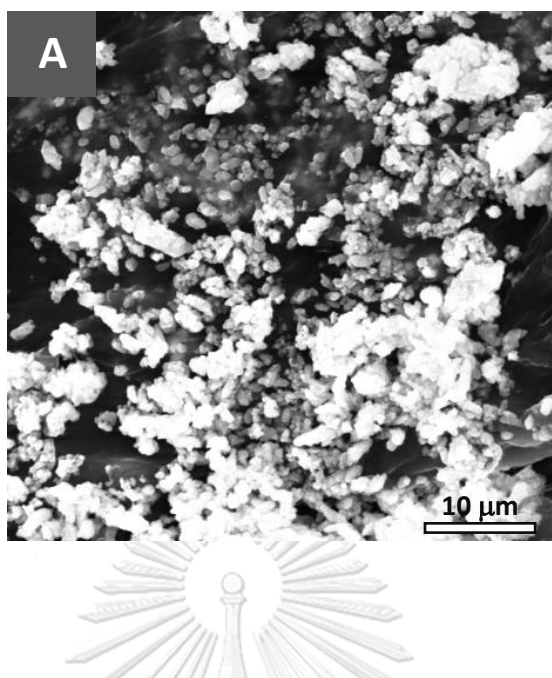


Figure 4.16 SEM/EDX results of NR-E; (A) SEM image, and (B) EDX spectrum.

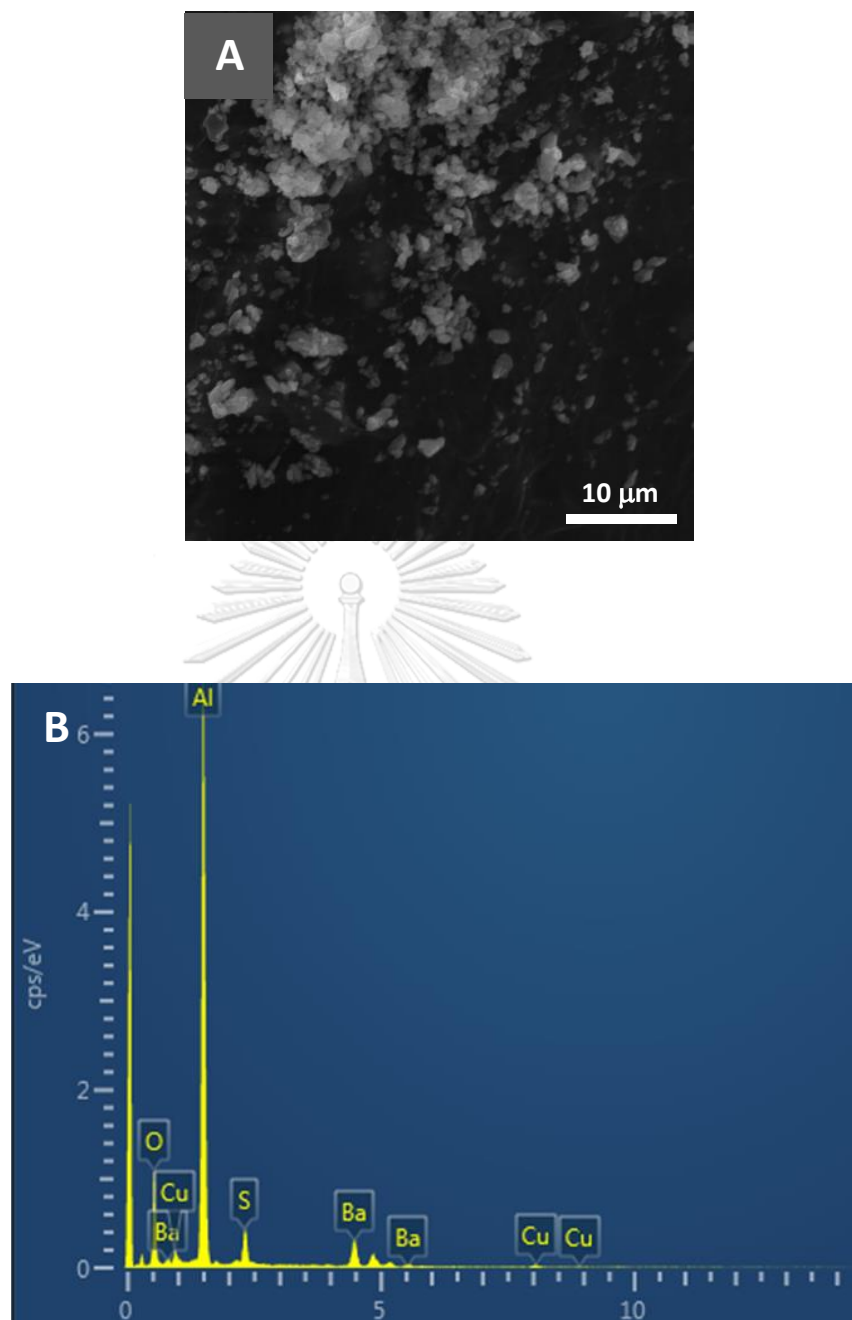


Figure 4.17 SEM/EDX results of NR-P; (A) SEM image, and (B) EDX spectrum.

4.5 Investigation of X-ray attenuation property

The NR-W, NR-E, and NR-P have been carried out the X-ray attenuation study by varying the concentration of filler at 40, 50, and 60 %w/w, and exposed with the X-ray generator at a tube voltage of 30, 40, and 60 kV.

4.5.1 The radiation attenuation ratio

The results indicated that the radiation attenuation ratio enhanced when increasing the filler loading, as shown in Figure 4.18 to Figure 4.20.

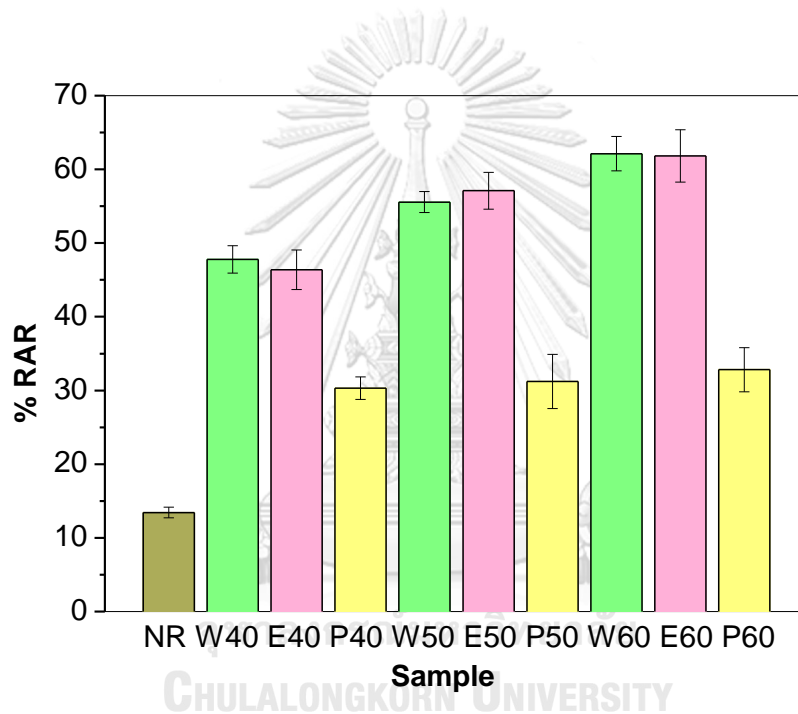


Figure 4.18 The % RAR of RVNR samples mixed with BaSO₄ fillers and irradiated at 30 kV X-ray tube voltage.

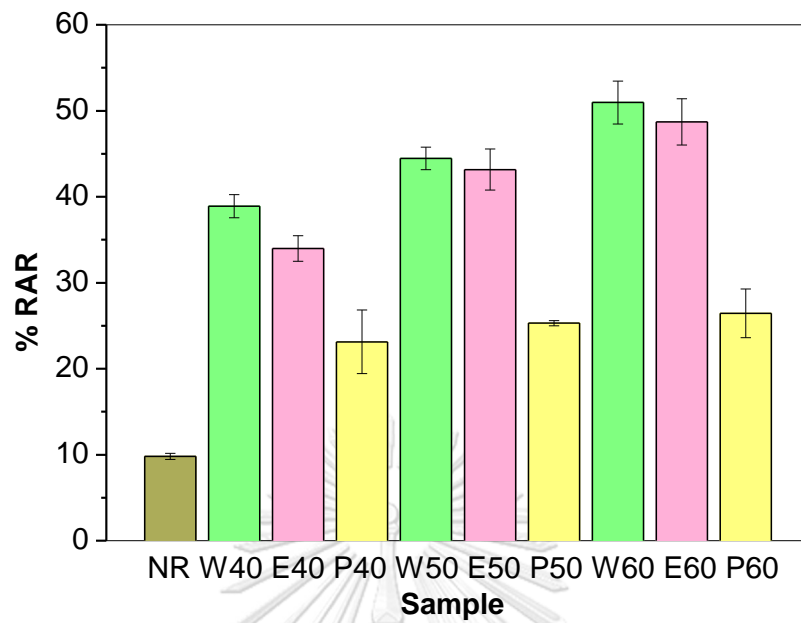


Figure 4.19 The % RAR of RVNR samples mixed with BaSO_4 fillers and irradiated at 40 kV X-ray tube voltage.

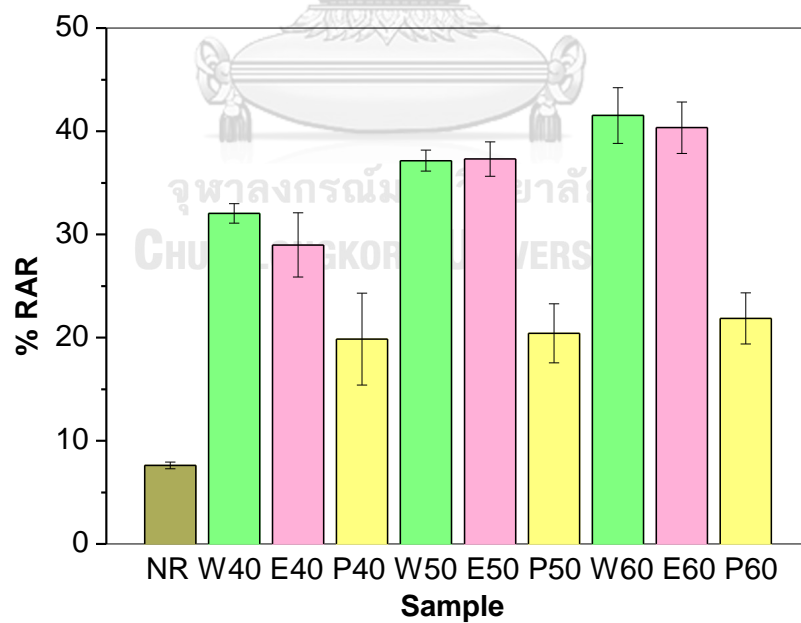


Figure 4.20 The % RAR of RVNR samples mixed with BaSO_4 fillers and irradiated at 60 kV tube voltage.

The BaSO_4 plays an important role in absorbing the incident X-ray; nonetheless, some X-rays can penetrate through the porosity, causing the transmittance radiation of the material. The high amount of filler dispersed in the material could improve the X-ray attenuation; however, the BaSO_4 behavior would be packed into a large molecule that affects increasing space in the materials. The Ba/AC illustrated a high shielding efficiency than using the BaSO_4 powder as the conventional method. It was because the amorphous cellulose could distribute the BaSO_4 particle, which could prevent the collecting of particles compared to the BaSO_4 powder. The NR-W and NR-E provided a homogeneous distribution of BaSO_4 particles throughout the natural rubber that leading to decreased X-ray transmittance opportunity through space.

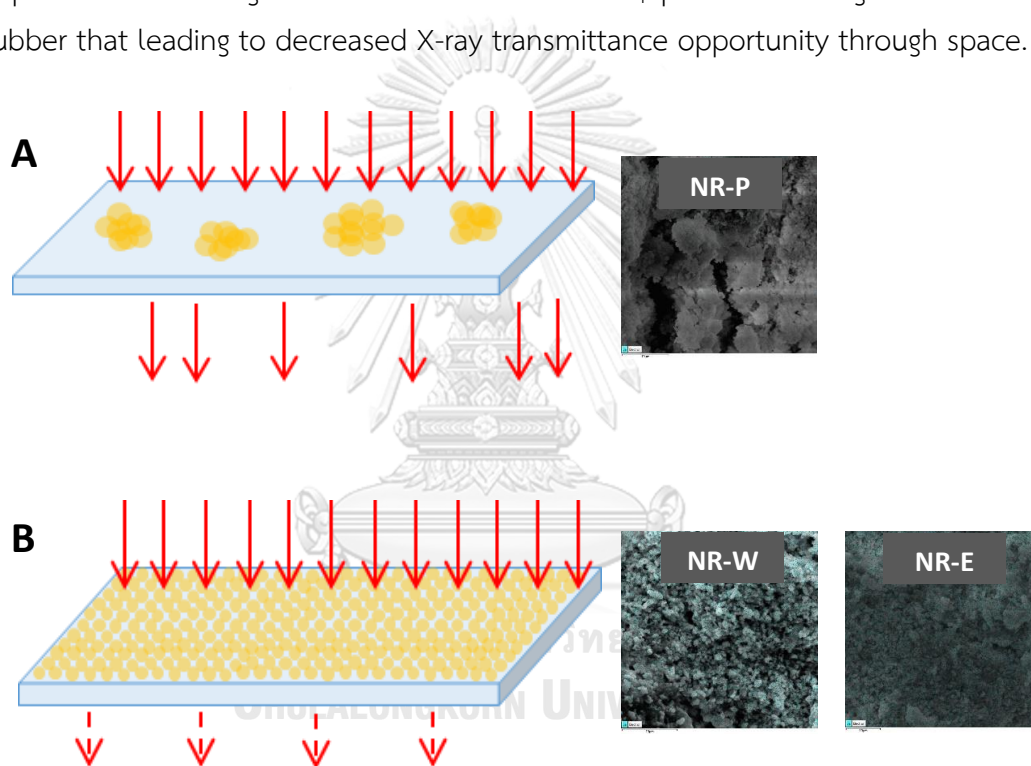


Figure 4.21 BaSO_4 particle distribution affects with X-ray transmittance; (A) BaSO_4 powder, and (B) Ba/AC.

4.5.2 The linear attenuation coefficient

Figure 4.22 demonstrates linear attenuation coefficient of the RVNR composites from Ba/AC were higher than that of BaSO_4 powder when irradiated at 30, 40, and 60 kV. The filler concentration in the materials impacted the linear attenuation coefficient. The increased BaSO_4 particles provide a high linear attenuation coefficient, which

improved the shielding performance. The linear attenuation coefficient describes the fraction of the X-rays, which are absorbed or scattered per the thickness of the materials. The value generally expresses the number of atoms in cubic millimeters, volume of material, and the probability of incident X-rays will be absorbed or scattered from the BaSO_4 particles.

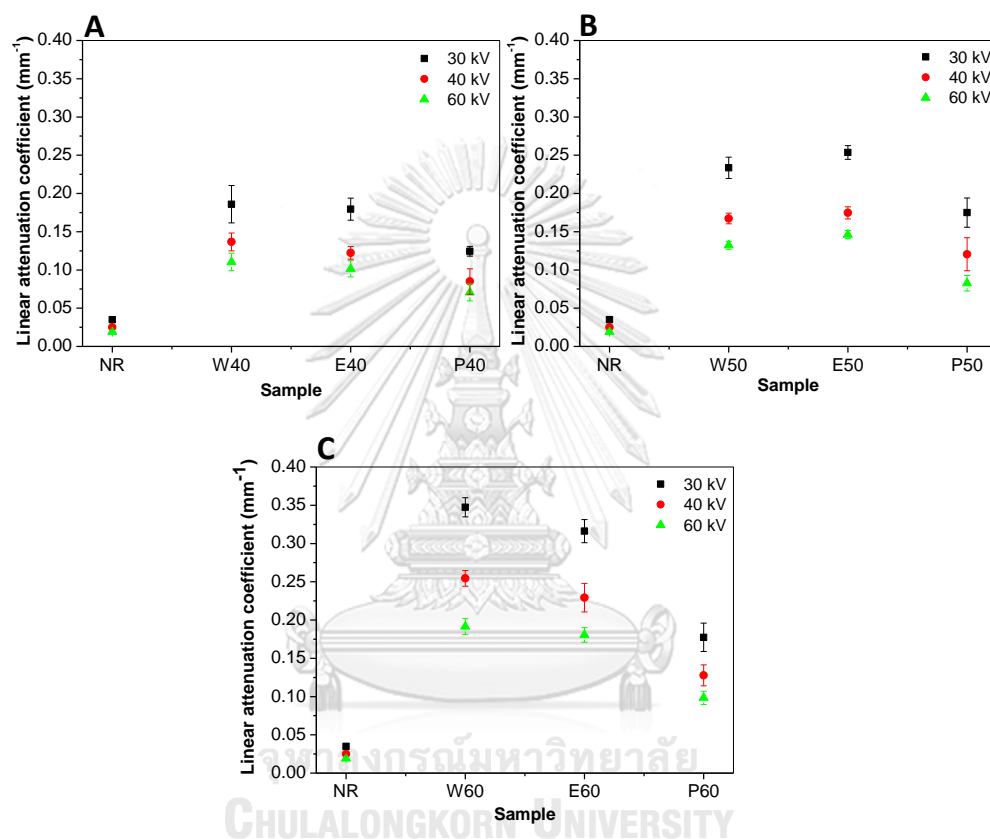


Figure 4.22 The linear attenuation coefficient of RVNR samples mixed with BaSO_4 fillers; (A) 40 %w/w, (B) 50 %w/w, and (C) 60 %w/w.

4.5.3 The half-value layer

The results in Figure 4.23 illustrates half-value layer of the natural rubber composites from Ba/AC is lower than that of the BaSO_4 powder. The amount of BaSO_4 contained in the materials plays a significant role in the X-ray shielding efficiency because the half-value layer describes the thickness of materials in which 50% of incident X-rays attenuated. The higher volume of BaSO_4 filler was added, the

greater X-ray absorption was achieved. The lower thickness of materials that can absorb the radiation representing the higher efficient shielding of the materials. Moreover, enhancing the X-ray tube voltage results in increasing the half-value layer of materials because of high X-ray densities than lower voltage.

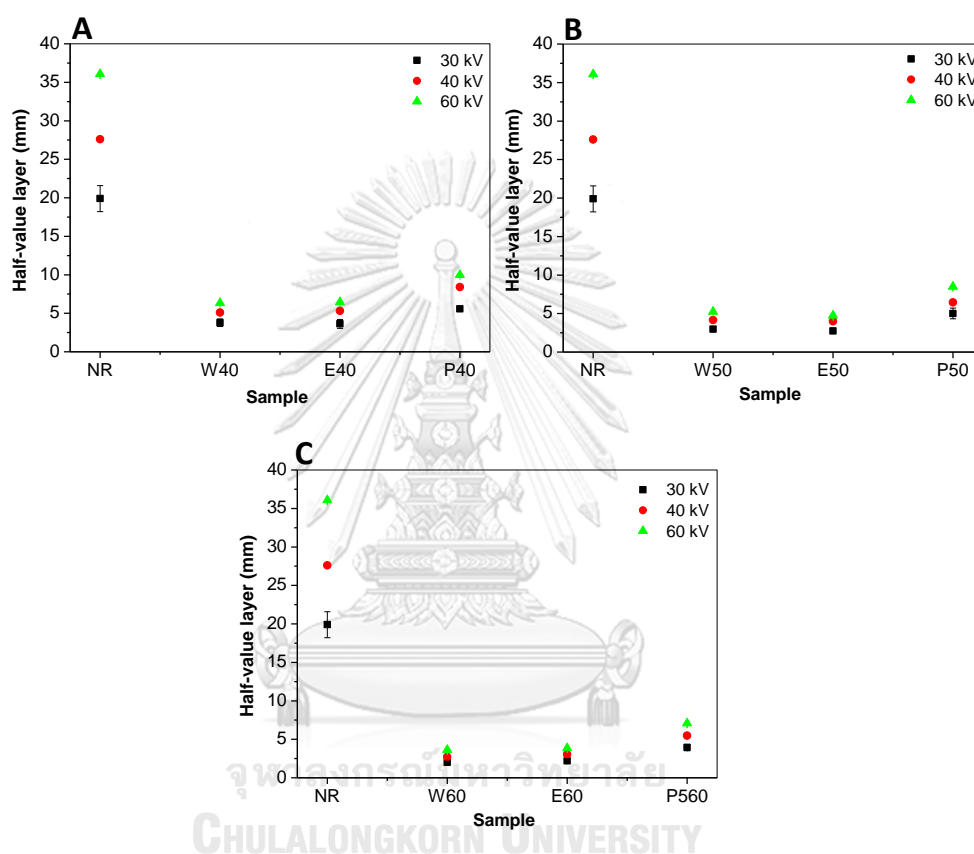


Figure 4.23 The half-value layer of RVNR samples mixed with BaSO_4 fillers; (A) 40 %w/w, (B) 50 %w/w, and (C) 60 %w/w.

The results indicate that BaSO_4 /amorphous cellulose/natural rubber tends to prevent X-ray efficiency. The radiation attenuation increased when enhancing the BaSO_4 in the materials. The X-ray tube voltage also affects the radiation penetration: increased tube voltage provides a high density of X-ray incidents at the materials. The greater voltage was utilized, the lower the X-ray absorption was obtained, comparing to the same ratio of Ba/AC composites. The Ba/AC substrates incorporates with RVNR illustrated higher X-ray shielding performance than the BaSO_4 powder. It

was because the amorphous cellulose plays a role in BaSO_4 distribution, including reducing the particle aggregation to large molecules. As a result, the X-ray can penetrate the several porosities that occurred from particle packing. Moreover, the Ba/AC-W showed similar results without significant differences, comparing to the Ba/AC-E. It could be concluded that RVNR incorporated with Ba/AC-W from recycled pulp tends to utilization as an X-ray shielding substrate with equality properties to the purified pulp.

However, it is difficult to compare the attenuation efficiency with previous researches because we can not maintain the beam quality for each experiment to be the same. The beam quality of X-rays depends on the tube voltage, current, source distance, and environmental control during irradiation. Therefore, this research employed the lead equivalent to comparing the X-ray shielding efficiency that is normally used in the manufacturing commercial.

4.5.4 The mass attenuation coefficient

Mass attenuation coefficient can describe how the sample will be absorbed X-ray per unit mass. The mass attenuation coefficient is a ratio of photons removed from a Monochromatic X-ray beam by the absorbed material per unit mass. In Table 4.1, the NR-W60 illustrated similar results with the NR-E60, which meant both materials provided the same X-ray shielding efficiency. While the NR-P60 demonstrated less X-ray attenuation property than the NR-W60, and NR-E60 as shown in the lower attenuation coefficient.

Table 4.1 The density and mass attenuation coefficient of the varied thickness for RVNR composites.

Sample	Density (g/cm ²)	Mass attenuation coefficient (cm ² /g)		
		30 kV	40 kV	60 kV
NR	0.92	0.381	0.273	0.209
NR-W60	1.20	2.895	2.121	1.596
NR-E60	1.10	2.874	2.085	1.642
NR-P60	0.98	1.810	1.303	1.005

4.5.5 The varied thickness of BaSO₄/amorphous cellulose/natural rubber

The BaSO₄/amorphous cellulose/natural rubbers have been studied the tendency to be used as X-ray protective materials. Each sample layer was stack in several thicknesses and compared to the lead sheet at the thickness of 0.3 mm. The radiation attenuation ratio, the linear attenuation coefficient, and the half-value layer were taken into consideration. The sample sheets were carried out to irradiate at 60 and 80 kV. Figure 4.24 shows the radiation attenuation ratio and the linear attenuation coefficient that increased when enhancing the thickness, while the half-value layer provided the opposite value. As a result, the samples with adequate thickness can present the performance of radiation attenuation equivalent to lead. The higher thickness by layering the specimens can increase the shielding abilities. The BaSO₄ and particles provided well-distributed to fulfill the space that array the layers on the stack, which resulted in most incident radiation could be absorbed by the BaSO₄. W1, W2, W3 were the sample sheet prepared from office waste paper, while E1, E2, and E3 were produced from the eucalyptus pulp at different thicknesses, as shown in Table 4.2.

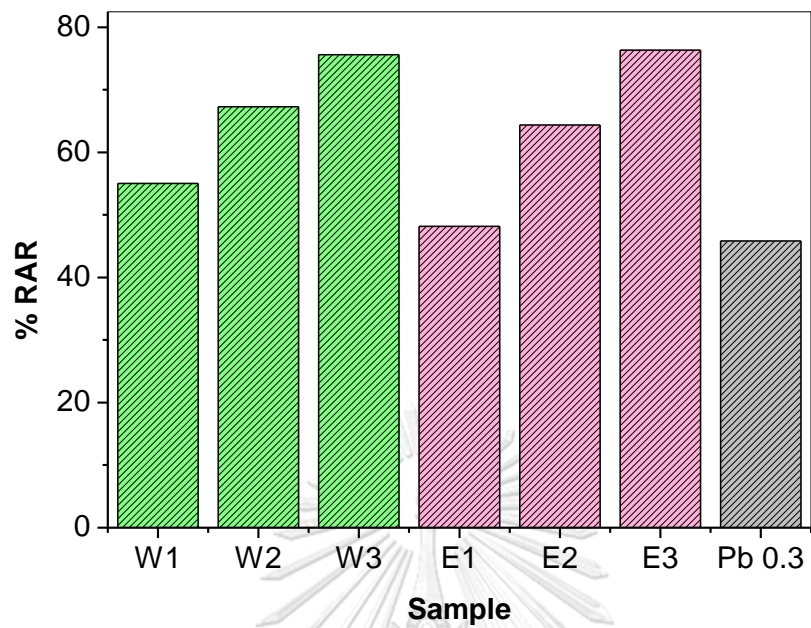


Figure 4.24 The radiation attenuation ratio of NR-W and NR-E with different thicknesses compared to the lead sheet when exposing with 60 kV.

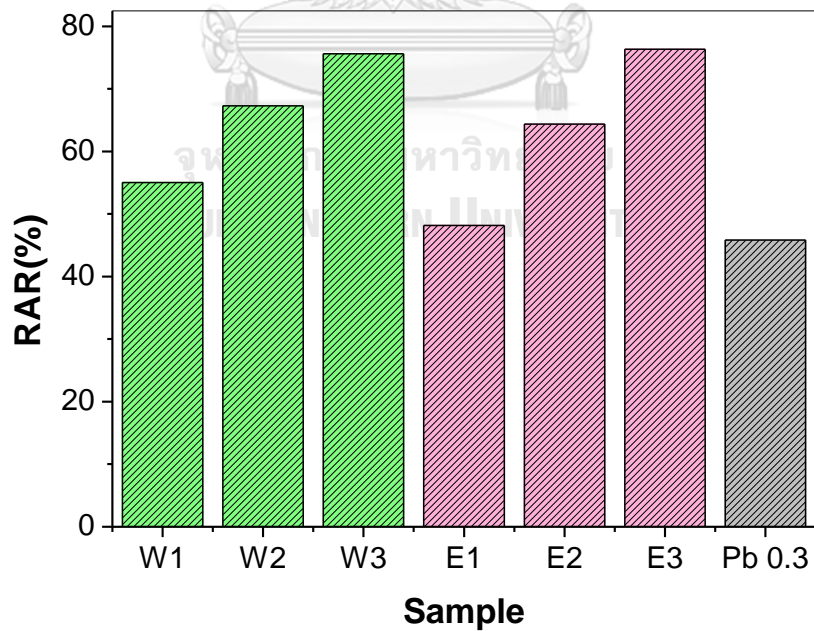


Figure 4.25 The radiation attenuation ratio of NR-W and NR-E with different thicknesses compared to the lead sheet when exposing with 80 kV.

Table 4.2 The thickness of the sample sheet that array in the layer stack.

Sample code	W1	W2	W3	E1	E2	E3
Thickness (mm)	5.821	8.543	10.689	6.769	9.123	12.354

Table 4.3 The linear attenuation coefficient and the half-value layer of samples.

Sample	Linear attenuation coefficient (mm ⁻¹)		Half-value layer (mm)	
	60 kV	80 kV	60 kV	80 kV
	W1	0.239	0.147	2.904
W2	0.240	0.155	2.884	4.461
W3	0.259	0.160	2.677	4.342
E1	0.180	0.112	3.859	6.201
E2	0.182	0.115	3.801	6.051
E3	0.189	0.129	3.668	5.363
Pb	4.665	2.542	0.149	0.273

The linear attenuation coefficient and the half-value layer of the samples and the lead presented the lead has greater values than the samples. Because the lead provides a high atomic number and density than BaSO₄, which meant it is necessary to prepare the natural rubber composites in thick sheets to obtain the shielding efficiency equivalent to 0.3 mm Pb. However, the very thick shielding material may not suitable for an occupational worker in daily use. Therefore, it is essential to concern the density and amount used of the BaSO₄ to compensate between the shielding abilities and the thickness. An insufficient amount of BaSO₄ affects the inadequate shielding performance compared to utilize in high concentration. Consequently, to produce the practical X-ray protective materials, it is required to increase the BaSO₄ loading in the substrate before combining it with the natural rubber to reduce the thickness of RVNR sheets.

4.6 Preparing of X-ray shielding protective prototypes

X-ray shielding protectives had been fabricated with optimized thickness for practical use. The high BaSO₄ amounts were utilized during the Ba/AC regeneration process to enhance the attenuation efficiency. Subsequently, the Ba/AC was incorporated with RVNR at the ratio of 40%, 50%, and 60%, and then study the X-ray shielding performance by exposing at 60, 80, and 100 kV. The radiation attenuation ratio of the X-ray shielding sheets was compared to the 0.3 mm lead thickness and 0.5 mm thyroid shield. The NR-E60 PROTO provided a radiation attenuation ratio similar to the lead sheet at the thickness of 0.3 mm when exposed with 60 kV. While the NR-W60 PROTO demonstrated a lower shielding efficiency than the NR-E60 PROTO. It was because the BaSO₄ content in NR-W60 PROTO (16.51 %w/w) was less than the NR-E60 PROTO (22.46 %w/w). The lead sheet was trailable to the thyroid shield in the commercial, which illustrated the 0.3 mm lead that complying with the 0.5 mm thyroid shield, as shown in Table 4.4.

Table 4.4 The radiation attenuation ratio of X-ray shielding sheets of prototype development when exposed with 60, 80, and 100 kV.

Materials	Thickness (mm)	Radiation attenuation ratio (%)		
		60 kV	80 kV	100 kV
NR-E40 PROTO	7.821	51.13	36.97	21.08
NR-E50 PROTO	6.698	54.42	37.08	25.86
NR-E60 PROTO	3.808	72.77	42.21	31.31
NR-W40 PROTO	5.592	46.12	30.15	18.99
NR-W50 PROTO	4.833	55.49	34.60	20.61
NR-W60 PROTO	4.182	55.30	35.42	22.68
Pb	0.3	70.19	46.49	42.00
Thyroid shield	0.5	92.37	75.50	72.91

The linear attenuation coefficient of the lead sheet was used for calculating the thickness of X-ray protective prototypes equivalent to 0.25 mm of lead, as expressed in Table 4.5.

Table 4.5 The linear attenuation coefficient of X-ray shielding sheets to study the prototypes producing.

Materials	Linear attenuation coefficient (mm ⁻¹)		
	60 kV	80 kV	100 kV
NR-E40 PROTO	0.092	0.054	0.030
NR-E50 PROTO	0.144	0.077	0.049
NR-E60 PROTO	0.342	0.142	0.068
NR-W40 PROTO	0.112	0.056	0.037
NR-W50 PROTO	0.167	0.083	0.049
NR-W60 PROTO	0.199	0.094	0.060
Pb	4.034	1.937	1.800
Thyroid shield	5.146	2.725	2.602

The thickness of the prototype equivalent to 0.25 mm was calculated from the linear attenuation coefficient of 0.3 mm Pb, showing the results in Table 4.6.

Table 4.6 The required thickness of the prototypes that equivalency to 0.25 mm of Pb.

Materials	Materials thickness at lead equivalent to 0.25 mm Pb		
	(mm)		
	60 kV	80 kV	100 kV
NR-E40 PROTO	10.93	8.95	14.97
NR-E50 PROTO	7.00	6.30	6.62
NR-E60 PROTO	2.95	3.42	9.19
NR-W40 PROTO	9.02	8.57	12.18
NR-W50 PROTO	6.02	5.85	9.16
NR-W60 PROTO	5.07	5.16	7.46

The X-ray protective prototypes were categorized into two purposes; attenuation of the primary X-ray beam and scattered beam. The linear attenuation coefficient at 80 kV is selected for preventing the primary X-ray beam, while the 60 kV is represented for the scattering X-ray beam. [72] The X-ray protectives for the intervention of direct beam were formulated by incorporating RVNL and 60% w/w Ba/AC prepared from office waste paper at the thickness of 5.16 mm. Subsequently, the shielding sheets were cut into a specific shape to produce the head shield, thyroid shield, and breast shield shown in Figure 4.26.



Figure 4.26 Prototypes for X-ray protective materials; (A1-A3) shielding sheets in various shapes and prototypes of (B1) head shield, (B2) thyroid shield, and (B3) breast shield.

The lab coat shielding for X-ray scattering was also fabricated using the 60% w/w Ba/AC prepared from eucalyptus pulp at the thickness of 3.42 mm, then attached in the middle of the lab coat as demonstrated in Figure 4.27.

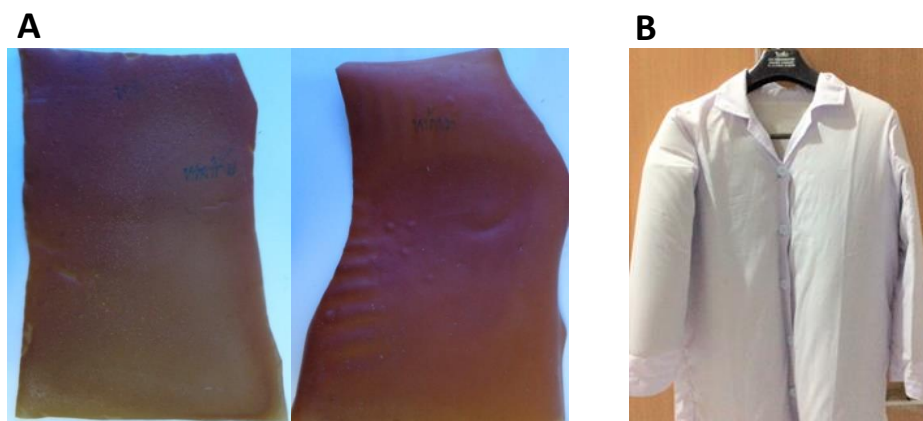


Figure 4.27 The X-ray shielding prototype; (A) shielding sheet prepared for attaching with the lab coat, and (B) lab coat for X-ray scattering attenuation.

4.7 Interaction of X-ray with barium sulphate/amorphous cellulose/natural rubber using XCOM program

To estimate the attenuation performance of X-ray interaction with barium sulphate/amorphous cellulose/natural rubber, the XCOM program from NIST was employed to investigate each mass attenuation coefficient (cm^2/g). The photon energy from 24.6 keV to 83.3 keV representing the X-ray energy from 30 kV to 100 kV that was utilized in this research. The coherent scattering, incoherent scattering, and photoelectric absorption were examined at the concentration of Ba/AC composites 60 %w/w. The mass attenuation coefficients associated with the energy range demonstrated the photoelectric absorption is predominant for all photon energy ranges. The barium sulphate provides the K-absorption edge at 37.4 keV, which affects photoelectric absorption. The absorption of photon will increase remarkably at the K-edge absorption above the binding energy of the K shell. The probability of a photoelectric interaction dramatically increases for photons of energies above the absorption edge relative to energies below the edge.

In addition, the coherent scattering (Rayleigh scattering) was reduced when enhancing the photon energy because the coherent scatter interacts with an electron

of an atom in the excited state and emitted the photon with the same energy but in a different direction. As a result, there are no ionization occurs, and no electrons were ejected. Therefore, they emitted photons in the change of direction but without change in wavelength.

According to the incoherent scattering (Compton scattering), the trend of mass attenuation coefficient demonstrated no difference significantly compared to the behavior of photoelectric absorption and coherent scattering. The photon interacts with an outer shell electron of an atom, leading the electron is ejected from the atom including the photon is scattered with some energy reduction.

Therefore, it could be summarized that the BaSO₄/amorphous cellulose/natural rubber provides the mass attenuation coefficient in the dominant behavior of photoelectric absorption depending on the K-edge absorption. While the coherent scattering present mass attenuation coefficient will be decreased when increasing the photon energy that is different from the incoherent scattering, illustrated the consistent trend of shielding performance, as show in Figure 4.28.

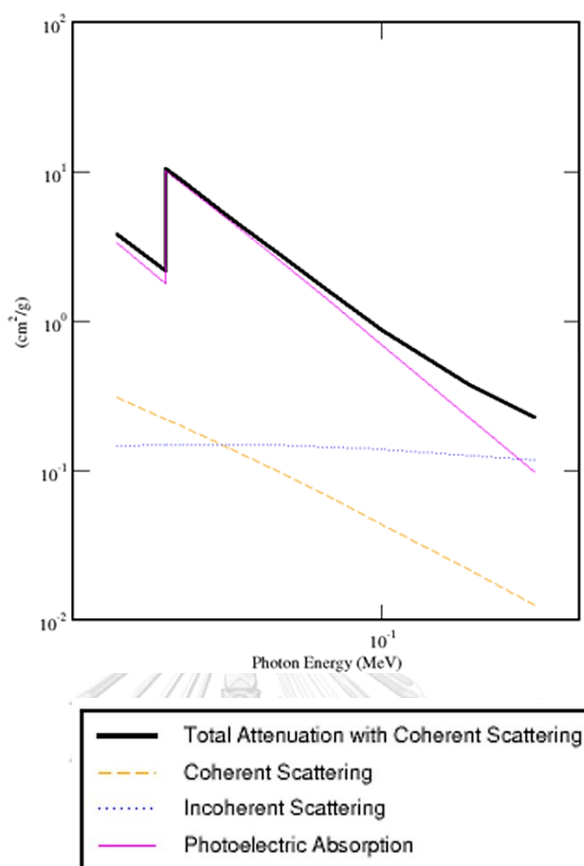


Figure 4.28 X-ray interaction of BaSO₄/amorphous cellulose/natural rubber.

4.8 Physical property of X-ray protection products

Density, tensile strength, and elongation at break of the X-ray shielding sheet were studied, as shown in Table 4.7.

Table 4.7 The densities and physical properties of representative for X-ray shielding sheets.

Sample	BaSO ₄ (%)	Density (g/cm ³)	Tensile strength (MPa)	Elongation at break (%)
NR	0	0.925 ± 0.003	10.02 ± 0.88	733 ± 5
NR-W60 PROTO	16.51	1.119 ± 0.003	11.24 ± 0.69	595 ± 15
NR-E60 PROTO	22.46	1.309 ± 0.001	8.39 ± 1.07	558 ± 19

The BaSO_4 concentration of NR-E60 PROTO is higher than NR-W60 PROTO even though prepared in an equal ratio. It was because the NR-E60 PROTO produced from the eucalyptus pulp is purified cellulose (100 %), while the NR-W60 PROTO originated from recycled cellulose of office waste paper. In general, waste paper is fiber sheets composing chemical agents, which are limestone (calcium carbonate), clay (kaolinite), starch, and ink. [73] The impurities may have an effect on the preparation of amorphous cellulose and Ba/AC composites during the cellulose pulp regeneration when produced in large scale.

In addition, increased Ba/AC amounts, result in a decrease in the tensile strength and elongation at break compared to RVNR without filler. The quantity of BaSO_4 in Ba/AC correlates to the density of material and mechanical properties; enhanced the BaSO_4 amounts lead to reduce mechanical strength in materials. The BaSO_4 concentration of NR-W60 PROTO (16.51 %w/w) demonstrated higher mechanical properties than the NR-E60 PROTO (22.46 %w/w) due to the filler-filler interactions affect in the materials, tending to aggregation of BaSO_4 in the materials.[74] The more fillers were added, the probability of the interaction was increased, resulting in worse particle dispersion and decreased tensile strength and elongation at break, shown in Figure 4.29. Consequently, it was because BaSO_4 contain in materials correlated to the mechanical properties of X-ray shielding sheets. It is necessary to consider the optimal amount corresponding to the shielding efficiency to obtain the X-ray protective materials with high-quality mechanical properties when producing in manufacture in the future.

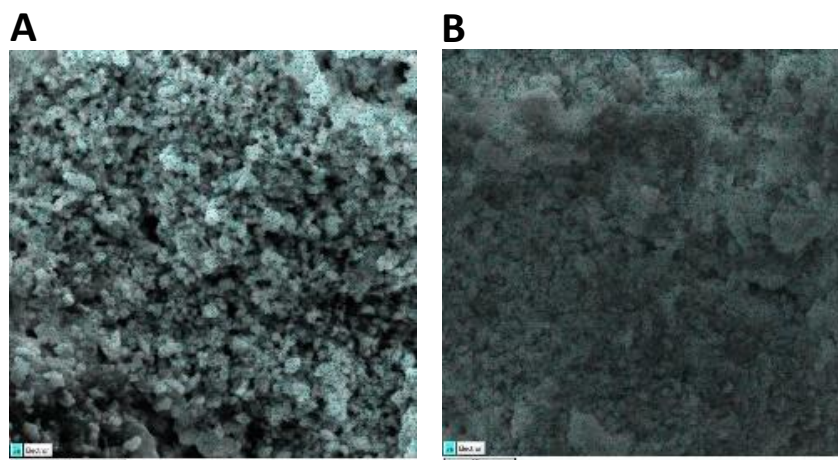


Figure 4.29 The Ba/AC particles dispersion in natural rubber;
(A) Ba/AC NR-W60 PROTO and (B) Ba/AC NR-E60 PROTO.

4.9 Comparison of investment for X-ray shielding prototypes and commercial products.

The price of raw materials and prototype production were investigated by comparing with commercial manufacturing. The X-ray shielding prototypes present a lower investment than the commercial products, approximately two times shown in Table 4.8.

Table 4.8 Comparison of price for X-ray shielding prototypes and commercial products.

Protective materials	Price (bath)	
	Shielding prototypes	Commercial products [75], [76], [77]
Head shield	~ 1,400	3,000 - 3,500
Thyroid shield	~ 1,000	1,900 - 2,500
Breast shield	~ 1,500	3,500 - 3,800
Lab coat/ Apron	~ 4,000	7,800 - 10,000

CHAPTER 5

CONCLUSION

The Ba/AC was successfully fabricated as the substrate in X-ray shielding applications. The benefits of amorphous cellulose are to improve the features of barium sulphate compounds, which are biodegradable, environment-friendly, non-toxic, and low-cost. The flow injection techniques are employed to prepare the composites with barium sulphate compounds to obtain the sub-micron particles preventing material aggregation. These advantageous properties lead the X-ray substrates can utilize in many applications. Due to the simple method without using several chemical substances, this technique is proper to scale up for commercial applications.

The X-ray shielding lab coat was produced for the occupational worker to protect the scatter radiation with equivalency to 0.25 mm Pb. The Ba/AC plays a role in enhancing the x-ray attenuation efficiency. The advantages of the Ba/AC are well-dispersed when combining with the RVNR due to amorphous cellulose surrounded barium sulphate in Ba/AC, resulting in decreased aggregation of barium sulphate particles compare with the barium sulphate powder. Moreover, the Ba/AC can combine in RVNR in high loading up to 60 %w/w to obtain thin material, which is practically utilized for the worker in terms of more comfortable movement. In addition, the X-ray protection prototypes from office waste paper as base materials were fabricated for the direct X-ray beam equivalent to the thickness of lead 0.25 mm. The Ba/AC from office waste paper was also studied the properties correlate with the eucalyptus pulp. The characterization results have illustrated the consistency with both substrates, which means no significant properties between recycled pulp and purified pulp. Moreover, the RVNR was combined with the filler to investigate the

shielding efficiency. The Ba/AC from office waste papers indicated the attenuation property the same as Ba/AC from eucalyptus pulp.

The self-life of BaSO₄/amorphous cellulose/natural rubber is drawn attention to estimating the aging of the prototypes by consideration from the radiation vulcanized natural rubber. It could be concluded that the materials possible to expired approximately three to five years after production under normal utilization condition. [78], [79]

In terms of environmental benefits, the Ba/AC was produced from the office waste paper as recycled materials to produce cellulose pulp. The recycling of waste paper can preserve trees, water, and economics. The waste paper can reduce chemicals used, including save electricity during the manufacturing process. Moreover, utilizing waste paper is wealth to cut down on the pollution, which is greenhouse gases. The decomposing of paper can release greenhouse gases composing carbon dioxide, methane, nitrous oxide, ozone, chlorofluorocarbons, and hydrofluorocarbons, which contributed to climate change in the long term.



จุฬาลงกรณ์มหาวิทยาลัย
CHULALONGKORN UNIVERSITY

REFERENCES

1. Ma, C.M., Coffey, C.W., Dewerd, L.A., Liu, C., Nath, R., Seltzer, S.M., and Seuntjens, J.P., AAPM protocol for 40-300 kV x-ray beam dosimetry in radiotherapy and radiobiology. *Medical Physics*, 2001. **868-893**.
2. Glees, J.P., and Wolstenholme, V., *The Role of Kilovoltage X-rays in the Treatment of Skin Cancers*. European Oncological Disease, 2006.
3. Simon, N., *Radiation in the Diagnosis and Treatment of Disease*. American Journal of Public Health and the Nation's Health, 1964. **54(Suppl 1)**: p. 57-62.
4. Sciences, D.o.M., *Quality Standards of Medical Diagnostic X-ray Machines*. 2019.
5. Beck, T.J., *A multi-layer light-weight garment material with low radiation buildup providing scattered-radiation shielding*, W.I.P. Organization, Editor. 2011: USA.
6. Management, O.o.R., *X-Ray Safety Training for Analytical and Cabinet X-ray*.
7. Munro, L., *Basics of radiation protection: how to achieve ALARA: Working tips and guidelines*. 2004, Malta: World Health Organization.
8. Khong, P.-L., Ringertz, H., Donoghue, V., Frush, D., Rehani, M., *Radiological protection in paediatric diagnostic and interventional radiology*. *Annals of the ICRP*. ICRP Publication 121, 2013. **42(2)**.
9. BMWG, *Basic radiation physics & Fundamentals of radiation protection*, in *Train-the-Trainer on Radiation Detection Techniques and Procedures for the region of SEA*. Ispra, Italy.
10. Gazette, G., *Ministrial regulation of radiation safety*. 2018: Bangkok, Thailand.
11. Florida, U.o. *Radiation Safety Short Course Study Guide*. [cited 2021; Available from: https://webfiles.ehs.ufl.edu/rssc_stdy_chp_3.pdf].
12. Ngaile, J.E., Uiso, C.B., Msaki, P., and Kazema, R., *Use of lead shields for radiation protection of superficial organs in patients undergoing head CT examinations*. *Radiation Protection Dosimetry*, 2008. **130**: p. 490-498.
13. Movahedi, M.M., Abdi, A., Mehdizadeh, A., Dehghan, N., Heidari, E., Masumi, Y., and Abbaszadeh, M., *Novel paint design based on nanopowder to protection*

- against X and gamma rays. *Indian Journal of Nuclear Medicine*, 2014. **29(1)**: p. 18-21.
14. Gwon, S., H., Oh, J. H., Kim, M., Choi, S., Oh, K., H., and Sun, J., Y., Sewable soft shields for the gamma-rays radiation Scientific Report, 2018. **8**: p. 1-7.
 15. Hulbert, S.M., and Carlson, K.A., Is Lead Dust Within Nuclear Medicine Departments a Hazard to Pediatric Patients? *Journal of Nuclear Medicine Technology*, 2009. **37(3)**: p. 170-172.
 16. AbuAlRoos N. J., A., N. A. B., and Zainona, R., Conventional and new lead-free radiation shielding materials for radiation protection in nuclear medicine: A review. *Radiation Physics and Chemistry*, 2019. **165**.
 17. MaCaffrey, J.P., Mainegra-Hing, E., and Shen, H., Optimizing non-Pb radiation shielding materials using bilayers. *Medical Physics*, 2009. **36(12)**: p. 5586-5594.
 18. Kim, S.C., Dong, K. R., Chung, W. K., Performance evaluation of a medical radiation shielding sheet barium as an environment-friendly material. *Journal of the Korean Physical Society*, 2012. **60**: p. 165-170.
 19. Kim, S.C., and Jung, H. M., A study on performance of low-dose medical radiation shielding fiber (RSF) in CT scans. *International Journal of Technology*, 2013. **2(1)**: p. 178-187.
 20. Levine, M.S., and Rubesin, History and Evolution of the Barium Swallow for Evaluation of the Pharynx and Esophagus. *Dysphagia*, 2017. **32**: p. 55-72.
 21. Zhou, C., and Wu., O., Recent development in applications of cellulose nanocrystals for advanced polymer-based nanocomposites by novel fabrication strategies.
 22. Plermjai, K., Boonyarttanakalin, K., Mekprasert, W., Pavasupree, S., Phoohinkong, W., and Pecharapa, W. Extraction and characterization of nanocellulose from sugarcane bagasse by ball-milling-assisted acid hydrolysis. in *International Conference on Science and Technology of Emerging Materials*. 2018. Pattaya, Thailand.
 23. Popescu, C.M., Larsson, P.T., Olaru, N., and Vasile, C., Spectroscopic study of acetylated kraft pulp fibers. *Carbohydrate Polymer*, 2012. **88**: p. 530-536.

24. Popescu, C.M., Tibirna, C., M., Raschip, I., E., Popescu, M.C., Ander, P., and Vasile, C., Bulk and surface characterization of unbleached and bleached softwood kraft pulp fibers. *Cellulose Chemistry and Technology*, 2008. **42 (9-10)**: p. 525-547.
25. Ciolacu, D., Clolacu, F., and Popa, V., Amorphous cellulose chemistry and technology. *Cellulose Chemistry and Technology*, 2011. **45(1-2)**: p. 13-21.
26. Zhang, B.X., Azuma, J.I., Uyama, H., Preparation and characterization of transparent amorphous cellulose film. *RSC Advances*, 2015. **5**: p. 2900-2907.
27. Hong, J., Wang, Y., Ye, X., Zhang, Y.H.P., Simple protein purification through affinity adsorption on regenerated amorphous cellulose followed by intein self-cleavage. *Journal of Chromatography A*, 2008. **1194**: p. 150-154.
28. Yang, Q., Fukuzumi, H., Saito, T., Isogai, A., and Zhang, L., Transparent cellulose films with high gas barrier properties fabricated from aqueous alkali/urea solutions. *Biomacromolecules*, 2011. **12**: p. 2766-2771.
29. Fink, H.P., Weigel, P. Purz, H.J., and Gangster, J., Structure Formation of Regenerated Cellulose Materials from NMMO-Solutions. *Progress in Polymer Science*, 2011. **26**: p. 1413-1542.
30. Qi, H., Chang, C., and Zhang, L., Properties and applications of biodegradable transparent and photoluminescent cellulose films prepared via a green process. *Green Chemistry*, 2009. **11**: p. 177-178.
31. Hattori, K., and Arai, A., Preparation and Hydrolysis of Water-Stable Amorphous Cellulose. *ACS Sustainable Chemistry & Engineering*, 2016. **4**: p. 1180-1186.
32. Tsao, G.T.a.C., T.Y., Process for recovering and utilizing cellulose using sulfuric acid. 1981.
33. Su, H., Zhu, P., Zhang, L., Zhou, F., Li, G., Li, T., et.al., Waste to wealth: a sustainable and flexible supercapacitor based on office waste paper electrodes. *Journal of Electroanalytical Chemistry*, 2017. **786**: p. 28-34.
34. Joshi, G., Naithani, S., Varshney, V.K., Bisht, S. S., Rana, V., and Gupta, P.K., Synthesis and characterization of carboxymethyl cellulose from office waste paper: a greener approach towards waste management. *Waste Management*, 2015. **38**: p. 33-40.

35. Department, P.C. Minimization of paper usage and utilization of office waste paper. Available from: http://pcd.go.th/info_serv/waste_paper.html.
36. Ikeda, Y., Park, E.Y., and Okuda, N., Bioconversion of waste office paper to gluconic acid in a turbine blade reactor by the filamentous fungus *Aspergillus niger*. *Bioresource Technology*, 2006. **97**: p. 1030-1035.
37. Danial, W.H., Majid, Z.A., Muhid, M.N.M., Triwahyono, S., Bakar, M.B., and Ramil, Z., The reuse of wastepaper for extraction of cellulose nanocrystals. *Carbohydrate Polymer*, 2015. **118**: p. 165-169.
38. Makuuchi, K., Environmentally friendly vulcanization technology of natural rubber latex by radiation. *Advanced Materials*, 1994. **18A**: p. 721-724.
39. Zhang, C., Zhang, M., Wu, G., Wang, Y., and Zhang, L., Radiation Cross-Linking and Its Application, in *Radiation Technology for Advanced Materials*. 2019, Elsevier Inc.
40. Commission, C.N.S., Introduction to Radiation 2012, Canada. 38.
41. Academy, H.s.a.I.L.E., Radiation Safety and Awareness Radiological and Nuclear Smuggling and Detection for Law Enforcement Awareness Course. 2018, Bangkok, Thailand.
42. Uo, M., Wada, T., and Sugiyama, T., Applications of X-ray fluorescence analysis (XRF) to dental and medical specimens. *Japanese Dental Science Review*, 2014. **51**: p. 2-9.
43. ICRP, The recommendations of the International Commission on Radiological Protection. ICRP Publication 103, 2007. **37(2-4)**.
44. ITU-JRC, Introduction to Radiation Detection Equipment, in *Training Course on Radiological Crime Scene Management and the Way to Nuclear Forensics*. 17-27 June 2013.
45. Selbert, J.A., and Boone, J.M., X-ray imaging physics for nuclear medicine technologists. Part 2: X-ray interactions and image formation. *Journal of Nuclear Medicine Technology*, 2005. **33(1)**.
46. Khan, F.M., and Gibbons, J.P., *The Physics of Radiation Therapy*. 2014, USA: LIPPINCOTT WILLIAMS & WILKINS, a WOLTERS KLUWER business.

47. Aral, N., Nergis, F.B., and Candan, C., An alternative x-ray shielding material based on coated textiles. *Textile Research Journal*, 2015: p. 1-9.
48. Burns, K.V., Shoag, J.M., Kahlon, S.S., Parsons, P.J., Bijur, P.E., Taragin, B.H., and Markowitz, Lead Aprons Are a Lead Exposure Hazard. *Journal of the American College of Cardiology*, 2017. **14(5)**: p. 641-647.
49. Rebar, A.V., Crawford, A.B., Moses, N.A., and Krug, D.M. , Flexible highly filled composition, resulting protective garment, and methods of making the same, U.S. Patent, Editor. 2014: USA.
50. Apell, P., and Gellerstedt. F., Radiation protective material, U.S. Patent, Editor. 2019: USA.
51. Kujuktham, B., Wichayasiri, C., and Udon, S., X-Ray Attenuation of Cotton Fabrics Coated with Barium Sulphate. *Journal of Metals, Materials and Minerals*, 2016. **26 (1)**: p. 17-23.
52. Maghrabi, H.A., Vijayan, A., Mohaddes, F., Deb, P., and Wang, L., Evaluation of x-ray radiation shielding performance of barium sulphate-coated fabrics. *Fibers and Polymers*, 2016. **17(12)**: p. 2047-2054.
53. Kim, S.C., Choi, J.R., and Jeon, B.K., Physical analysis of the shielding capacity for a lightweight apron designed for shielding low intensity scattering X-rays. *Scientific Report*, 2016. **6(27721)**.
54. Pulford, S., and Fergusson, M., A textile platform for non-lead radiation shielding apparel. *The Journal of The Textile Institute*, 2016. **107 (12)**: p. 1610-1616.
55. Jiang, X., Zhu, X., Chang, C., Liu, S., and Luo, X., X-ray shielding structural and properties design for the porous transparent BaSO₄/ cellulose nanocomposite membranes. *International Journal of Biological Macromolecules*, 2019. **139**: p. 793-800.
56. Kalkornsurapranee, E., Kothan, S., Intom, S., Johns, J., Kaewjaeng, S., Kedkaew, C., Chaiphaksa, Sareein, T., and Kaewkhao, J., Wearable and flexible radiation shielding natural rubber composites: Effect of different radiation shielding fillers. *Radiation Physics and Chemistry*, 2021. **179(109261)**.

57. kim, S.C., and Son, J. K., Double-layered fiber for lightweight flexible clothing providing shielding from low-dose natural radiation. *Scientific Report*, 2021. **11**(3676).
58. Orue, A., Santamaria-Echart, A., Eceiza, A., Pena-Rodriguez, and Arbelaiz, A., Office waste paper as cellulose nanocrystal source. *Journal of Polymer Science*, 2017.
59. Khelle, H.L., Abd, A.N., and Ali, K.M., Preparation of Nano-Cellulose from Industrial Waste by Ultrasonic Device. *Journal Of Biochemical Technology*, 2018. **9(1)**: p. 35-39.
60. Oliva, C., Huang, W., Badri, S.E., Lee, M.A.L., Ronholm, J., Chen, L., and Wang, Y., Concentrated sulfuric acid aqueous solution enables rapid recycling of cellulose from waste paper into antimicrobial packaging. *Carbohydrate Polymers*, 2020. **241**.
61. Lei, W., Fang, C., Zhou, X., Yin, Q, Pan, S., Yang, R., Liu, D., and Quyang, Cellulose nanocrystals obtained from office waste paper and their potential application in PET packing materials. *Carbohydrate Polymers*, 2018. **181**: p. 376-385.
62. Lei, W., Zhou, X., Fang, C., LI, Y., Song, Y., Wang, C., and Huang, Z., New approach to recycle office waste paper: Reinforcement for polyurethane with nano cellulose crystals extracted from waste paper. *Waste Management*, 2019: p. 59-69.
63. Sridee, J., Rheology properties of natural rubber latex, in *Engineering in Polymer Engineering*. 2006, Suranaree University of Technology.
64. Kohjiya, S., Introduction, in *Chemistry, Manufacture and Applications of Natural Rubber*. 2014, Woodhead Publishing.
65. Kato, H., Nakatsubo, F., Abe, K., and Yano, H., Crosslinking via sulfur vulcanization of natural rubber and cellulose nanofibers incorporating unsaturated fatty acids. *RSC Advances*, 2015. **5**: p. 29814-29819.
66. Makuuchi, K., An introduction to radiation vulcanization of natural rubber latex. 2003: T.R.I. Global Co., Ltd., : Thailand.

67. El-Sayed, S.A., and Mostafa, M.E., Thermal pyrolysis and kinetic parameter determination of mango leaves using common and new proposed parallel kinetic models. *RSC Advances*, 2020. **10**: p. 18160-18179.
68. Wypych, G., *Handbook of Fillers*. 4 ed. 2016: ChemTec Publishing.
69. Moonlek, B., and Saenboonruang, K., Mechanical and electrical properties of radiation vulcanized natural rubber latex with waste eggshell powder as bio-fillers. *Radiation Effect & Defects in Solids*, 2019. **174 (5-6)**: p. 452-466
70. Songsri, A., Mechanical properties improvement of radiation pre-vulcanized natural rubber latex films by controlling of irradiation temperature, in Department of Nuclear Technology. 2006, Chulalongkorn University. p. 98.
71. Kim, S.C., Dong, K. R., Chung, W. K., Medical radiation shielding effect by composition of barium compounds. *Annals of Nuclear Energy*, 2012. **47**: p. 1-5.
72. Zuguchi, M., Chida, K., Taura, M., Inaba, Y., Ebata, A., and Yamada, S., USEFULNESS OF NON-LEAD APRONS IN RADIATION PROTECTION FOR PHYSICIANS PERFORMING INTERVENTIONAL PROCEDURES. *Radiation Protection Dosimetry*, 2008. **131(4)**: p. 531-534.
73. Villanueva, A., and Eder, P., End-of-waste criteria for waste paper: Technical proposals, in 2011: Spain. p. 101.
74. Lim-aroon, P., Wimolmala, E., Sombatsompop, N., and Saenboorung, K., Manufacturing process and properties of lead-free natural rubber sponge for use in X-ray and gamma ray shielding applications. *ICOP Conference Series: Materials Science and Engineering*, 2019. **526**.
75. Medvine. X-ray materials. July 9, 2021]; Available from: <https://www.medvine.com/th-th/product/dental-equipment/x-ray-materials/taiyo-thyroid-shield>.
76. METRO GLOBAL CO., L. Radiation Shielding Materials. July 9, 2021]; Available from: <https://www.mgcbkk.com/category/7/%E0%B8%A7%E0%B8%B1%E0%B8%AA%E0%B8%94%E0%B8%B8%E0%B8%9C%E0%B8%A5%E0%B8%B4%E0%B8%95%E0%B8%A0%E0%B8%B1%E0%B8%93%E0%B8%91%E0%B9%8C%E0%B8%9B%E0%B9%89%E0%B8%AD%E0%B8%87%E0%B8%81%E0%B8%B1%E0%B8%99%>

E0%B8%A3%E0%B8%B1%E0%B8%87%E0%B8%AA%E0%B8%B5-radiation-shielding-materials-2.

77. Expo, M. X-ray protective breast shield. July 9, 2021]; Available from: <https://www.medicaexpo.com/prod/rothband/product-121480-841350.html>.
78. Vulcanite. Technical Data Sheet: Shelf Life of Rubber Components. [cited 2021, 7 July]; Available from: <http://vulcanite.com.au/wp-content/uploads/technical/TDS-Shelf-Life-of-Rubber-Components.pdf>.
79. Hwang, S. Shelf Life vs. Service Life in Rubber Products. July 7, 2021]; Available from: <https://warco.com/shelf-life-vs-service-life-in-rubber-products/>.





APPENDIX

จุฬาลงกรณ์มหาวิทยาลัย
CHULALONGKORN UNIVERSITY

1. X-ray beam set-up for Secondary Standard Dosimetry Laboratory (SSDL)

The X-ray tube is set up to generate a narrow spectrum following the ISO 4037-1. The characteristics of the radiation qualities used for X-ray calibration are shown in Table S1. The chamber with the build-up cap is positioned free in the air as a reference point on the beam central axis. The reference plane of the chamber must be perpendicular to the central axis of the beam. The size of the radiation field at the reference plane is diameter 340 mm as shown in Figure S1. This procedure provides an overall uncertainty ($k = 2$) of about 6 % to 10 % for the phantom related to operational quantities.



Figure S1 X-ray calibration facilities in terms of the physical quantity air kerma.

Table S2 Radiation qualities at the IAEA for the ISO 4037-1 Narrow Spectrum Series.

Short name	Mean energy (keV)	Resolution (%)	Tube potential (Kv)	Recommended inherent filtration	Additional filtration			
					Pb (mm)	Sn (mm)	Cu (mm)	Al (mm)
N-30	24.6	32	30	1 mm Be	-	-	-	4.0
N-40	33.3	30	40	4 mm Al	-	-	0.21	-
N-60	47.9	36	60	4 mm Al	-	-	0.6	-
N-80	65.2	32	80	4 mm Al	-	-	2.0	-
N-100	83.3	28	100	4 mm Al	-	-	5.0	-

2. Gamma dosimetry for RVNR using Red 4034 Harwell dosimeters

The quality control for gamma irradiation can perform using polymethylmethacrylate (PMMA) dosimeters. In general, the Red 4034 Harwell dosimeters (Figure S2) are widely used in routine high dose rate dosimetry in the field of industrial radiation processing. The main advantages of this dosimetry method are ruggedness, stability, simplicity, and low price. The interaction of ionizing radiation with PMMA produces free radicals that affect its optical absorbance in certain wavelength bands. This dosimeter is cover in the range of 5 to 50 kGy. The PMMA dosimeters were attached to the natural rubber to measure the absorbed dose of gamma irradiation, as shown in Figure S3. After irradiation, the PMMA dosimeters were determined the intensities by comparing with the calibration curve as shown in Figure S4. The average absorbed dose from each point was obtained to ensure that the RVNR is the desired dose.



Figure S2 Red 4034 Harwell dosimeters before and after radiation.



Figure S3 Red 4034 Harwell dosimeters positioned for quality control of radiation dosimetry.

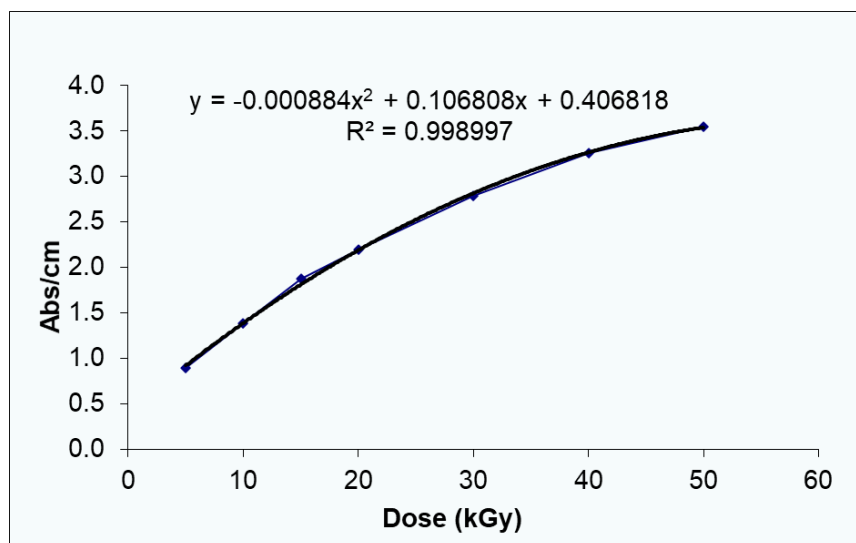


Figure S4 Calibration curve of Red 4034 Harwell dosimeters.

3. The results of X-ray attenuation study

Table S3 The radiation attenuation ratio (%) of X-ray shielding sheets.

Sample Code	X-ray tube voltage (kV)					
	30		40		60	
	% RAR	SD	% RAR	SD	% RAR	SD
NR	13.43	0.73	9.82	0.35	7.60	0.32
W40	47.77	1.86	38.90	1.35	32.03	0.94
E40	46.38	2.69	33.98	1.49	28.97	3.11
P40	30.31	1.55	23.13	3.68	19.85	4.45
W50	55.56	1.43	44.45	1.31	37.15	1.01
E50	57.10	2.50	43.15	2.39	37.31	1.66
P50	31.24	3.68	25.29	0.30	20.42	2.86
W60	62.13	2.35	50.97	2.50	41.53	2.70
E60	61.81	3.56	48.70	2.68	40.35	2.49
P560	32.81	2.99	26.46	2.84	21.85	2.47

Table S4 The linear attenuation ratio (mm^{-1}) ratio of X-ray shielding sheets.

Sample Code	X-ray tube voltage (kV)					
	30		40		60	
	μ	SD	μ	SD	μ	SD
NR	0.35	0.03	0.25	0.01	0.19	0.01
W40	1.86	0.24	1.37	0.12	1.10	0.11
E40	1.79	0.14	1.22	0.08	1.02	0.11
P40	1.24	0.06	0.85	0.17	0.71	0.11
W50	0.23	0.01	0.17	0.01	0.13	0.01
E50	0.25	0.01	0.17	0.01	0.15	0.01
P50	0.17	0.02	0.12	0.02	0.08	0.01
W60	3.474	0.126	2.545	0.103	1.916	0.102
E60	3.161	0.151	2.294	0.187	1.806	0.096
P560	1.774	0.185	1.277	0.137	0.985	0.086

Table S5 The half-value layer (mm) ratio of X-ray shielding sheets.

Sample Code	X-ray tube voltage (kV)					
	30		40		60	
	HVL	SD	HVL	SD	HVL	SD
NR	1.99	0.17	2.76	0.01	3.61	0.00
W40	0.38	0.05	0.51	0.12	0.63	0.11
E40	0.36	0.06	0.53	0.08	0.65	0.11
P40	0.56	0.03	0.84	0.17	1.00	0.11
W50	2.98	0.18	4.15	0.01	5.25	0.01
E50	2.74	0.20	3.98	0.01	4.75	0.01
P50	5.02	0.69	6.45	0.02	8.50	0.01
W60	0.20	0.01	0.27	0.10	0.36	0.10
E60	0.22	0.02	0.31	0.19	0.39	0.10
P560	0.39	0.04	0.55	0.14	0.71	0.09

Table S6 The attenuation properties of shielding sheets when exposed with 60 kV.

Sample code	Thickness (mm)	%RAR	μ	HVL
W1	5.821	77.870	0.239	2.904
W2	8.543	86.960	0.240	2.884
W3	10.689	92.330	0.259	2.677
E1	6.769	72.542	0.180	3.859
E2	9.123	86.998	0.182	3.801
E3	12.354	96.853	0.189	3.668
Pb	0.300	75.330	4.665	0.149

Table S7 The attenuation properties of shielding sheets when exposed with 80 kV.

Sample code	Thickness (mm)	%RAR	μ	HVL
W1	5.821	55.025	0.147	4.727
W2	8.543	67.273	0.155	4.461
W3	10.689	75.621	0.160	4.342
E1	6.769	48.184	0.112	6.201
E2	9.123	64.372	0.115	6.051
E3	12.354	76.352	0.129	5.363
Pb	0.300	45.845	2.542	0.273

VITA

NAME Harinate Mungpayaban
DATE OF BIRTH 31 December 1975
PLACE OF BIRTH Bangkok
INSTITUTIONS ATTENDED Chulalongkorn University
HOME ADDRESS 39 Rangsit-Pathumtani 12 Soi 5, Prachathipat sub-district,
Thanyaburi district, Pathum Thani Province 12130

